THE USE OF FINITE ELEMENT METHODS IN THE DETERMINATION OF NORMAL AND SHEAR STRESSES IN SLOPES

by

Diana Louise Michels

A thesis submitted to the Faculty and Board of Trustees of the Colorado School of Mines in partial fulfillment of the requirements for the degree of Master of Science (Engineering Systems).

Golden, Colorado

Date 16 November 1998

Signed: _____
Diana Louise Michels

Approved: _____
Dr. D. V. Griffiths
Thesis Advisor

Golden, Colorado

Date 11-20-98

_____
Dr. Joan Gosink
Department Head
Engineering

ABSTRACT

This thesis describes the influence on the calculated results of stresses in slopes due to several key factors. By the use of finite element methods based on linear-elastic theory, the effects slope angle and Poisson's ratio of the soil that forms embankments are investigated in order to determine the sensitivity of the stresses in the slopes to these properties. In addition, the finite element method itself is scrutinized to ascertain effects induced by the location of mesh boundaries with respect to embankment dimensions as well as the density of elements used in the formation of the finite element meshes.

An instance in which the Mohr-Coulomb failure criterion is violated when using elastic theory is presented and discussed. A finite element program that uses a visco-plastic algorithm, which iteratively redistributes stresses until the failure criterion is met, is introduced and the results are compared with those obtained with elastic theory. Additionally, the changing stresses and nodal displacements that occur during the stress redistribution process by the visco-plastic algorithm are investigated and presented.

The elastic finite element model is found to be quite suitable for calculating the stresses in soil slopes. It is shown that Poisson's ratio has a profound influence on the elastic solution, but a relatively mild influence on the converged elasto-plastic solution. It is further determined that for slope angles of 45°, stress concentrations at the toe and crest appear and increase with steeper grades. Whereas, for flatter slopes, these stress concentrations are altogether absent.

TABLE OF CONTENTS

LIST OF FIGURES

Page

LIST OF TABLES

Page

ACKNOWLEDGMENTS

It is with grateful acknowledgement that I would like to thank my Thesis Committee for their time and efforts to guide me through this research.

Thank you:

Dr. Vaughan Griffiths, for introducing me to the application of finite element analysis to geotechnical problems, and for inspiring me to explore several facets of each;

Dr. Graham Mustoe, for guiding me to a more intuitive understanding of the mechanical properties of soils;

Dr. Hal Olsen, for helpful suggestions toward improving the organization of my written work;

Dr. Jerry Higgins, for support and encouragement when I desired and needed it most;

and finally, I extend my thanks to Bill Savage, who shared his time and experience as my research progressed.

LIST OF SYMBOLS

SYMBOL	MEANING
$\angle$	Angle
ϕ	Angle of Friction
$^{\circ}$	Angular Degrees
σ	Normal Stress
ν	Poisson's Ratio
τ	Shear Stress
γ	Unit Weight
σ_x	Horizontal Stress
τ_{xy}	Shear Stress
σ_y	Vertical Stress
c	Cohesion
E	Modulus of Elasticity
FE	Finite Element
g	Acceleration of Gravity
K_0	Coefficient of Earth Pressure at Rest

Table of Abbreviations and Symbols

Section 1

INTRODUCTION

The effects of several key factors that influence the calculated results of stresses in slopes are sought. By the use of finite element methods based on linear-elastic theory, the influence of slope angle and Poisson's ratio of the soil that forms embankments are investigated in order to determine the sensitivity of the stresses in the slopes to these properties.

As with many calculative tools, the use of the finite element method requires certain assumptions to be made. Of particular interest to this researcher are the choice of mesh size and element density and their respective effects upon calculated results. Accordingly, these aspects are scrutinized to ascertain their effects on the finite element solutions to elastic stresses in slopes.

1.1 Background

Initially, in addition to studying the changes in stresses in embankments when properties of the slopes are modified, the research for this thesis was to include a comparison of results from the finite element program with results obtained from a closed-form analytic solution. During the course of that research, concern with respect to

the accuracy of the analytic solution evolved. It was decided instead to pursue the parametric studies using finite element analysis.

The analytic solution considered employs a conformal mapping routine, which could possibly be used in the generation of finite element meshes. This idea was successfully attempted and an example is presented herein. In part, due to the questions surrounding the analytic solutions, it seemed reasonable to run some additional tests that would establish the suitability of the finite element program for use in this study. To this end, a comparison of finite element solutions to the Boussinesq strip load solutions for normal and shear stresses is also presented.

During the examination of the parametric results, an occasion for which the elastic solution for the Mohr-Coulomb failure criterion is violated was encountered. A latent cross-examination of the combination of parameters that produced this situation was performed by the application of an additional finite element program based on an iterative visco-plastic algorithm. The results from this program were then compared with the elastic solution.

Finally, a brief inquiry into the redistribution process of the visco-plastic algorithm was made. A new visualization technique employing animation was implemented for better understanding of the changes in the failure function and the displacements of the slope during the redistribution process.

1.2 Thesis Objectives

The intent of this thesis is to use finite element analysis in the characterization of variations of normal and shear stresses in slopes concomitant with Poisson's ratio and grade changes. A parallel aim included in this research is the determination of the manner and severity with which mesh size and element density affect the finite element results.

1.3 Approach

At the outset, the tools, methods and terminology key to this research are described. Following this denotation is a brief description of the conformal mapping technique broached in the "Background" section above. Three stress normalization methods are then discussed and compared. Thereupon, the results of the parametric studies are presented and discussed. The last section is devoted to the visco-plastic solution and the transformations it generates in order to resolve stresses in violation of the Mohr-Coulomb failure criterion.

Section 2

EXPERIMENTAL METHODS AND TOOLS

The comparisons of the finite element results are all made by visually inspecting contour plots of the stresses, etc. The contouring process is not trivial, as many choices with respect to the generation and presentation of the plots. The software package used for this purpose is described in this section. Also covered in this division are several of the basic details of the geotechnical problem under study as they relate to the finite element method in general and to the elastic FE program in particular.

2.1 Graphics Packages

SURFER® for Windows by Golden Software, Inc. is used for the contouring graphics. Several point estimation routines are offered in this package and all produce essentially identical contours for the work included herein in part because the input data is relatively dense and regularly spaced. All methods except triangulation yield contours in the "air" region above the slope as shown in Figure 2-1. This is merely an artifact of the point estimation procedures and in no way affects the validity of the contours in the embankments.

A "blanking" procedure which essentially "whites out" the air space region and

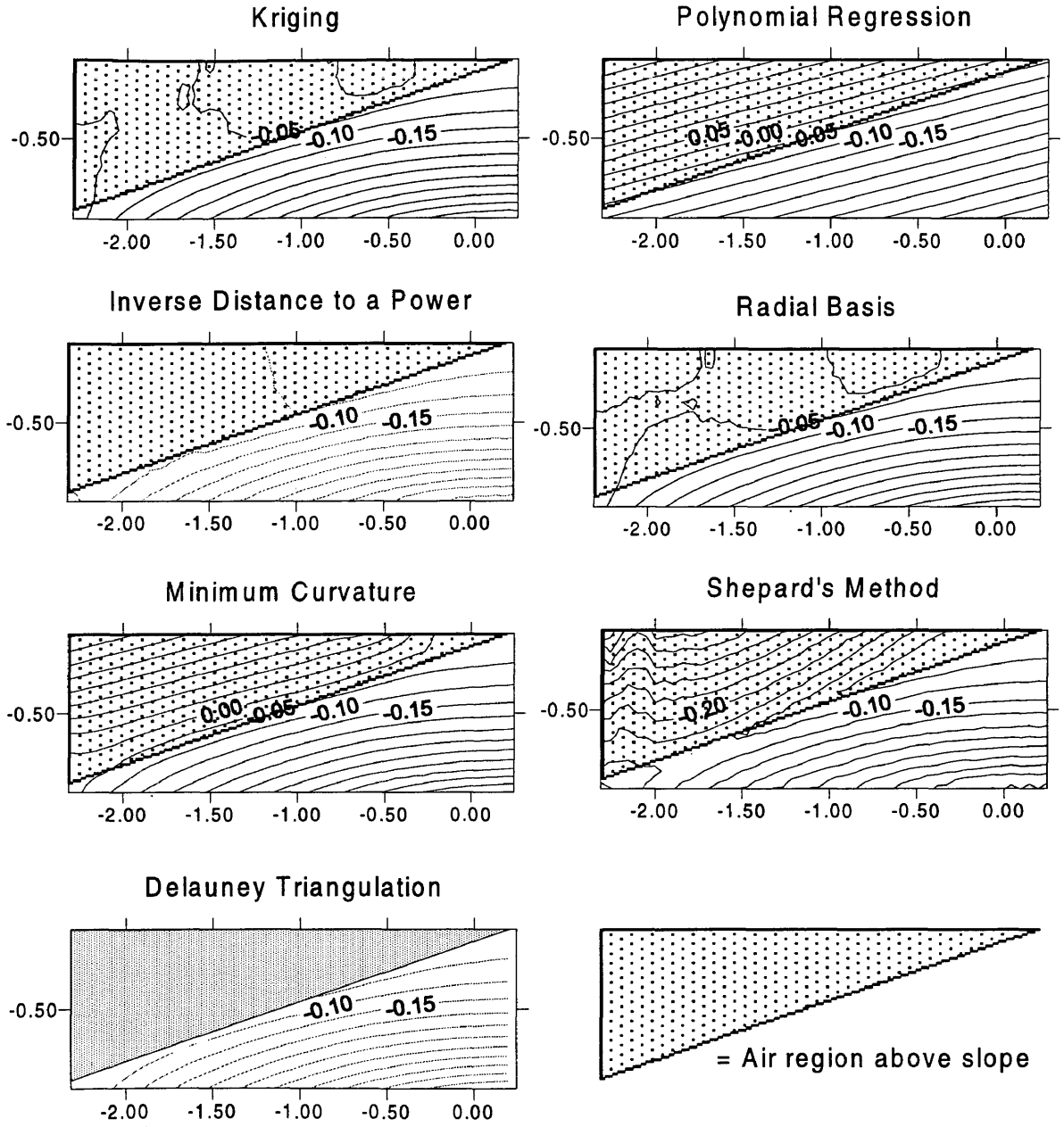

Figure 2-1: Comparison of Contouring Methods Available in SURFER®

has no effect on the remaining contours may be utilized. Unfortunately, the results so generated have not consistently been to this researcher's satisfaction. For clarification it has been found necessary to draw in the slope and upper front boundary. To this end, opaque polygons are used to fulfill the dual roles of blanking out the contours in the airspace and delineation of the physical boundaries.

SURFER® offers a variety of options for each point estimation method. The Kriging method has been used throughout this work, employing all of the default selections with the single exception of the point estimation grid line spacing, which has been set to a value of 0.25 in both the x- and y- directions. This grid line spacing refers to the distance in data units between adjacent rows and columns used for point estimation purposes by the contouring program. (For the shear stresses with a Poisson's ratio of 0.4999, it was found necessary to increase this spacing to 1.25 in order to obtain fairly smooth contour lines.) A graphical example of the effects of the Kriging options is included in Appendix A.

Finite element meshes presented were derived from postscript files produced by the mesh.f subroutine included in the finite element program code and converted to JPEG[1] format for inclusion within the text. The graphics conversion was done in a

[1] "Joint Photographic Expert Group"

Linux[2] environment using *XV*, by John Bradley (v. 310a, Copyright 1994). The mesh.f subroutine was originally written by R. Daniel Lohnes and subsequently updated by Gordon A. Fenton and D. V. Griffiths. The sole alteration made to this routine for the present work was to insert lines that override the scaling of the mesh to fill a full page. The override renders all mesh graphics in a consistent scale.

Graphs and illustrations of calculation points, in the case of analytic meshes à la Savage, Powers and Swolfs (1984), were done using Microsoft® Excel 97.

2.2 Finite Element Method

The finite element scheme used for this work is that developed and described by Smith and Griffiths (1988). The general routine used is based on the 8-node quadrilateral element for plane strain analysis of linear-elastic soils as illustrated in Chapter 5 of Smith and Griffiths' book.

Because all of the analyses are elastic, the soil cohesion and friction angle do not affect the results but nominal values of $c/\gamma h = 0.30$ and $\phi = 30°$ are used for later comparisons with the Mohr-Coulomb failure function.

Young's modulus is set to a value of $1*10^2$ kPa--due to normalization, this value does not affect the outcome of the results presented in this work. Clough and Woodward (1967) have shown that values of stress under gravity loading, when calculated using

---

[2] PC version of UNIX

linear elastic theory, vary in proportion to the unit weight of the material and the size of the embankments. The value of the modulus of elasticity therefore does not affect the calculated stress values. However, the effects of Poisson's ratio on the values of stress are somewhat more complex (Lefebvre, *et al*, 1973).

The slope angle is varied by changing the major dimensions of the finite element mesh. These dimensions are shown in Figure 2-2. The number of elements is also changed for specific reasons to be stated in later sections as this issue becomes imperative. The FORTRAN listing of the finite element code used is included in Appendix B.

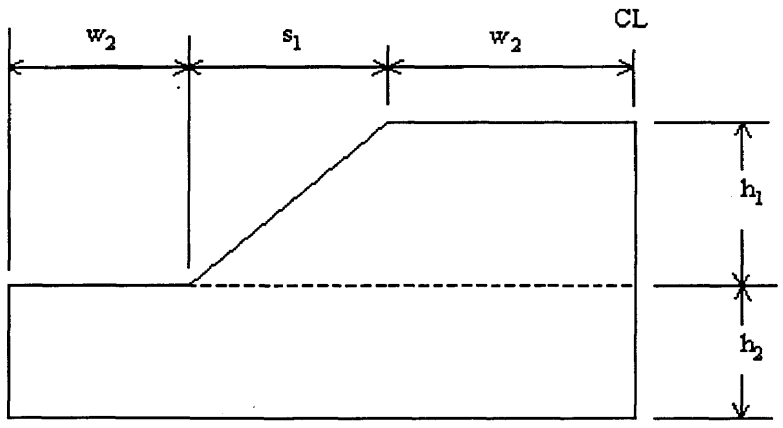

Figure 2-2: Finite Element Slope Dimensions

The embankments studied are considered symmetric and so only one half of each structure is employed in the solutions. The boundary conditions along the centerline ("CL" in Figure 2-2) restrict horizontal motion and allow vertical motion. The lower boundary is fully fixed and may be thought to represent a rough, rigid base; perhaps bedrock and/or simply a no-slip condition between the base of the embankment and the native floor material. The foundation of the embankments is assumed to be of the same material as the embankments. The boundary conditions on the edge of the foundation beyond the slope toe allow vertical motion only. The allowance for vertical motion on the left and right sides of the embankment models provides for the assumption of symmetry to either side of these boundaries.

2.2.1 Presentation of Results

All of the analytic and finite element results presented in this thesis have been non-dimensionalized. For instance, stresses are divided by the unit weight times a height (e.g. γh_1). In several instances, a measure of depth in "units" is given when describing specific results. This use of the term "unit" signifies a non-dimensional length, which is derived from the finite element mesh dimensions: $h_1 + h_2$ in the y-direction and $w_1+s_1+w_2$ in the x-direction. In general, one unit is equal to one embankment height (h_1). Additionally, these units will often be displayed on the axes of the contour plots or other graphs presented. In cases in which the unit numbers do not appear on contour plots, the

zero position on the horizontal axis is coincident with the crest of the embankments and the vertical zero position is along the top of the embankments, also coincident with the slope crests. Each tick mark along the axes represents one unit of distance unless otherwise noted.

2.2.2 Plane Strain and Gravity Loads

When slopes and embankments are quite a lot longer than they are wide, it may be assumed that the cross-sectional stresses are independent of position along the length of the structure. Thus, in an x-y-z coordinate system, where y is vertical x and z are mutually perpendicular and horizontal, and the z-direction is defined as that along the length of the embankments, when looking at the x-y plane, the z-position becomes inconsequential. The resulting conditions, in the context of the theory of elasticity, are called plane-strain conditions ($\varepsilon_z = 0$, see e.g. Davis and Selvadurai, 1996) and are adopted here. The governing equations then, based on Hooke's theory of elasticity are:

$$\varepsilon_{xx} = \frac{1}{E}\left[\sigma_{xx} - \nu\left(\sigma_{yy} + \sigma_{zz}\right)\right] \text{ and} \tag{2.1}$$

$$\varepsilon_{yy} = \frac{1}{E}\left[\sigma_{yy} - \nu\left(\sigma_{xx} + \sigma_{zz}\right)\right]. \tag{2.2}$$

Lefebvre, *et al* (1973) qualify this assertion in their statement that plane strain analyses in two dimensions provide an accurate representation of conditions in centrally located transverse sections of long dams of uniform cross sections. Further, they suggest

that plane strain analyses may not be suitable for transverse sections of dams located in steep-walled valleys due to the effects of cross-valley arching. These researchers found that on average, plane strain analyses for transverse sections typically yielded higher stresses than did three-dimensional finite element analyses. Depending upon the slope of the valley walls, the average variances could be as much as 3% lower than 3D analysis (minimum principal stress in a valley with 6:1 wall slopes) up to 38% greater than the 3D analysis (maximum shear stress in a valley with wall slopes of 1:1). Their conclusion with respect to the use of plane strain of central transverse sections of dams in valleys is that the degree of accuracy is most acceptable for valleys with wall slopes of 3:1 or flatter. The embankment cross sections studied herein unquestionably fall into this category.

The importance of the central location of the transverse cross section and flatness of valley walls, in the case of dams, is associated with the assumption in plane strain analysis that there is no out-of-plane deformation, and that cross-valley arching is not a substantial issue.

Gravity loads are those imposed by the self-weight of the soil. No additional forces are applied to any of the slopes or embankments considered herein. Due to this limitation of applied forces, all of the stresses are a function of the in-plane vertical and horizontal position and Poisson's ratio. The elastic modulus (E) does not affect these stresses because $\sigma_y = \gamma y$ (where γ is the unit weight of the soil and y is the thickness of the

soil above the point of interest) and the phenomenon described by Poisson's ratio is the cause of stress in the horizontal direction (σ_x).

Compressive stresses determined by the finite element method in this work are negative. In normally consolidated soils, horizontal stresses are typically smaller than vertical stresses and Hooke's law for elastic materials will yield reasonable results where the coefficient of earth pressure "at rest" is K_0, and $K_0 = \frac{\nu}{1-\nu}$. For this reason, it is assumed that soils are normally consolidated in all of the examples presented here.

2.2.3 Poisson's Ratio

Throughout this thesis the range of Poisson's ratios (ν) studied will include the extreme values of 0.00 and 0.4999. While the higher values of ν do have relevance in geotechnical practice for "undrained clays", the values below about 0.15 are not particularly meaningful with respect to soils. Nevertheless, the effects of the lower values of ν are pedagogically interesting and help to define trends that are less apparent when considering only results yielded with the higher ν values. Table 2-1, taken from Bardet (1997), summarizes representative values of ν for typical soils.

2.3 Suitability of the Use of Linear Elastic Theory

Linear elastic theory is the basis for the majority of the solutions presented in this work. It is well known that soil by definition is not a proper continuum and therefore cannot possess the properties of linear elastic materials as defined in conventional mechanics of materials. Nevertheless, soils can and do act nearly linearly and elastically under condition of small stresses, e.g. those which produce shear stresses which are considerably lower than the ultimate strength of the soil (Davis and Selvadurai, 1996).

Approximate values of Poisson ratio for various soils

Soil group	Soil type	Bowles (1988)	Cernica (1995)	Converse (1962)	Poulos (1975)
Clay	Soft	—	0.4		—
	Medium	—	0.3	—	0.3–0.35
	Hard		0.25	-	—
	Stiff plastic	—	—	0.4–0.45	- -
	Saturated	0.4–0.5		—	—
	Unsaturated	0.1 0.3	—		—
	Soft normally consolidated	—	—	—	0.35- 0.45
	Stiff overconsolidated	—	—	—	0.1–0.3
	Sandy	0.2–0.3	0.25	—	-
Silt		0.3–0.35	—	—	—
Loess		0.1–0.3		—	—
Sand	Loose	—	0.2	—	0.35–0.4
	Medium	-	—	- -	0.3–0.35
	Dense	0.3–0.4	0.3	0.3–0.36	0.25–0.3
Gravel	Loose	—	0.2	—	—
	Dense	—	0.3	—	— -

Table 2-1: Representative Values of Poisson's Ratio

Under the Mohr-Coulomb failure criteria, Smith and Griffiths (1988) have defined the failure criterion, F, which is a function of material properties and stress, for which

F > 0 indicates yielding and F < 0 signifies elasticity, where in terms of the principal stresses,

$$F = \frac{\sigma_1 + \sigma_3}{2}\sin(\phi) - \frac{\sigma_1 - \sigma_3}{2} - c\cos(\phi) \tag{2.3}$$

For the elastic analyses done for this thesis, the places at which F denotes yielding are not actual failure zones; rather, they illustrate the regions in which redistribution of stresses would occur in order to maintain structural integrity. This is illustrated for 45° slopes with Poisson's ratios of 0.20 through 0.30 (in increments of 0.01), and 0.49 in Figure 2-3 and Figure 2-4, and for 90° slopes with Poisson's ratios of 0.10, 0.20, 0.30, and 0.49, Figure 2-5. The redistribution of stresses will be discussed in a later section.

In these plots, it can be seen that in all cases the soil in the embankment region is elastic with the marginal exception right at the toe of the 90° slope with Poisson's ratio of 0.10 as the F = 0 contour coincides with this point. This latter distinction may indicate possible instability for these conditions. It should be noted again that with respect to soils, this low value for Poisson's ratio is not realistic and indicates that for small Poisson's ratios the stresses derived from linear elastic theory are not apparently valid for the foundation regions (Figure 2-3). This latter assertion assumes that there are no property changes with depth. It may be that if the elastic properties of the foundation soil change with depth and their variation is accounted for in the finite element model, the solution for the foundation may be quite different.

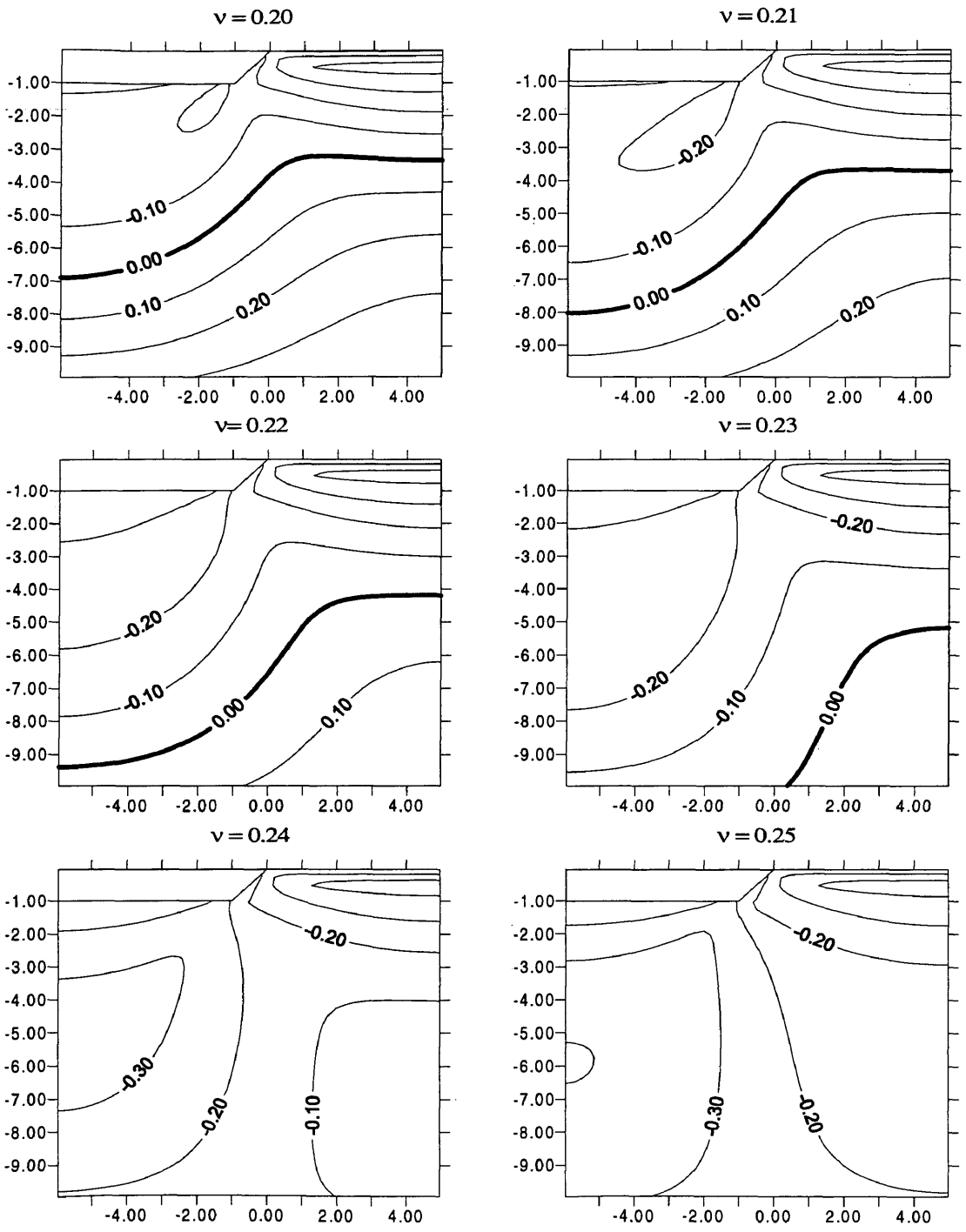

Figure 2-3: Contours of Mohr-Coulomb Function F With Increasing Poisson's Ratio (0.20 - 0.26); Slope Angle of 45°; $c/\gamma h_1 = 0.30$; ϕ, = 30°

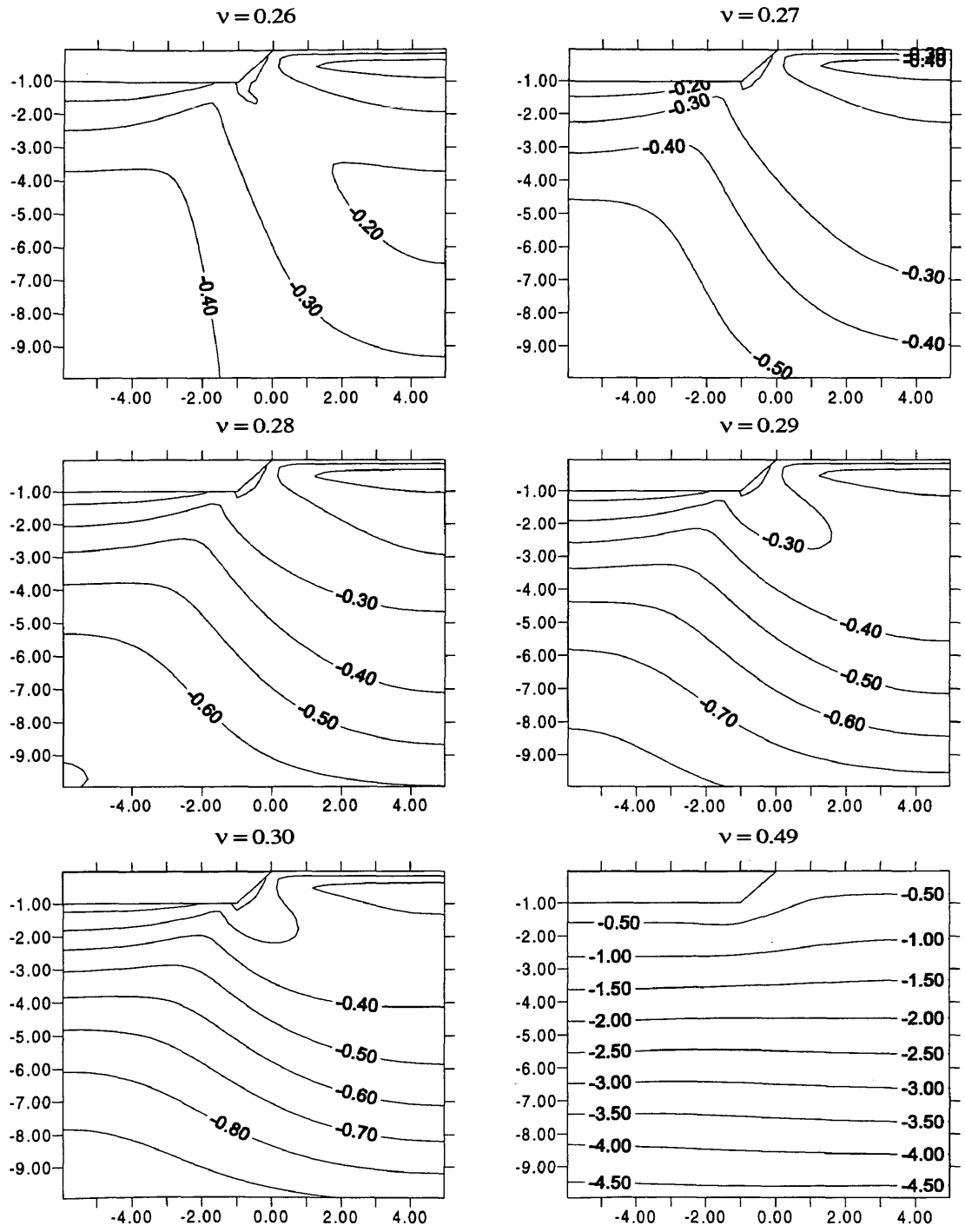

Figure 2-4: Contours of Mohr-Coulomb Function F With Increasing Poisson's Ratio (0.27 - 0.30, 0.49); Slope Angle of 45°; $c/\gamma h_1 = 0.30$; ϕ, = 30°

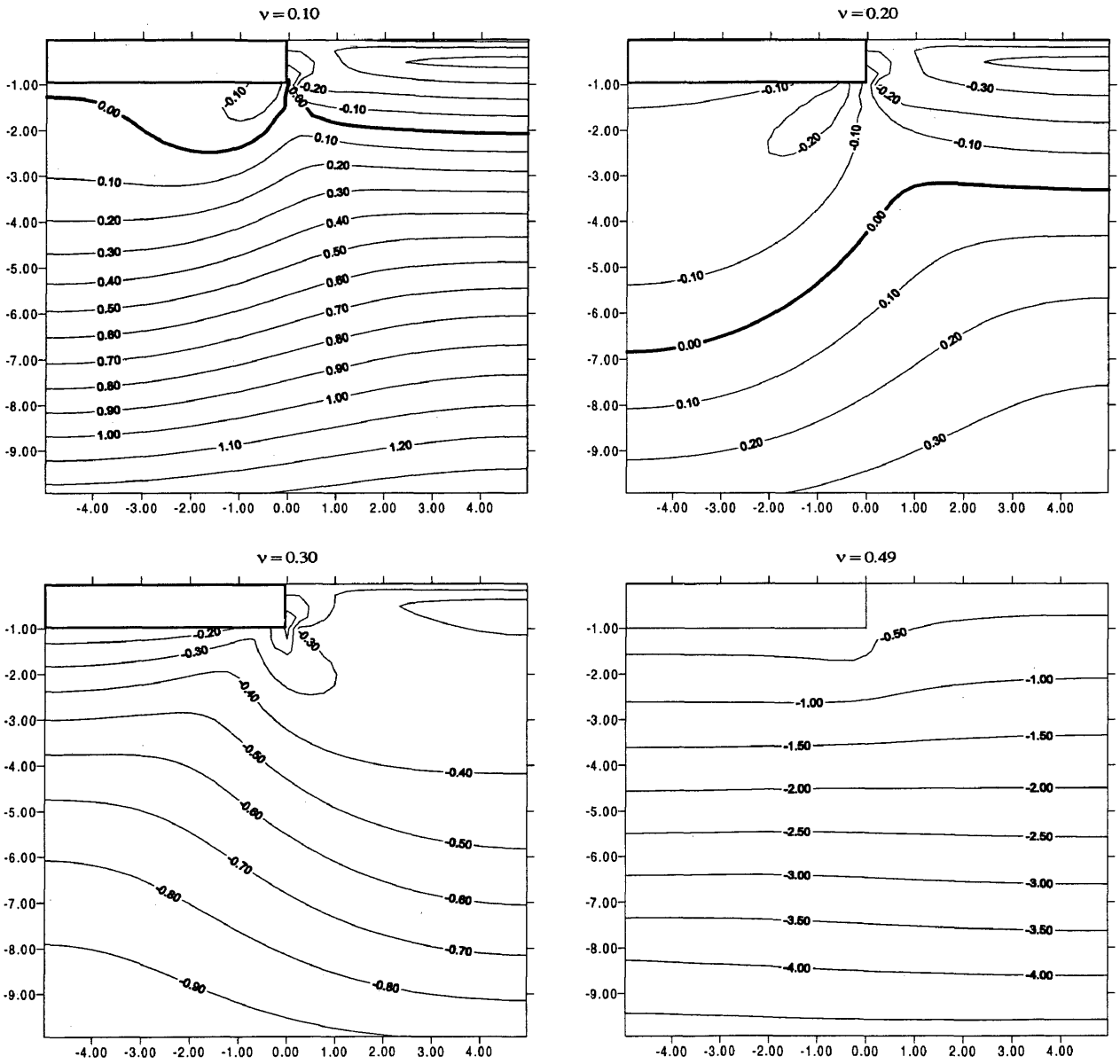

Figure 2-5: Contours of Mohr-Coulomb Function F With Increasing Poisson's Ratio (0.10, 0.20, 0.30, 0.49); Slope Angle of 90°; $c/\gamma h_1 = 0.30$; $\phi, = 30°$

Since it is not realistic to believe that the *in situ* property materials can be exactly known for all points of an embankment/foundation profile, the engineer using estimation methods such as those presented here which are based on linear elastic mechanics, must be aware of the necessarily approximate nature of the results. Furthermore, an understanding of how and why the numerical solutions may vary from actuality is imperative. At best, blind usage of such results may induce an engineer to use excessively conservative design constraints; at worst perhaps, a project might be abandoned or the design so conservative as to raise costs to prohibitive levels. At this time, remark must be made that while the "how and why" are not a primary focus of this thesis. However, they are mentioned here (and discussed in a later section) in order to establish the author's realization of their potential significance as well as to proclaim their existence to the reader.

Section 3

SLOPE TERMINOLOGY USED

Throughout this report, the following terms, as illustrated in Figure 3 - 1, are used with respect to specific points and regions of the slopes to be studied.

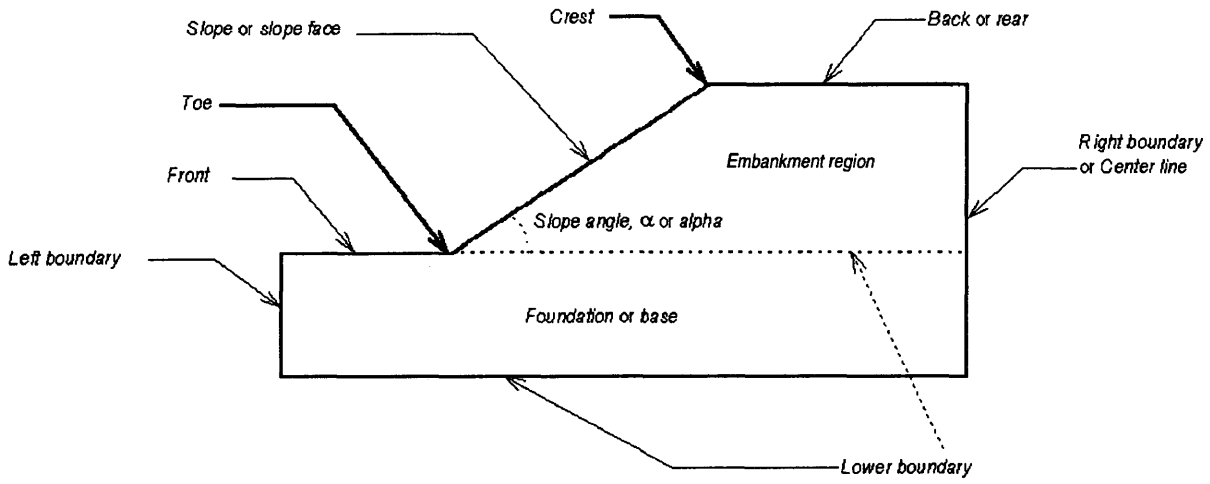

Figure 3 - 1: Slope Terminology

Three regions that are referred to with some regularity may be defined with respect to two imaginary vertical lines subtended from the toe and crest of the slopes. The region between these lines is the "center" or "central" region; that between the left boundary and the line subtended from the toe of the slope is the "left" or "front" region; and similarly, the area between the line subtended from the slope crest and the right

boundary (or center line) is the "right", "rear", or "back" region.

Except where otherwise stated, a negative-compression sign convention has been assumed.

Section 4

CONFORMAL MAPPING

The FE program used for the current research is particularly suited to slopes with straight boundaries. However, it is possible to extend its application to accommodate structures with more complex profiles.

4.1 Geotechnical Structures With Irregular Boundaries

Savage and Swolfs (1986) have obtained a closed-form solution for gravity-induced stresses in an elastic half-space bounded by a smooth curvilinear surface. The issue of interest with respect to the current research is the method in which the smooth surface was obtained for calculation purposes, and the application of this technique to the creation of finite element meshes.

Because of mathematical difficulties, few exact solutions exist for gravitational stresses in elastic media with irregular boundaries (Savage, Swolfs and Powers, 1985). Previous to the current work, the finite element programs developed by Smith and Griffiths have been used for slopes and embankments with finite limits and linear boundaries. The introduction of mapping routines may be relatively simple, as in the symmetric ridge example. The analytical evaluation of irregularly shaped structures can

be mathematically problematic; in contrast, the finite element method is quite capable of managing such tasks.

4.2 Conformal Mapping

Figure 4-1 compares a regularly spaced rectangular grid in (u,v)-space with its associated (x,y)-space grid as calculated by Savage and Swolfs' analytic solution. The subroutine quad.f, which creates a mesh within the finite element program, has been modified such that the (u, v) region is defined within the $(w_1 + w_2) \times h_2$ rectangular foundation region ($s_1 = 0$) is mapped into (x, y) coordinates, which describe the symmetric slope geometry. (see Appendix C). Once the mesh is defined, the finite element program operates normally.

The ability to arrange finite element boundaries in a curvilinear fashion as is made possible by this conformal mapping technique is worthwhile since all of the element nodes are mapped to the desired curves. This eliminates some of the discretization effects of placing mid-side nodes along the straight path between two corner nodes. A potential drawback of this mapping routine is the loss of some detail in areas where elements are quite large, thus making the calculation, or gauss points rarer in those regions. This consequence is evident in the upper left-hand element (shaded) of the mapped grid in Figure 4-1. However, depending upon the element density chosen, this may not be problematic at all. For instance, Figure 4-2 the elements in the mesh

generated by the modified quad.f subroutine in the finite element program are rather dense, and so their size does not vary appreciably.

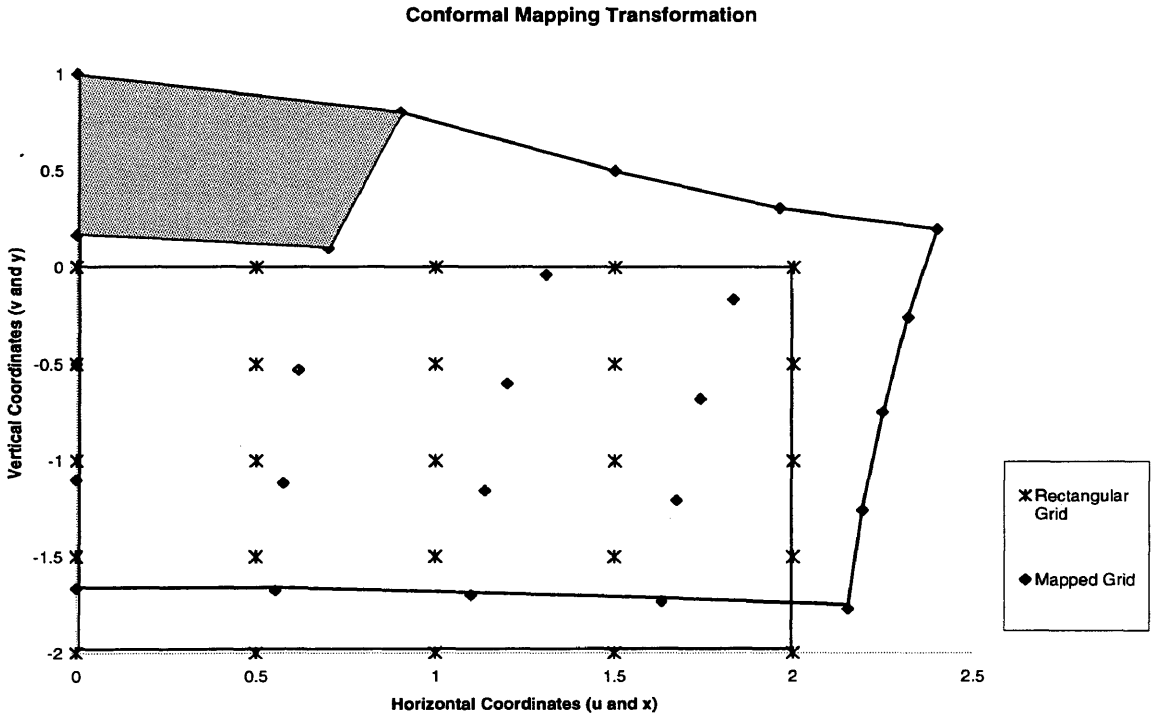

Figure 4-1: Conformal Map by Savage and Denlinger's RVT Program

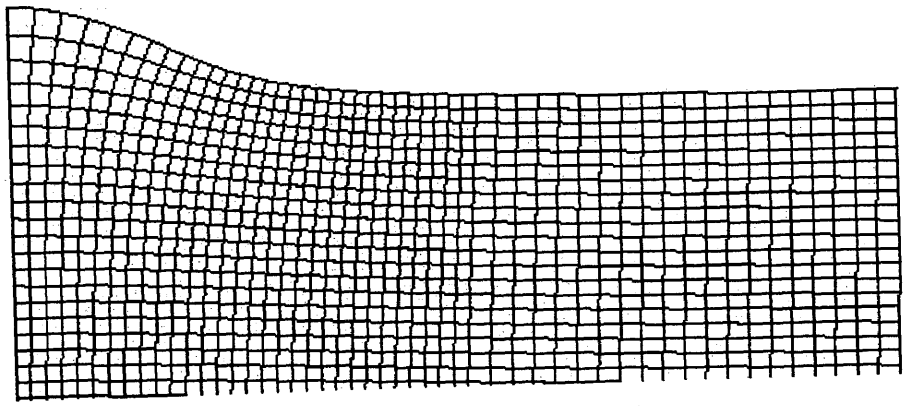

Figure 4-2: Conformal Map by Modified quad.f Subroutine

Section 5

EXAMINATION OF NORMALIZATION METHODS USED IN THE LITERATURE

Oddly enough, there does not seem to be a standard procedure for normalizing or representing the values of stress contours in slopes and embankments. Clough and Woodward (1967) simply contoured the stresses themselves but also contoured stress multiplication factors, which depend upon the dimensions of the embankment with respect to each calculation point. Poulos *et al* (1972) contoured non-dimensionalized stresses using a technique that relies on the maximum possible height of the slope (see Figure 5-7). Moreover, Savage (1994) normalizes stresses using the maximum actual height of the slope.

5.1 Clough and Woodward

In their often-referenced paper, investigators Clough and Woodward (1967) discuss the stresses and deformations developed in an earth dam during construction. Using finite element analysis with triangular plate elements, they determined stresses and deformations in a "standard" embankment (see Figure 5-1) on a rough rigid base as it was built up in several lifts. They determined that the stresses in an incrementally constructed

embankment and those in an embankment constructed in a single lift do not differ appreciably. (The deformations, on the other hand, do vary considerably but are not considered in this work.)

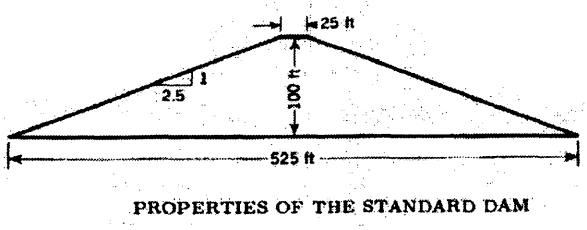

$\nu = 0.40$
$E = 200$ ksf $\cong 9.6$ kPa
$\gamma = 135$ pcf $\cong 21$ kN/m^3

Figure 5-1 : Clough and Woodward's Standard Dam

Figure 5-2 and Figure 5-3 show Clough and Woodward's stress and stress factor results for their "standard" embankment, which has a slope of 21.8°. Figure 5-4 and Figure 5-5 show corresponding results obtained by the finite element program used for this thesis. The correspondence between these is very good. The slight difference in the stress factor contours may be attributed to the simulated incremental construction used in the production of Clough and Woodward's figures.

The stress factors introduced by Clough and Woodward are calculated using: $K=\sigma/(\gamma H)$, where σ is the stress, γ is the unit weight of the soil, and H is the thickness of the soil above the point of interest. These factors must be multiplied by additional values which are tabulated to correspond to varied Poisson's ratios and side slopes (height-to-base ratios) and are to be used in conjunction with the "standard" embankment contours

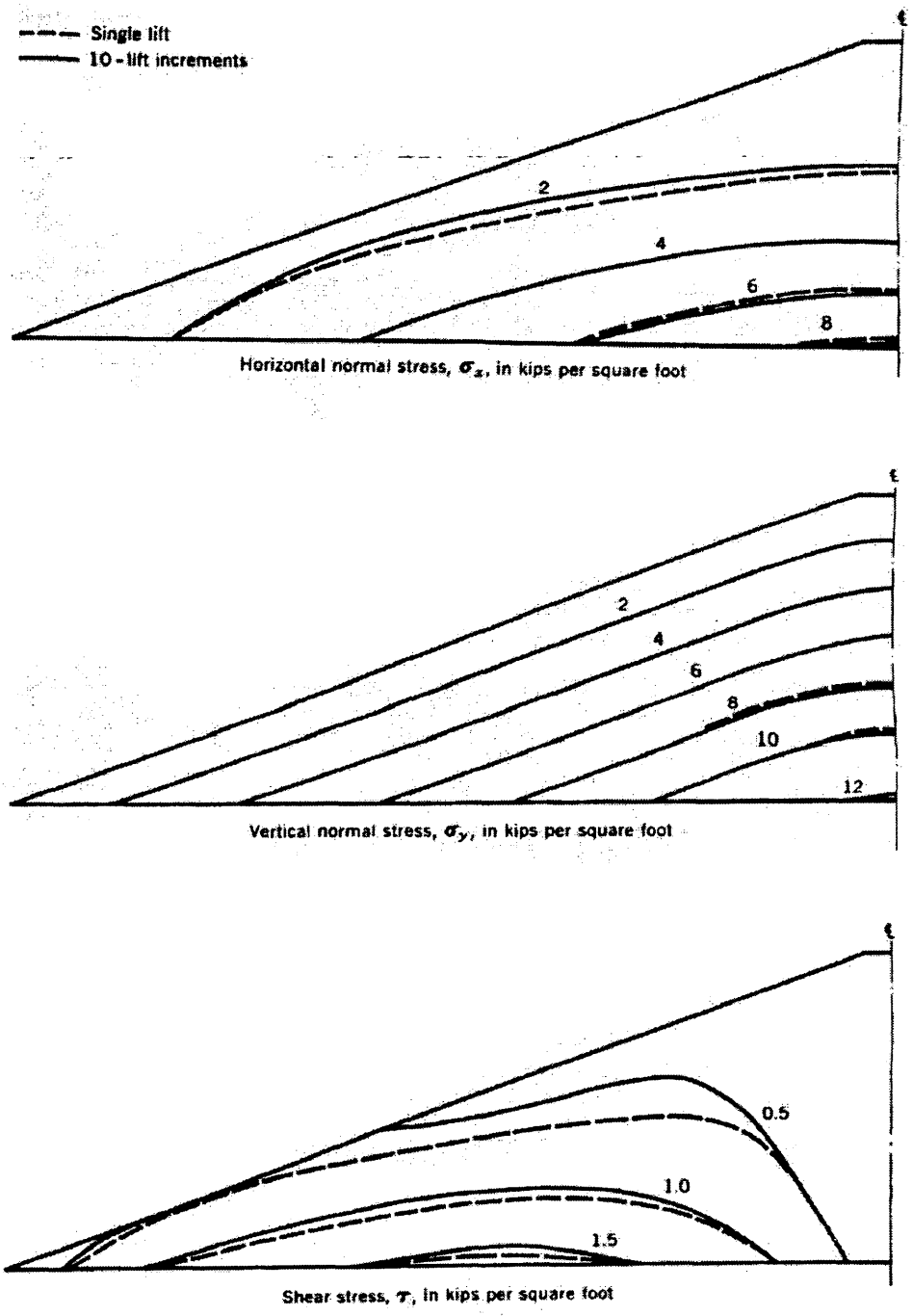

Figure 5-2: Clough and Woodward's Stress Contours for Single and Multiple Lift Construction Due to Dead Weight in Standard Dam

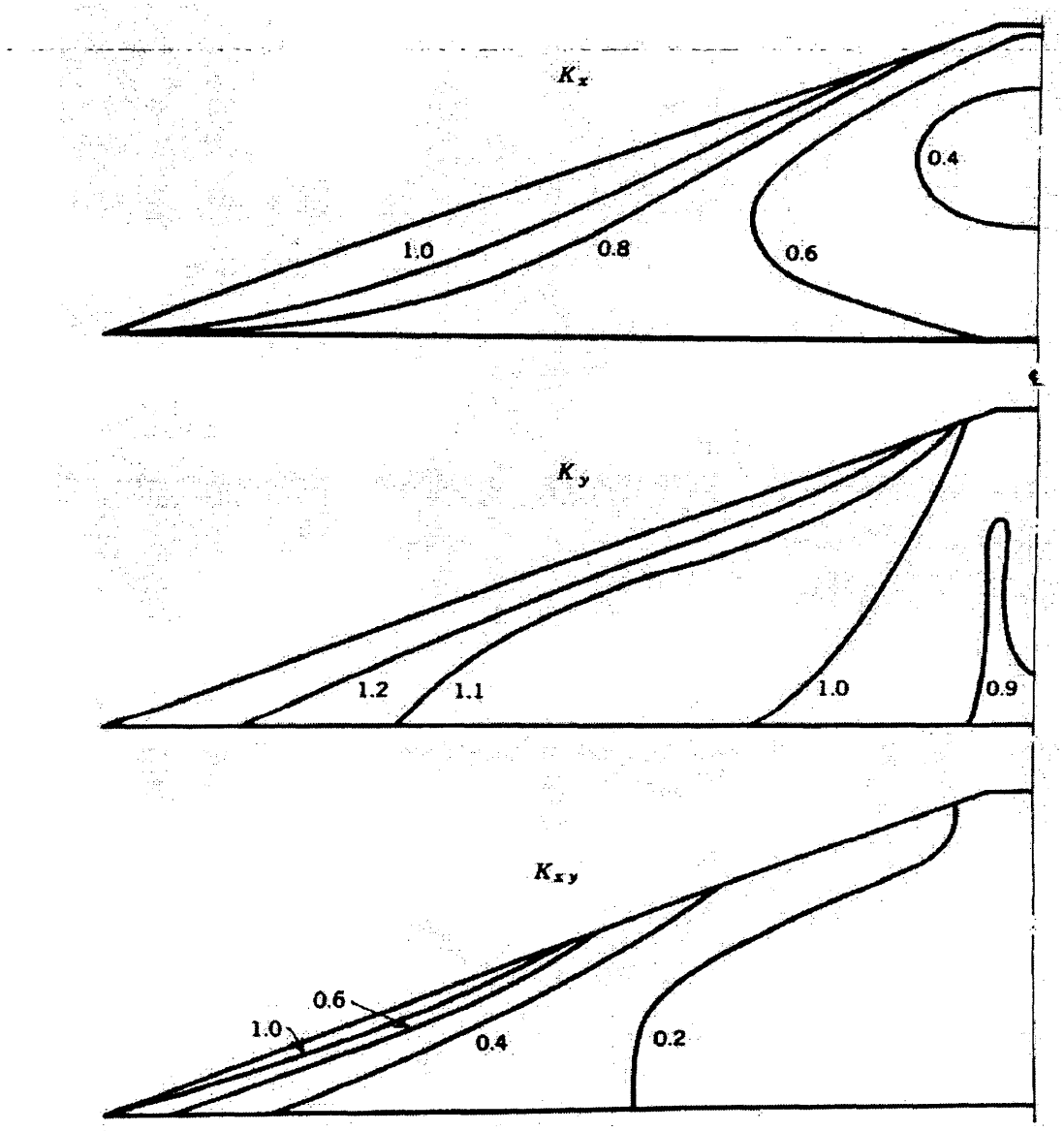

Figure 5-3: Clough and Woodward's Stress Factor Contours, K: Incremental Construction of Standard Dam.

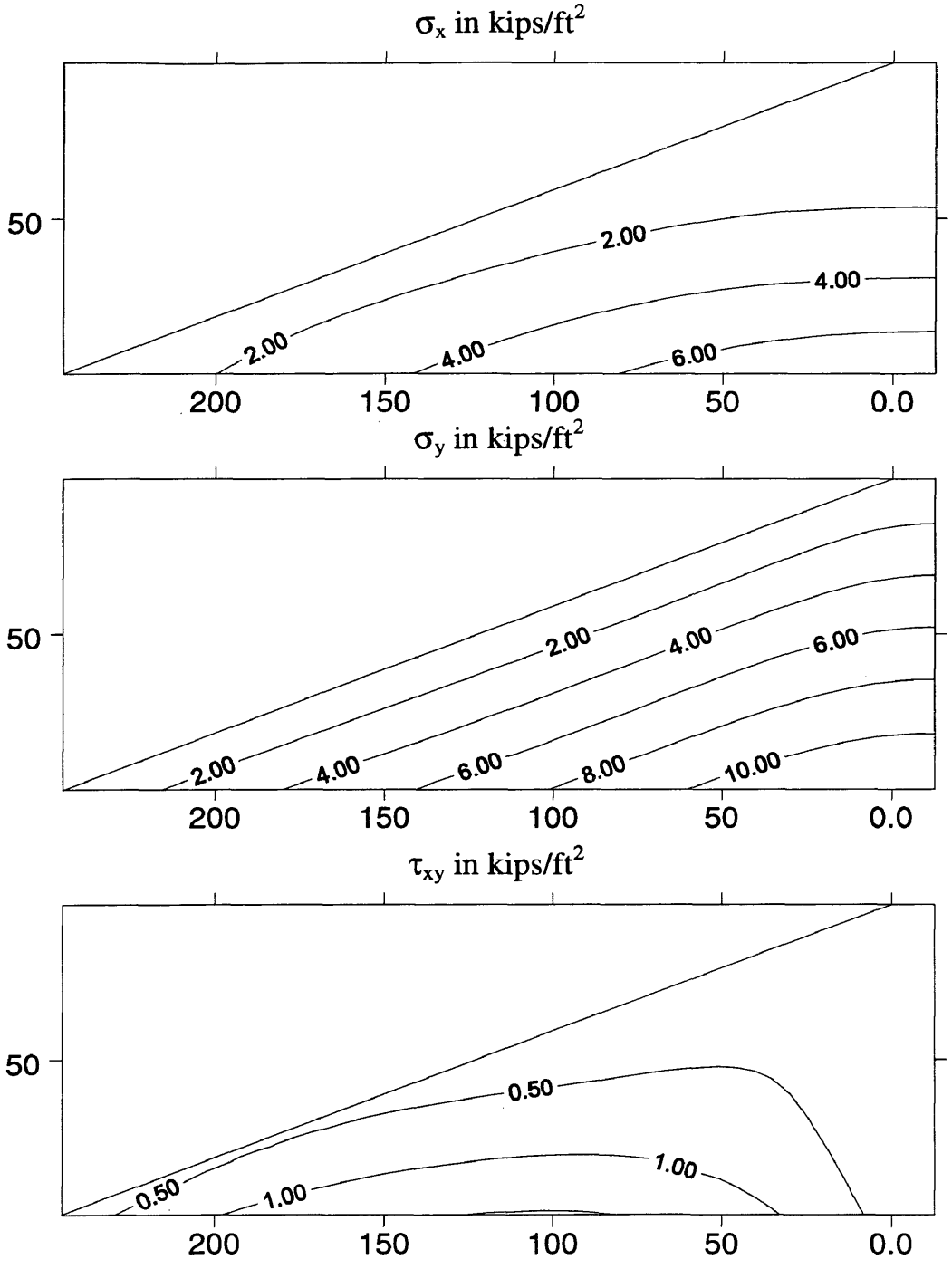

Figure 5-4: Stress Contours for Clough and Woodward/s "Standard Dam" as Determined by the Finite Element Method Used for the Current Study

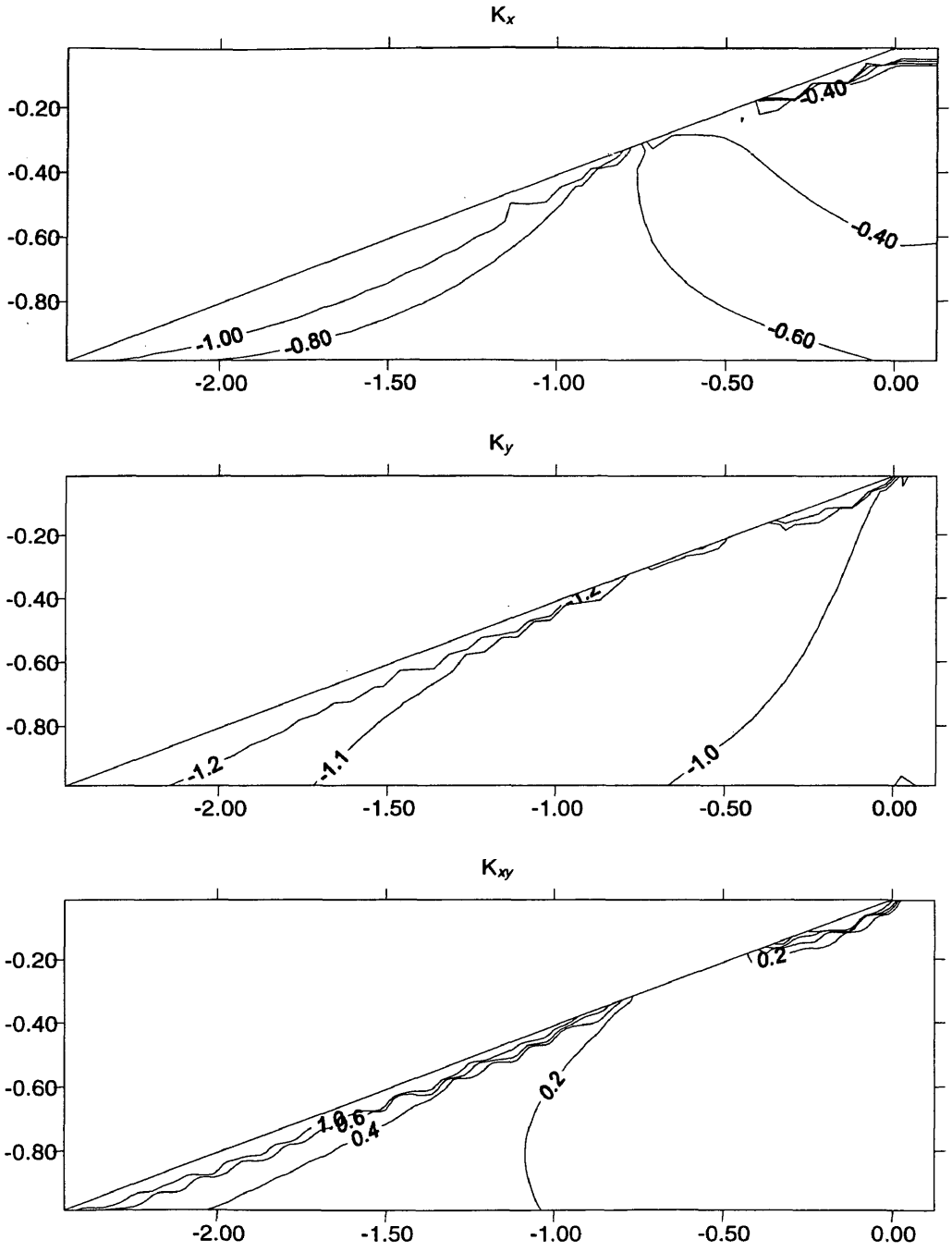

Figure 5-5: Stress Factor Contours for Clough and Woodward's "Standard Dam" as Determined by the Finite Element Method Used for the Current Study

for stress to determine the analogous values for any embankment. For completeness, an abridged form of the additional multiplication factors table is included in Figure 5-6.

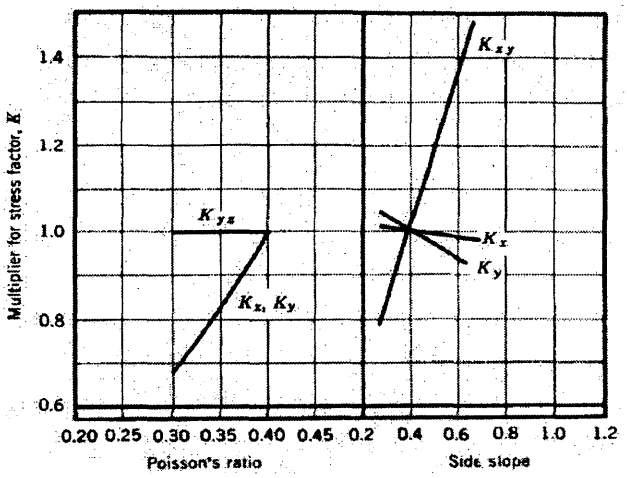

Figure 5-6: Clough and Woodward's Multipliers for the Stress Factors, K

These researchers point out that similitude exists between stresses and size and material density of embankments but that Poisson's ratio does not share this quality, thus the necessity to chart their multiplying factors. They state that this method of representing stresses is more convenient for some purposes, but do not elaborate.

The normalization methods discussed in the following subsections utilize constant factors, which seem to lend themselves to more intuitive and simple usage.

5.2 Poulos, Booker and Ring

Poulos, Booker and Ring (1972) present solutions for embankment deformations using a simplified calculation method that does not require the use of a computer. (Figure 5-7 illustrates the geometry adopted by these researchers.) However, as they state openly, once the slope reaches a certain size (h/H>0.5), finite element analysis should be used because while a slope's dimensions remain below this limit, the deformations are primarily vertical. Their method may be used for all slopes as quick preliminary calculative tools.

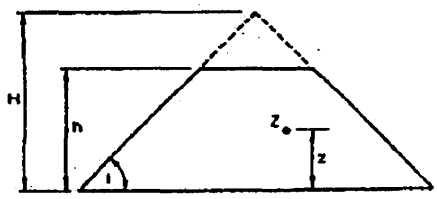

Figure 5-7: Poulos, Booker and Ring's Standard Embankment Geometry

While Poulos *et al* have extended their method to include embankments on flexible foundations as well as those with non-homogeneous properties, their results for embankments on rough rigid bases are referred to herein.

These investigators use a stress-normalization distinct from Clough and Woodward's. Here, they divide the stress by the unit weight of the soil and by the maximum possible height (H) of the slope.

5.3 Savage and Denlinger

Similar to Poulos *et al*, Savage and Denlinger use a constant divisor for their stress-normalization procedure: $\sigma/\gamma b$, where γ is the unit weight of the soil and b is the height of the slope; Figure 5-8 shows the geometric nomenclature. This is the method of normalization used for the remainder of the work done for this research.

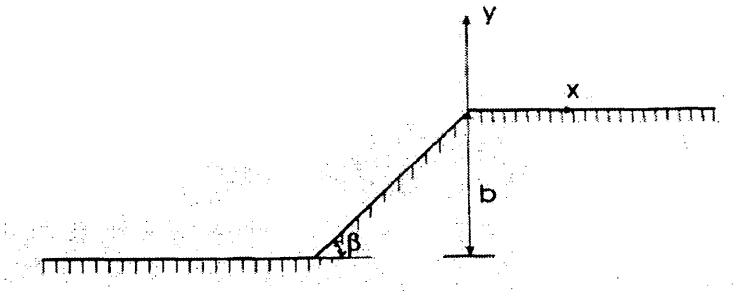

Finite slope of height b. The x, y-coordinate system and the slope angle β are also shown.

Figure 5-8: Savage and Denlinger's Embankment Nomenclature

Section 6

VERIFICATION OF THE FINITE ELEMENT METHOD FOR APPLICATION TO ELASTIC PROBLEMS

The Boussinesq solution for point loads was developed in 1885 by Joseph Boussinesq and was further developed to solve problems involving other various loading possibilities including infinite strip loads. These analytical results are well known and accepted by geotechnical engineers. Hence, a simple verification of the finite element package used for this thesis is to compare Boussinesq stress contours obtained from analytic and finite element methods.

In order to overlay the finite element results with the analytic Boussinesq solutions, a FORTRAN program has been developed which produces data files with Boussinesq stresses that can be contoured by SURFER®. The finite element routine used is slightly different than that used for the bulk of this thesis; however, the principles are identical as it was also developed from Smith and Griffiths (1988). Listings of the codes for these finite element and analytic Boussinesq routines are included in Appendices D and E, respectively.

Figure 6-1, Figure 6-2, and Figure 6-3 show the analytic and finite element results for normal and shear stresses to be coincident, thus verifying the finite element method.

The departures of the finite element solution from the analytic at the extreme boundaries are artifacts of the boundary conditions imposed in the finite element set-up. The analytic solution assumes an elastic half-space, whereas the finite element analysis imposes rather arbitrary boundaries to the side and bottom of the domain. The former is not necessarily realistic, and the boundaries of the latter may be moved to correspond to a particular region as desired. The point here is to illustrate the coincidence of the finite element solution with a well-known and historically accepted solution.

The Boussinesq solutions presented here are for infinite strip load supporting a stress q having width B = 1.0. The tick marks along the axes of these diagrams represent 0.50 units, and the strip load, B, is centered at the 0^{th} position in the x-, or horizontal direction.

It should be noted that these solutions numerically coincide best as Poisson's ratio approaches a value of 0.5. This is especially apparent in the horizontal stress (σ_x) solution and somewhat so for the shear stresses (τ_{xy}) as should be intuitive, given the dependency of these stresses on Poisson's ratio. Figure 6-4 demonstrates this phenomenon by comparing the finite element solutions of σ_x with Poisson's ratio at 0.0 and at 0.499 with the analytic Boussinesq solution; similarly, Figure 6-5 compares corresponding solutions for τ_{xy}. Furthermore, the finite element boundaries contribute to the differences in the contours in the areas closer to the edges of the plots.

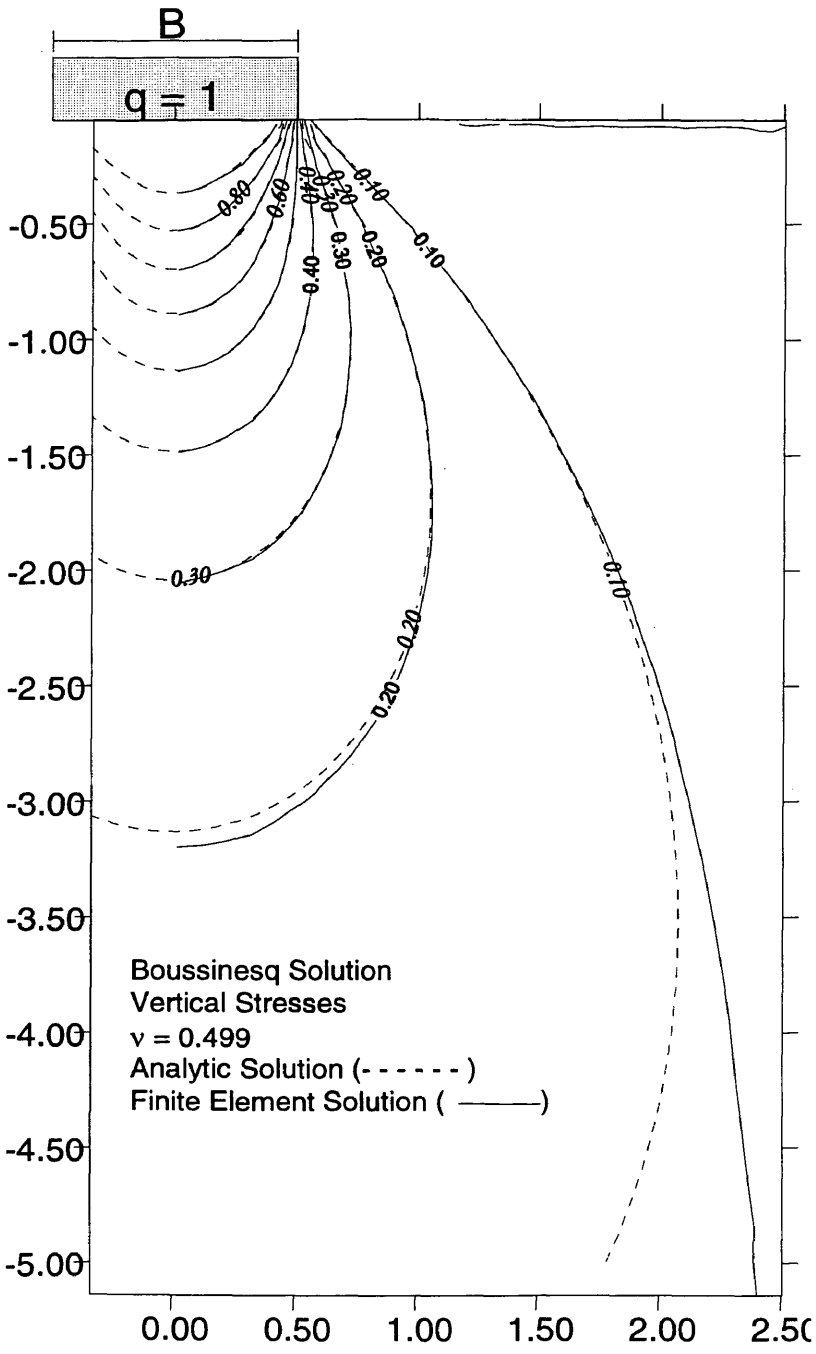

Figure 6-1 : Boussinesq Solution, σ_y/q

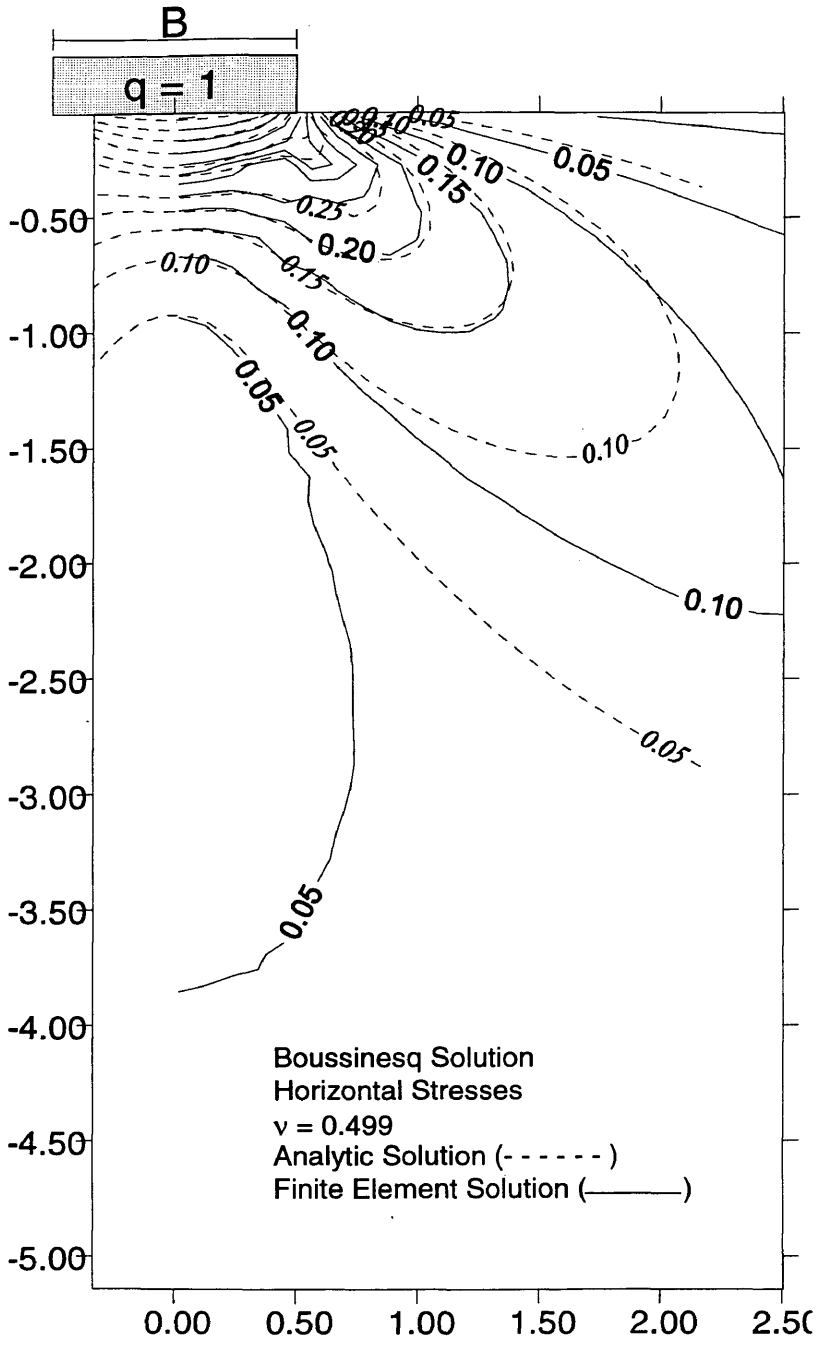

Figure 6-2: Boussinesq Solution, σ_x/q

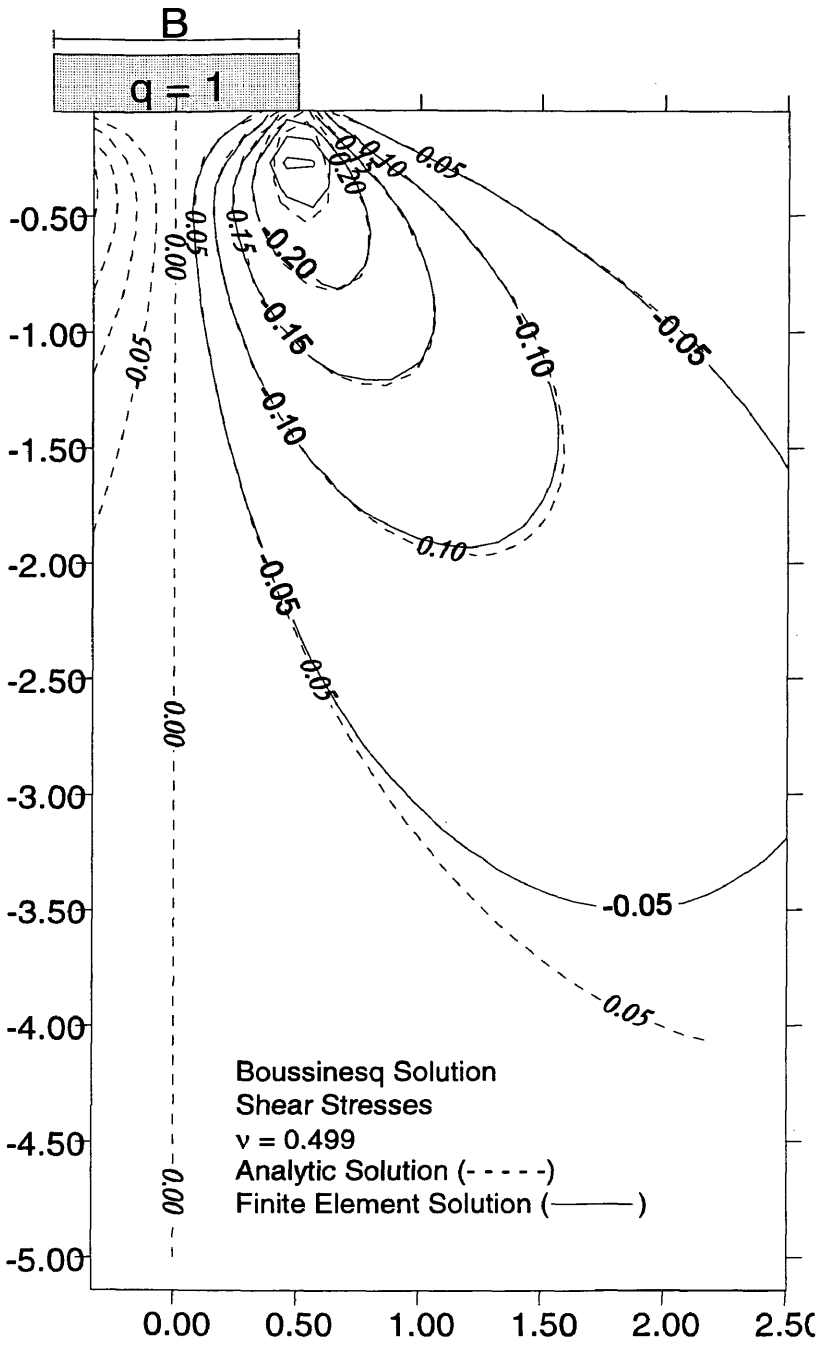

Figure 6-3: Boussinesq Solution, τ_{xy}/q

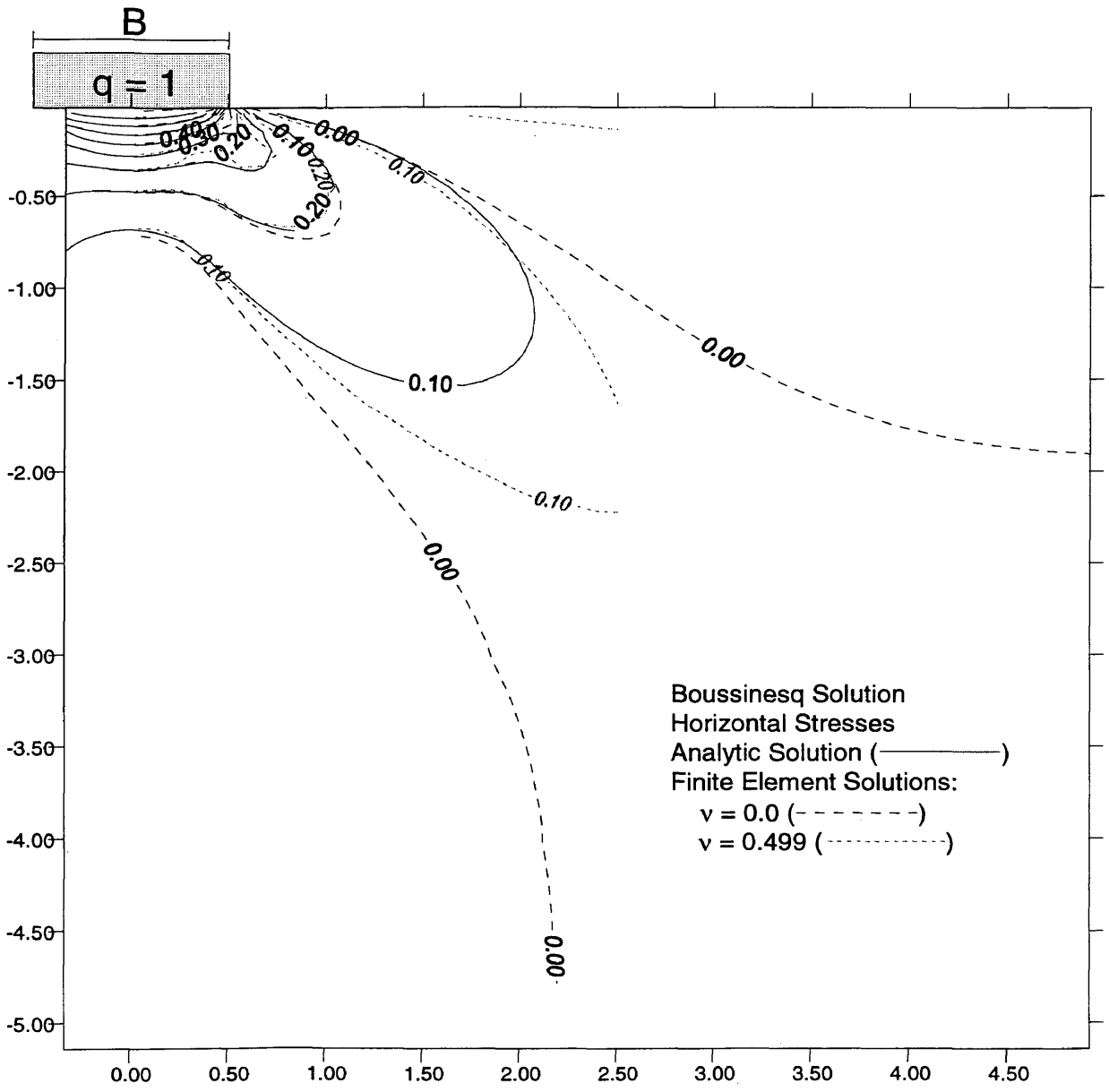

Figure 6-4: Boussinesq Solution, σ_x/Q, Effect of Poisson's Ratio

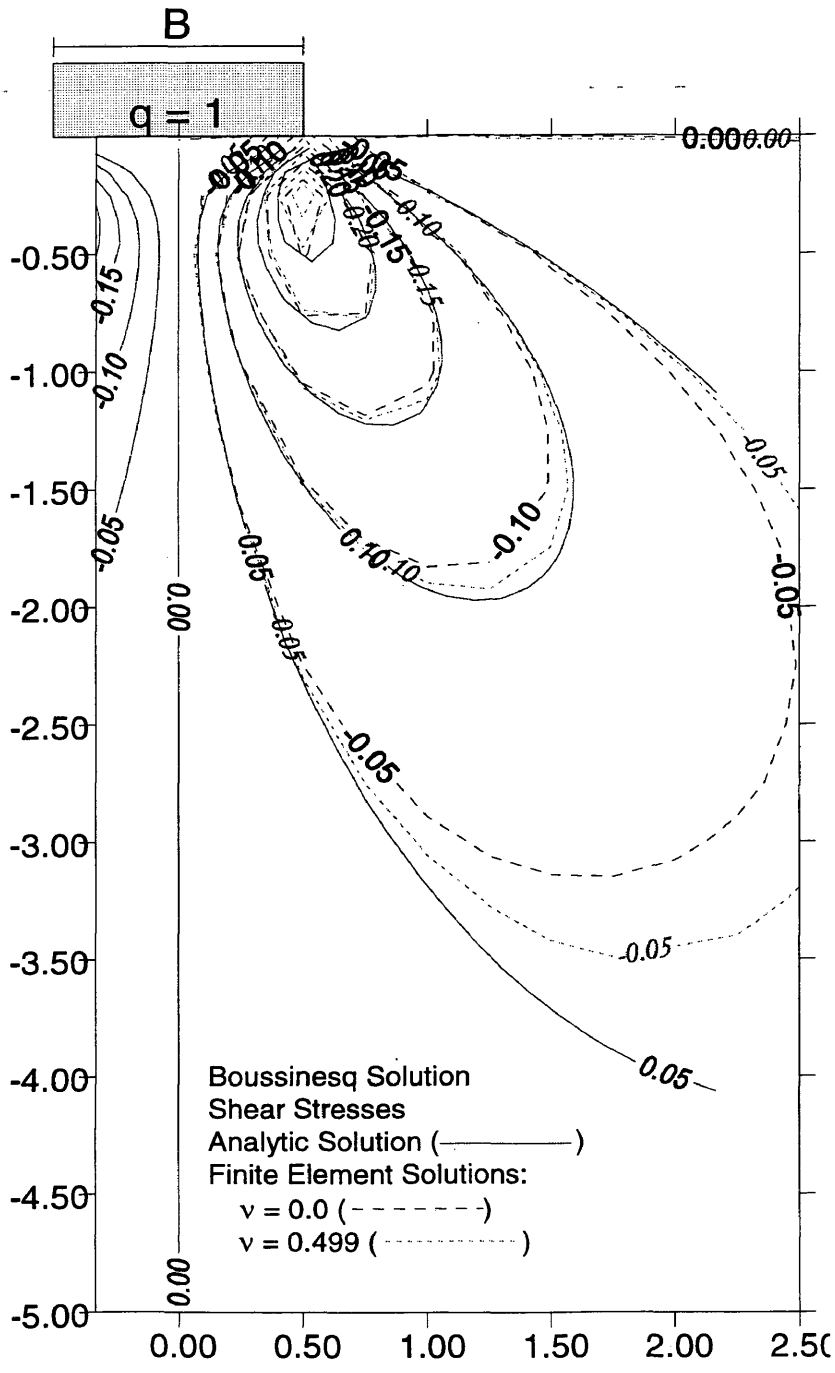

Figure 6-5: Boussinesq Solution, τ_{xy}, Effect of Poisson's Ratio

Section 7

INVESTIGATION OF MESH SIZE AND ELEMENT DENSITY EFFECTS

When using the finite element method, a balance must be struck between a reasonable description of the problem to be analyzed and computer time and space required to carry out the analysis. The mesh size refers to the placement of the mesh boundaries with respect to the structure under study, relating directly to its faithful representation. The density of elements that make up a mesh affects the amount of detail the solution can yield. The number of elements also define the computer requirements of the problem.

7.1 Mesh Size

In their paper describing the finite element analysis of an earth dam, De Wet and Hugo (1988) note some apparent boundary effects and explain them as their finite element program's[1] possible inability to model shear displacement at the boundary correctly. This correctly appreciates a potential weakness of modelling geotechnical

[1] FEADAM, developed by J. M. Duncan, K. S. Wong and Y. Ozawa for finite element analysis of dams and incorporating a hyperbolic model derived by J. M. Duncan and C. Y Chang.

structures. However, there are some important differences between the structure studied and reviewed by De Wet and Hugo and that used for the current research. The most relevant to this work, is that the boundary that they were modelling was between the dam material and the natural rock versus the assumption that the left and right boundaries used for the current work do not coincide with material changes. Therefore, the problems incurred in the joining of dissimilar materials are eliminated herein.

Incidentally, it is possible to affect similar contour deflections at the vertical boundaries simply by varying the Delauney triangulation point estimation grid size in the contouring program only, without changes to the finite element properties. This is yet further evidence that experimentation with graphics packages is strongly warranted.

In order to test the effects of mesh sizes, four meshes with equivalent element spacing for 15°, 45°, and 85° slopes have been used in the finite element program. The variables used in these meshes can be found in the Table in Appendix F along with graphical representations of the four mesh sizes. The "small" mesh is compared to a "deep/narrow" mesh, which is the same width as the small mesh but the lower boundary is extended. The small mesh is similarly compared to a "wide/shallow" mesh whose lower boundary coincides with that of the small mesh but the left boundary is extended. Finally, the coincident effects of depth and width are investigated in the comparison of the small mesh and "large" mesh, the latter of which has lower and left boundaries corresponding to the deep/narrow and wide/shallow meshes respectively. In order to

maintain congruity of the embankment geometries (e.g. h/H^2, after Poulos *et al*, 1972), the width behind the slope (the position of the centerline, or right-hand boundary) has not been altered.

The mesh size has no effect on vertical stress, as indeed it should not under simple gravity loading. Therefore, σ_y is considered a trivial case and is not further discussed in this section. In contrast, σ_x and τ_{xy} do demonstrate some effects due to the mesh extents. Their results, illustrated in Figure 7-1 through Figure 7-6, will be described forthwith.

7.1.1 Mesh Width Effects on σ_x

Horizontal stresses in the wider mesh (please refer to Figure 7-1) coincide well with those in the small mesh in the central and rear regions which is expected given that there are no changes in this area of the mesh. The variation in the front region, however, is quite interesting and depends subtly on Poisson's ratio. For the Poisson's ratios of 0.15 and 0.25, the horizontal stress is slightly greater in the wider mesh down to a depth just beyond 2 units, where the contours coincide exactly. Below this point, the horizontal stresses take on increasingly lower values with the wider mesh. The maximum difference in this example is approximately ± 0.05 for Poisson's ratios of 0.15 and 0.25. In the case where Poisson's ratio equals 0.45, the horizontal stresses are slightly smaller

[2] This ratio will be discussed in more detail in a later section.

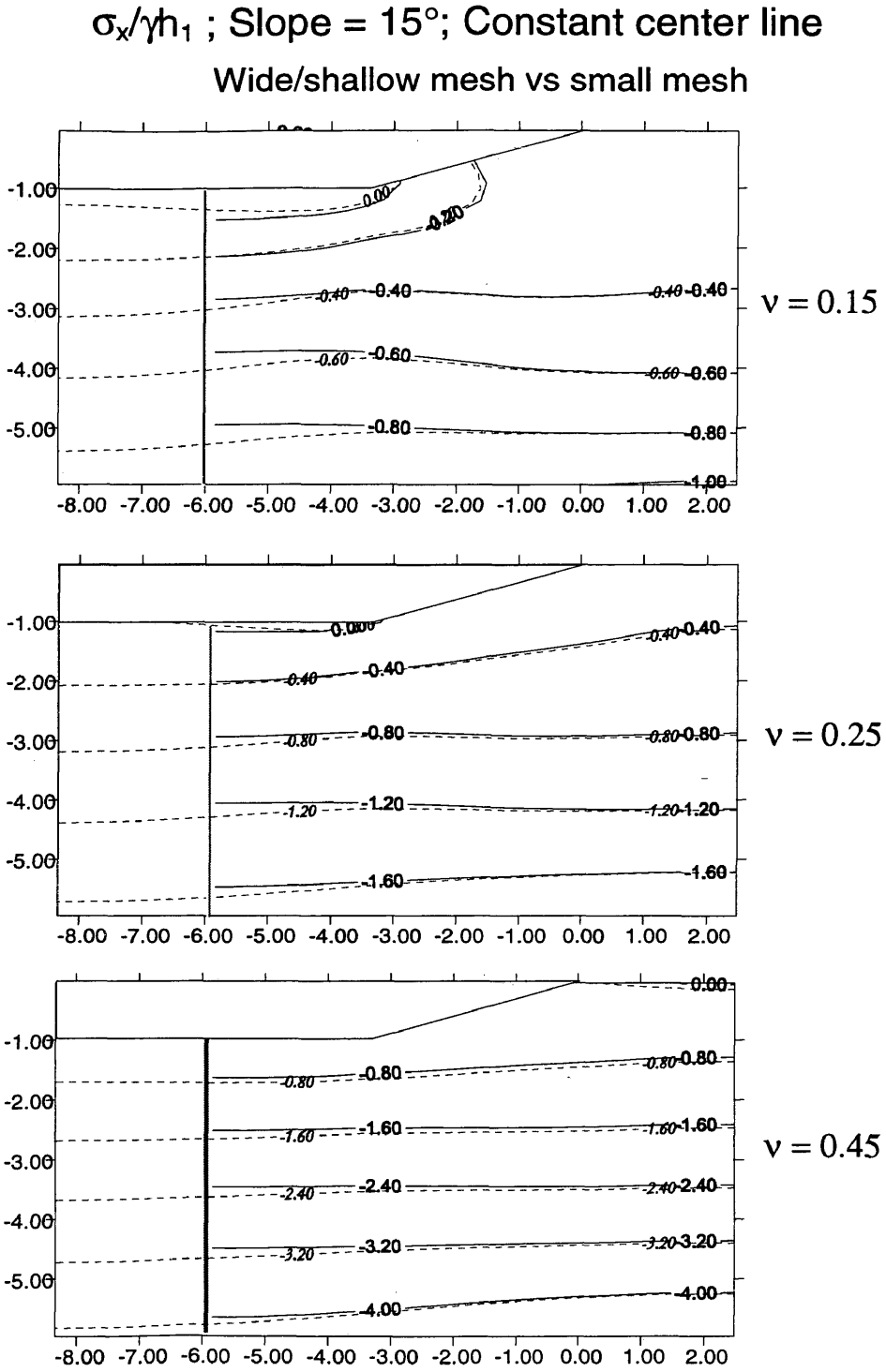

Figure 7-1: Finite Element Mesh Width Effects on Horizontal Stress

for the wider mesh in all three regions and at all depths. The difference is greatest in the left region with a maximum of –0.13 at 3.5 units' depth (±0.08 near the upper and lower boundaries).

7.1.2 Mesh Depth Effects on σ_x

The horizontal stress results for the deep mesh, illustrated in Figure 7-2, also vary subtly with Poisson's ratio but much less so than do the wide mesh results. For all three Poisson's ratios, the contours between 3 and 4 units' depth coincide well between the two mesh sizes. Above this level, the horizontal stresses in the deep/narrow mesh are generally smaller in the front region and larger in the rear region, with the reverse being the case below 3-4 units' depth. The numeric differences are –0.05 and +0.07 for Poisson's ratio of 0.15; ±0.11 for Poisson's ratio of 0.25; and ±0.25 for Poisson's ratio equals 0.45.

7.1.3 Overall Mesh Size Effects on σ_x

The large mesh versus small mesh diagrams, Figure 7-3, illustrate the combined effects of depth and width on horizontal stress and, as expected, yield virtually the superposition of the wider and deeper meshes. Overall, the effects of depth tend to be more apparent than those of width, particularly in the rear region, which is not affected by the width change. Generally speaking, the mesh effect, be it in width or depth, is quite

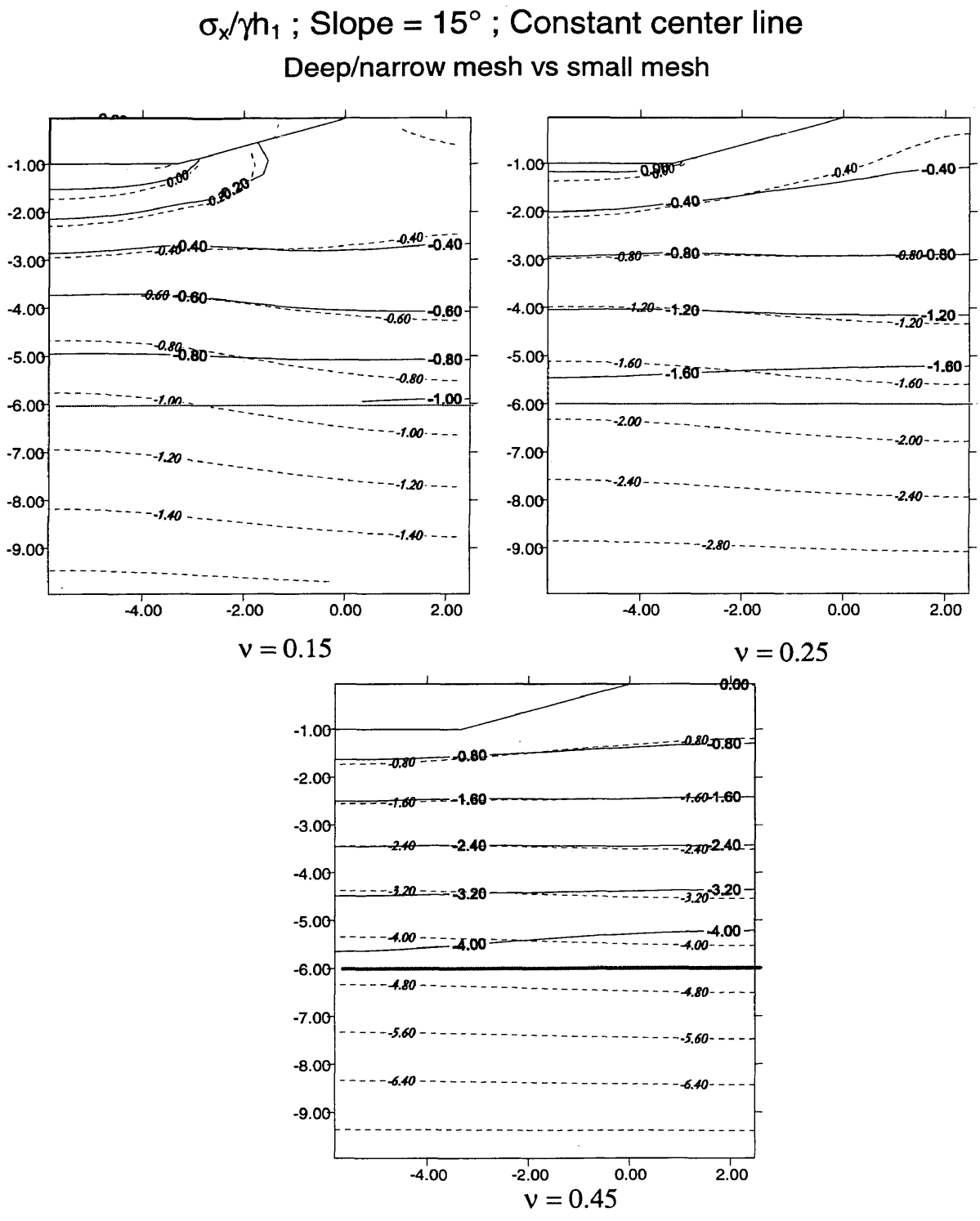

Figure 7-2: Finite Element Mesh Depth Effects on Horizontal Stress

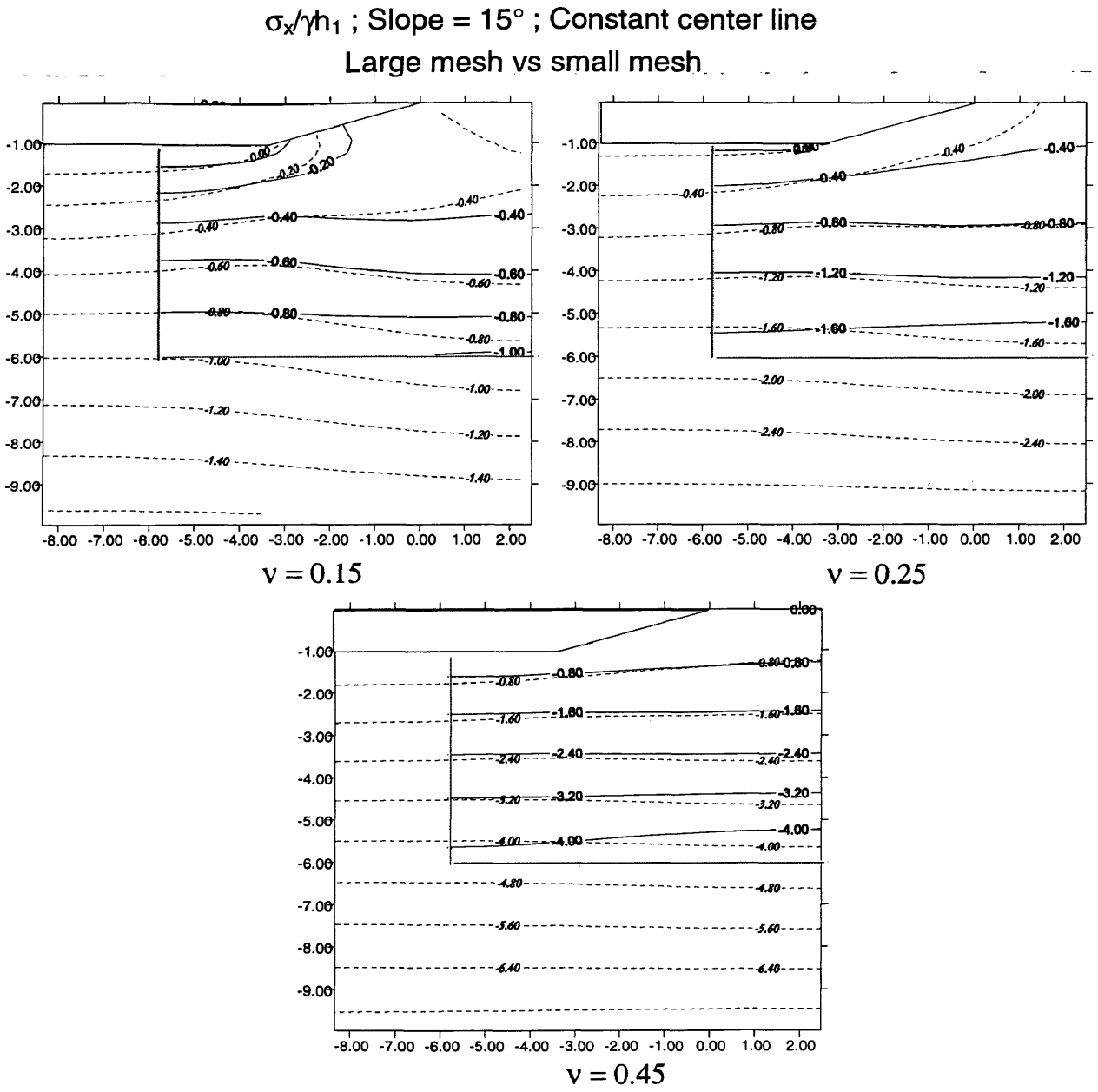

Figure 7-3: Finite Element Mesh Overall Size Effects on Horizontal Stress

modest.

7.1.4 . Mesh Width Effects on τ_{xy}

The effects of finite element mesh width are illustrated in Figure 7-4. For all three Poisson's ratios tested, the shear stress contours are nearly exactly coincident down to about 2 units' depth with the shear stress for the Poisson's ratio equals 0.45 case being slightly smaller in the wider mesh. Below this level, especially in the front region, the contours are strongly affected by the left-hand boundary as they tend toward parallelism with the same.

7.1.5 Mesh Depth Effects on τ_{xy}

Mesh depth affects the shear stresses, as shown in Figure 7-5, whose contours coincide for both deep and small meshes only just below the toe of the slope at about 1.5 units' depth. The shear stresses are characterized by circular contours in the central region which, as the lower boundary is approached, "break" apart at the bottom center, leaving the "ends" to run down toward that boundary. Increasing the mesh depth thus increases the number of closed circular contours and seems to relax the stresses some such that contours of the same numerical value form larger contour circles in the deeper mesh. The foregoing commentary holds for all three Poisson's ratios tested.

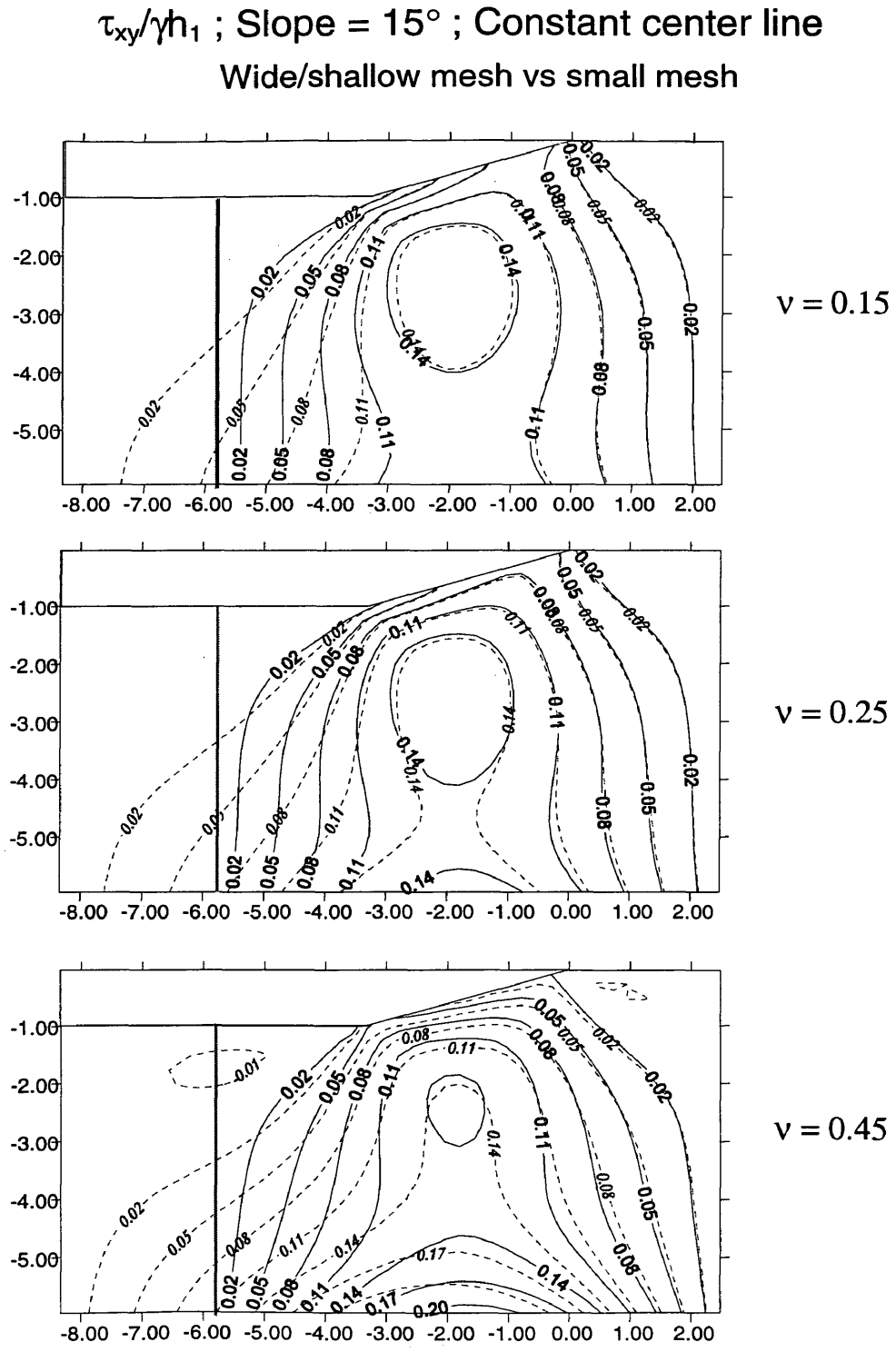

Figure 7-4: Finite Element Mesh Width Effects on Shear Stress

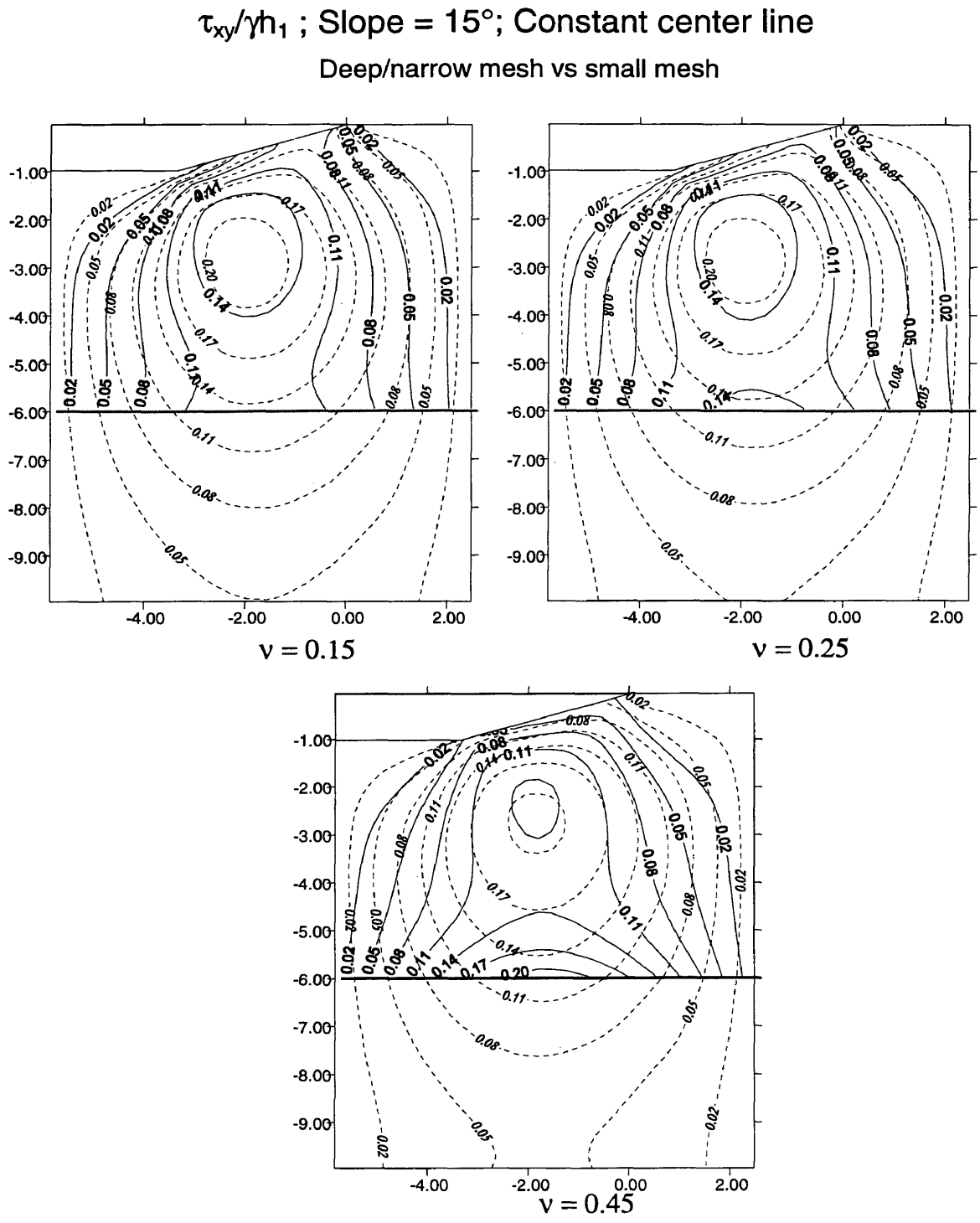

Figure 7-5: Finite Element Mesh Depth Effects on Shear Stress

7.1.6 Overall Mesh Size Effects on τ_{xy}

Again, the superposition of these effects is shown in large mesh versus small mesh diagrams (Figure 7-6). The overall effect suggests close likenesses between mesh size results exist only in the embankment region—that under and behind the slope down to just more than one unit of depth. From there to approximately 2.5 units' depth, the numeric difference is roughly 0.03. Beyond this level, the "bulbs" are so strongly influenced by the location of the lower boundary, a general characterization cannot be easily made. Nevertheless, the maximum differences are only on the order of 0.06.

7.1.7 Mesh Size Effects Summary

While heretofore the discussion has been with respect to the rather flat 15° slopes, as can be seen in similar diagrams (Appendix F), the mesh size effects are similar for all slope angles.

In essence, the maximum disparity in calculated stress values due to mesh sizes may be of an order significantly less than the strengths of embankment materials. Therefore, the variances imposed by mesh size are less of a concern than the creation of meshes that accurately depict the embankments under scrutiny.

In summary, the size of the finite element mesh does have an apparent affect upon the results they yield. However, reflecting upon the results presented by Clough and Woodward (1967), and Poulos *et al* (1972), the boundaries are not dissimilar from

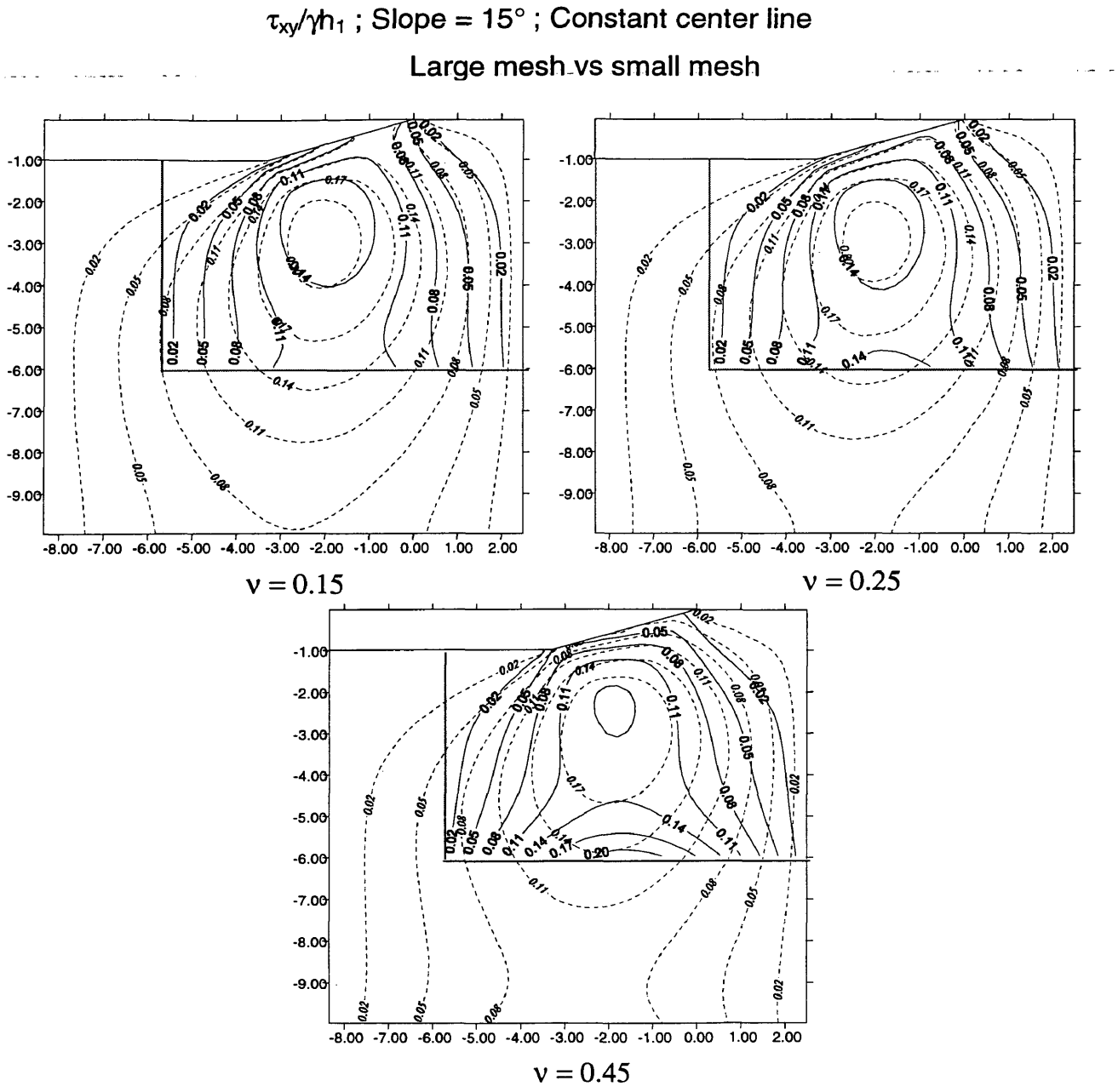

Figure 7-6: Finite Element Mesh Overall Effects on Shear Stress

physical confines such as "rough rigid" bases. The important issue is to use a mesh size that best represents the real problem. When the depth is such that it could be characterized as "infinite", judgment as to mesh size is up to the investigator and may depend on computer constraints. The point being that unless there are anomalies at depth, which may present issue with surface structures, a finite element mesh of extreme size in that direction is probably not necessary.

7.2 Element Density

Figure 7-7 illustrates effects of element density upon contoured stress results. The corresponding variable values used for this section are included in the table in Appendix G. Included in this appendix, and duplicated in Figure 7-8 below, are graphical representations of the meshes generated by these values.

None of the stresses are significantly affected by the element density. The shear stresses appear to be more sensitive than do the normal stresses; however, the magnitudes of shear stress are typically an order of magnitude smaller than the normal stresses. Accordingly, the element density may be chosen primarily in consideration of computer time and space. For example, De Wet and Hugo (1988) represented a lateral cross section of an embankment with a finite element mesh, which had approximately one element for

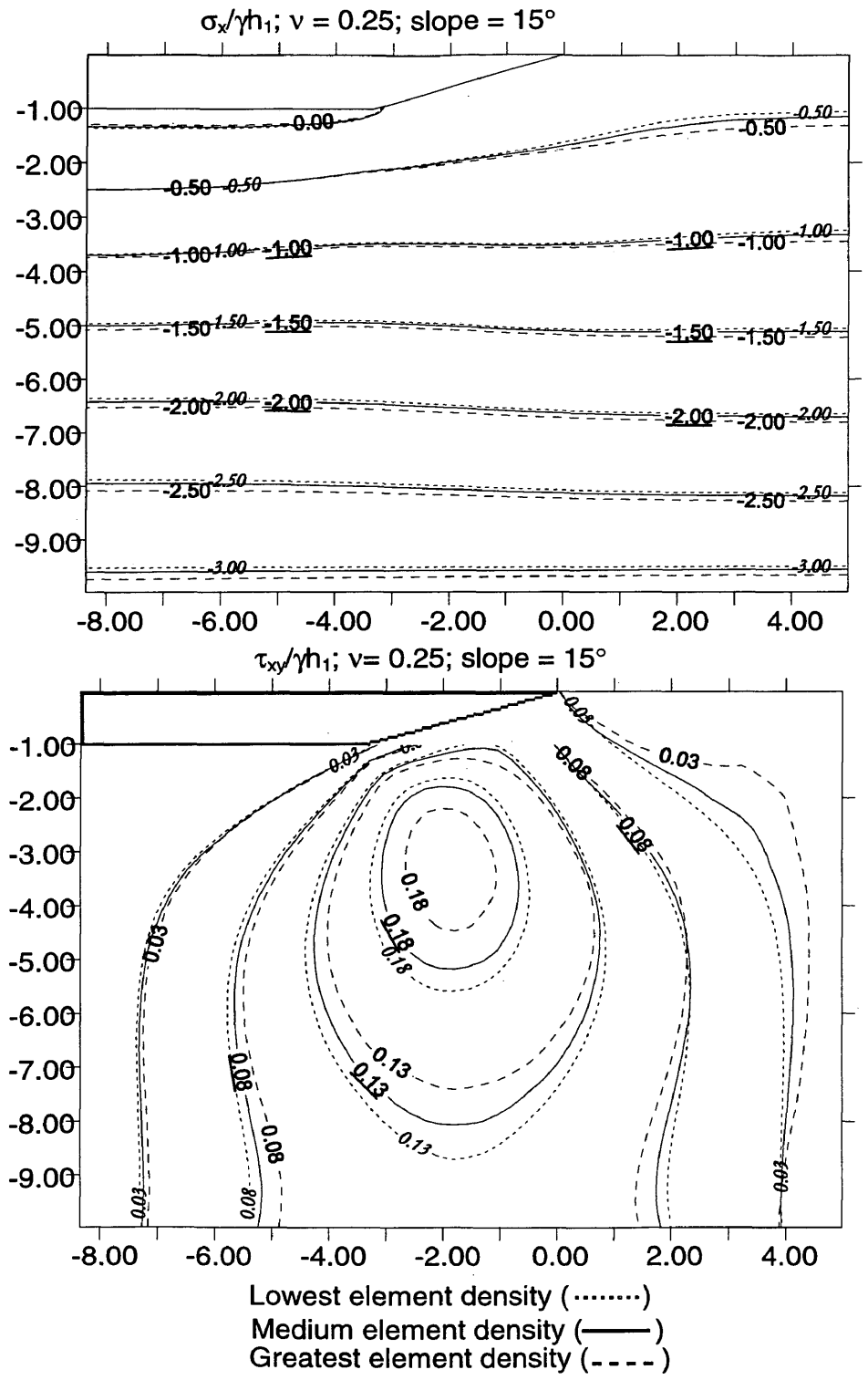

Figure 7-7: Element Density Effects on σ_x and τ_{xy}

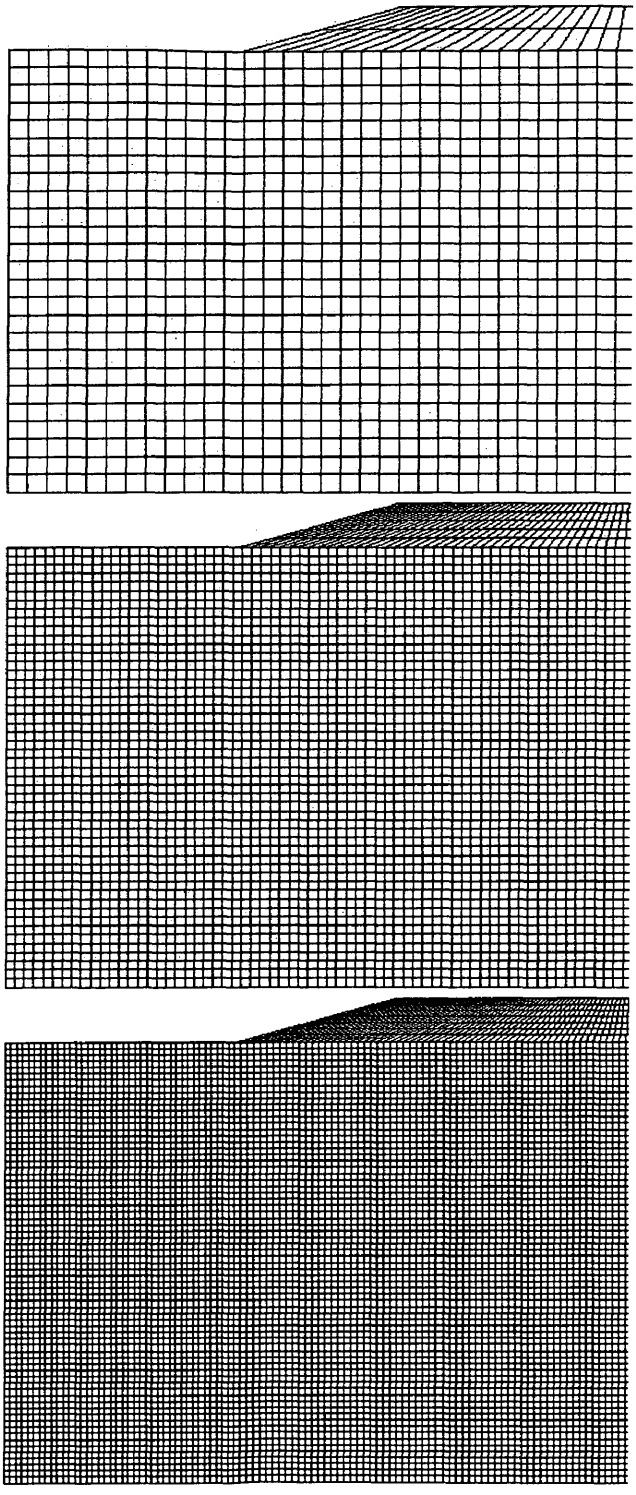

2.5 elements/unit^2

Lowest element density mesh

5.0 elements/unit^2

Medium element density mesh

7.0 elements/unit^2

Greatest element density mesh

Figure 7-8: Examples of Element Density Variants

each square unit[3]. The meshes used here have element densities averaging 2.5 elements per unit^2 for the sparsest meshes, 5 elements per unit^2 for the mid-dense meshes, and 7 elements per unit^2 for the densest meshes.

[3] The determination of the size of a "square unit" was made by correlating a non-dimensionalized version of De Wet and Hugo's embankment with the embankments represented in the current study.

Section 8

PARAMETRIC STUDY OF ELASTIC STRESSES: RESULTS AND DISCUSSION

It has been shown that the FE method is appropriate for the estimation of stresses in slopes. Furthermore, the impress of two assumptions required to use finite elements in this work were scrutinized and found to only mildly affects the calculated results. This section describes the influence of two intrinsic characteristics of slopes to the calculated stresses within the embankments.

8.1 Effects of Poisson's Ratio

The effects of Poisson's ratio on the stress contours for embankments of 90°, 45°, 30°, and 15° are investigated. Generally speaking, the effects are similar for all embankment grades. Figure 8-1, Figure 8-2 and Figure 8-3 illustrate these effects on horizontal, vertical and shear stresses for a slope angle of 45°. Similar illustrations for the other slope angles are included in Appendix I.

Regardless of the vicinity of the slope with respect to the underlying material, the horizontal stresses decrease significantly with depth. Figure 8-1 illustrates the "migration" of the $\sigma_x/\gamma h_1 = -1.0$ contour line as Poisson's Ratio is decreased from 0.49 to

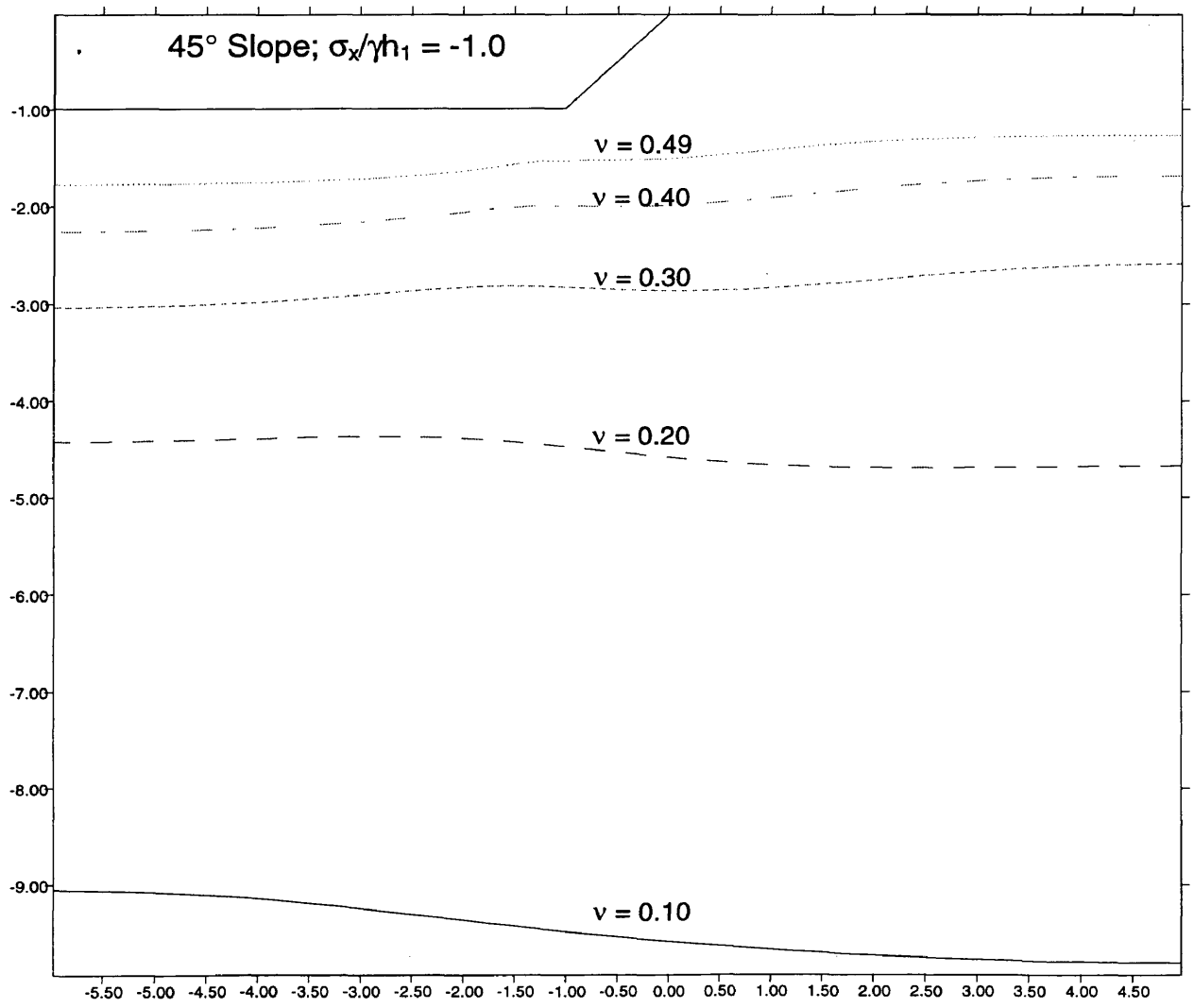

Figure 8-1: Effect of Poisson's Ratio on Horizontal Stress

0.10, thus graphically characterizing the inverse relationship between compressibility and horizontal stress.

The vertical stress does not change with Poisson's ratio in regions away from the embankment. However, directly under the slope, the greater Poisson's ratios tend to slightly depress the contours for $\sigma_y/\gamma h_1$, as illustrated by contours for Poisson's ratios of 0.10 and 0.49 in Figure 8-2.

The shear stress contours in general radiate from the surface of the slope and are affected by Poisson's ratio variations most greatly in the vertical region directly below the slope. As illustrated in Figure 8-3, increasing Poisson's ratios tend to increase τ_{xy} in a radial manner below the slope.

8.2 Effects of Slope Angle

Figure 8-4 shows stress contours for four slope angles (15°, 30°, 45°, and 90°) overlain such that the midpoint of each slope is aligned with that of the others. The Poisson's Ratio used in this demonstration is 0.30. This example reveals a distinct similarity among the various grades in stress patterns in the embankment and surrounding regions, suggesting that stresses proximal to the area of the slope region itself are of greatest importance when considering elastic failure mechanisms.

More detail with respect to the variation of stresses as grade changes is illustrated in the diagrams in Appendix I. Two distinct patterns evolve for both horizontal and shear

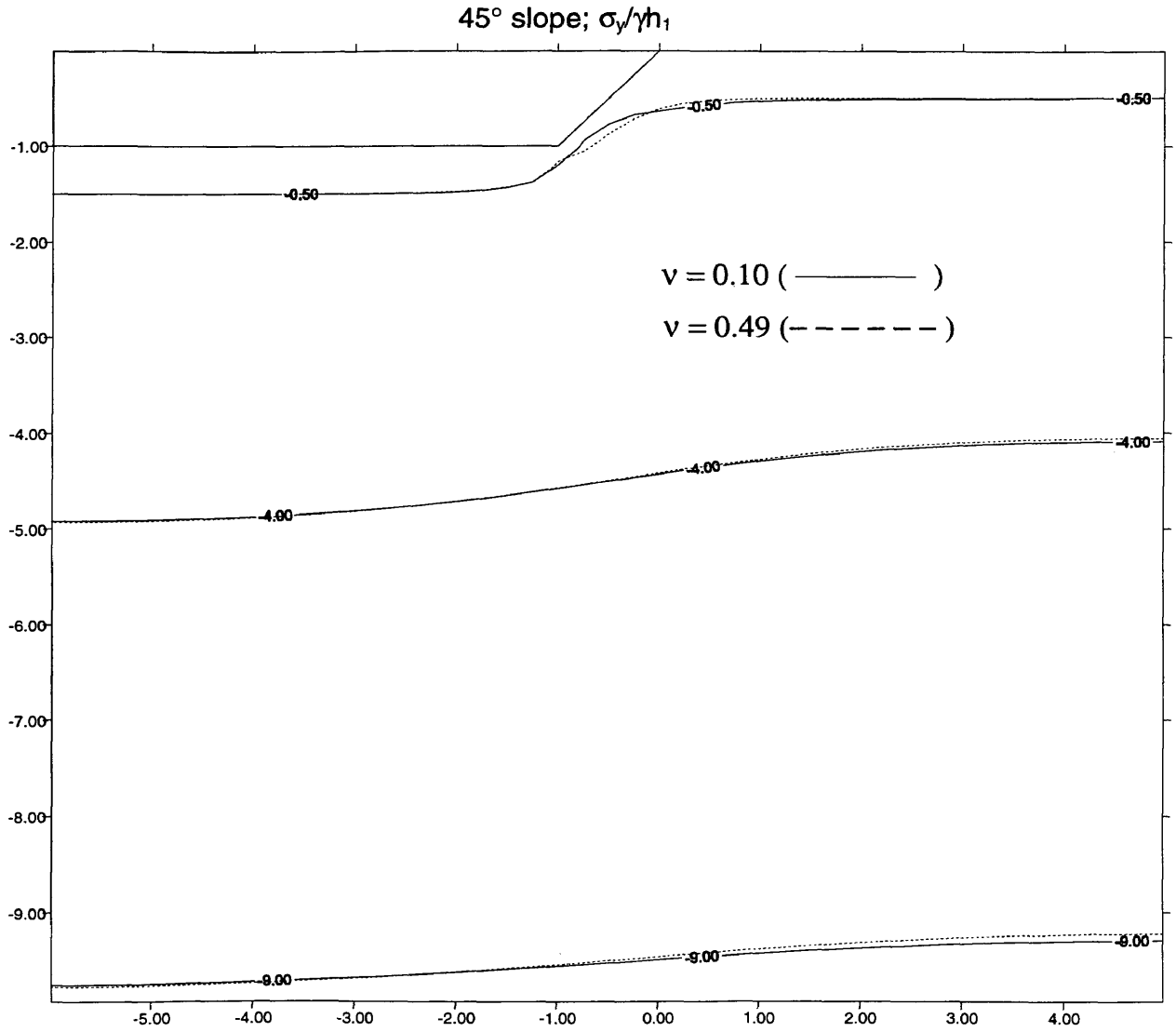

Figure 8-2: Effect of Poisson's Ratio on Vertical Stress

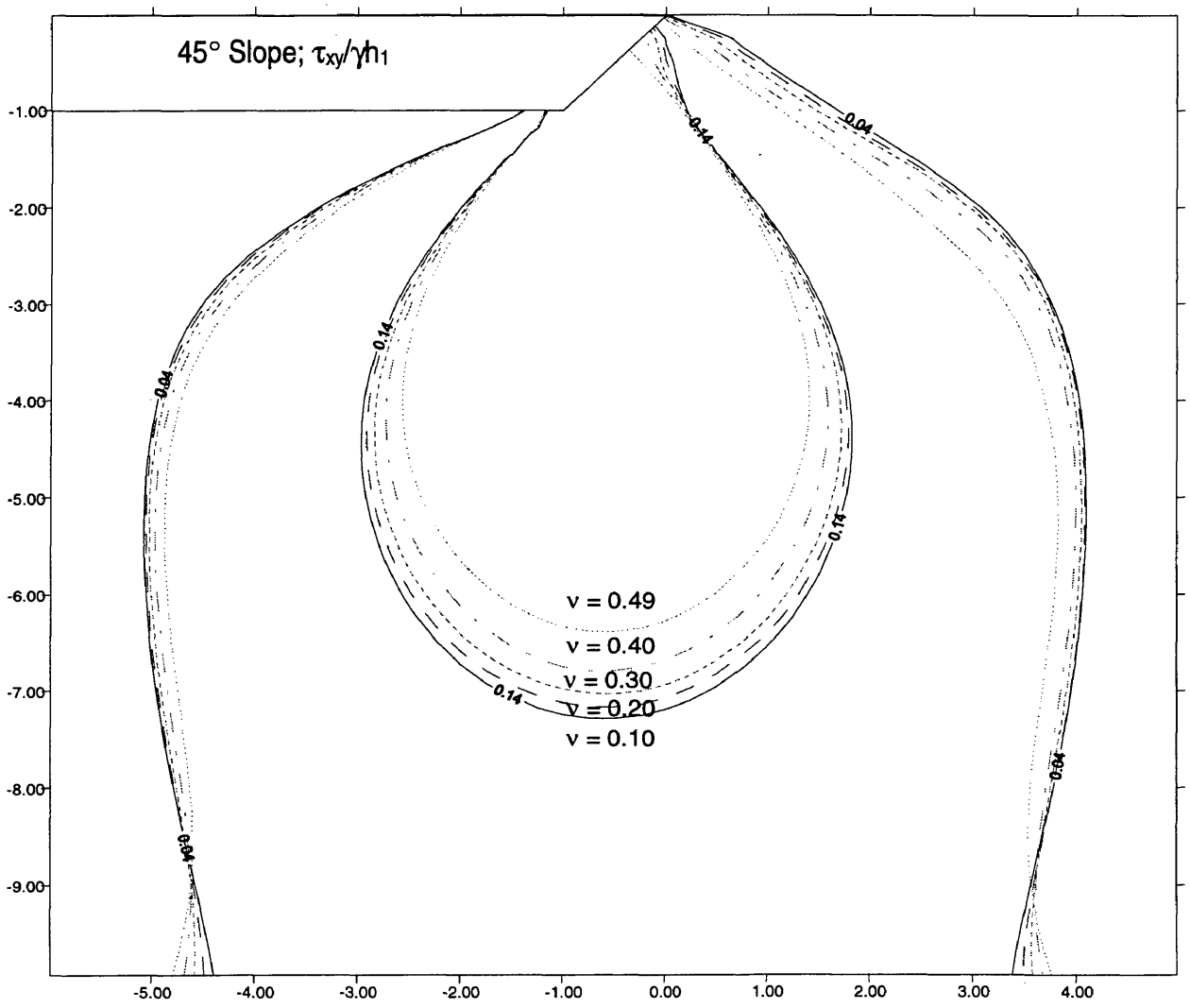

Figure 8-3: Effect of Poisson's Ratio on Shear Stress

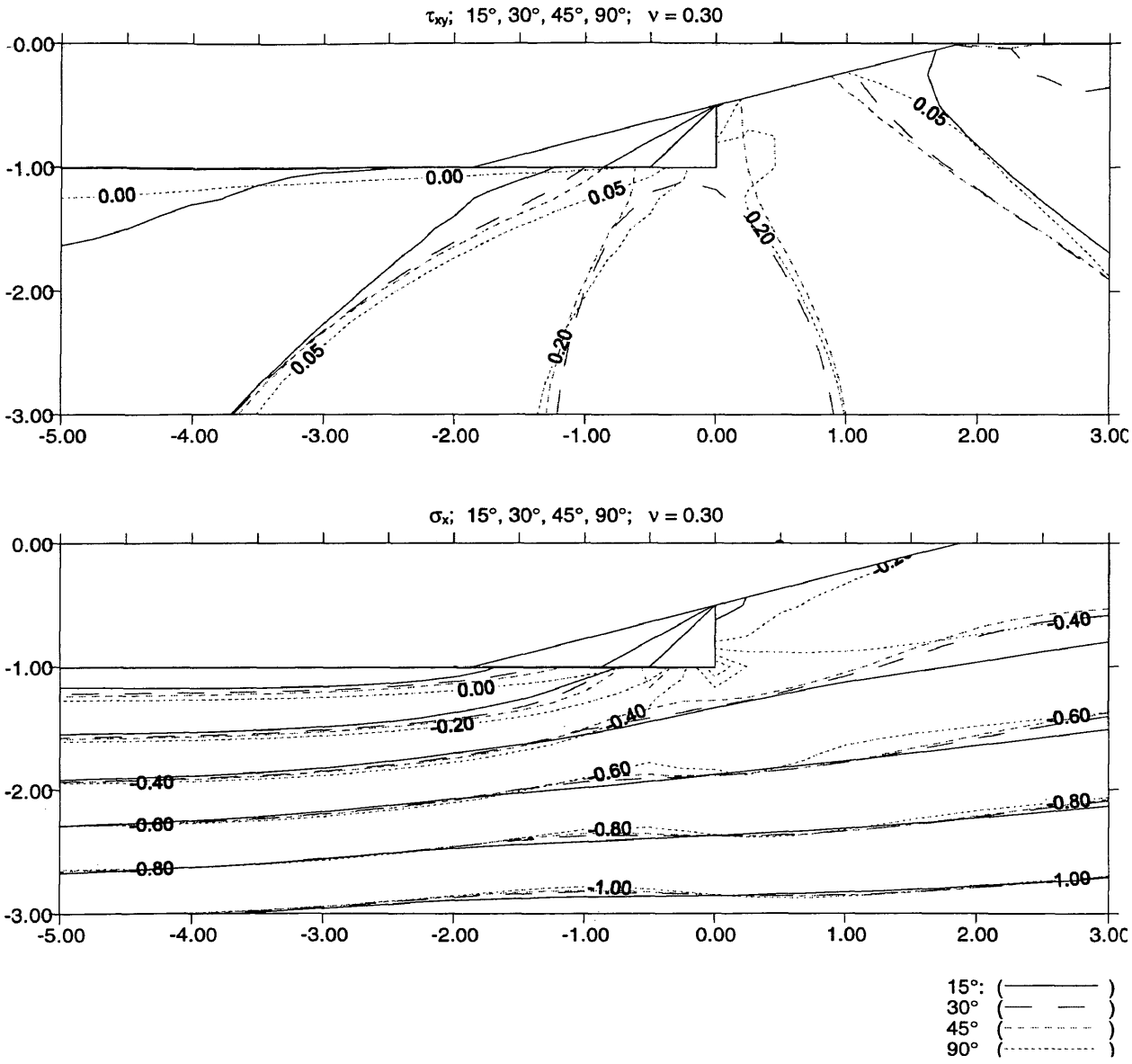

Figure 8-4: Effects of Slope Grade on Horizontal and Shear Stresses

stress as slope angle is increased. In both cases, the change from one pattern to another occurs between 35° and 45° slopes. The stress concentrations at the toes and crests do not appear in the 35° and flatter slopes. The shear stresses in the flatter slopes exhibit contours shaped like inverted bulbs, which rise toward the slope surface with increasing grade. When the slope angle reaches 45°, a combination of upright bulbs appear behind the lower half of the slope face and beneath the toe. As the angle further increases these latter bulbs rotate slightly in a clockwise fashion and demonstrate an increasing concentration of shearing stress in the region most proximal to these slope features. Figure 8-5 and Figure 8-6 show the same four slopes (as in Figure 8-4) and their respective shear and horizontal stresses individually with smaller contour intervals, serving to emphasize the contour pattern evolutions as grade increases.

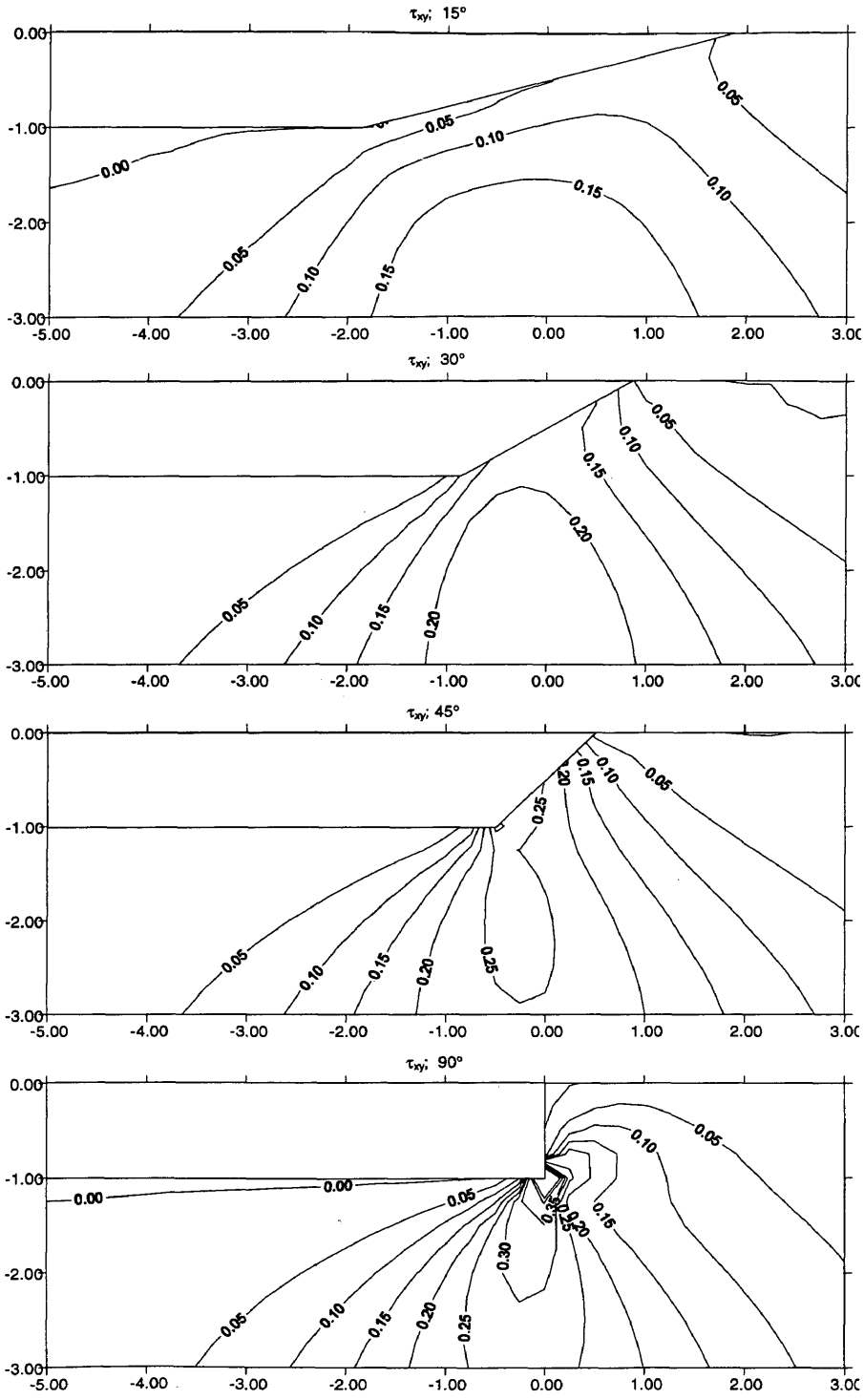

Figure 8-5: Shear Stresses in Various-Graded Slopes

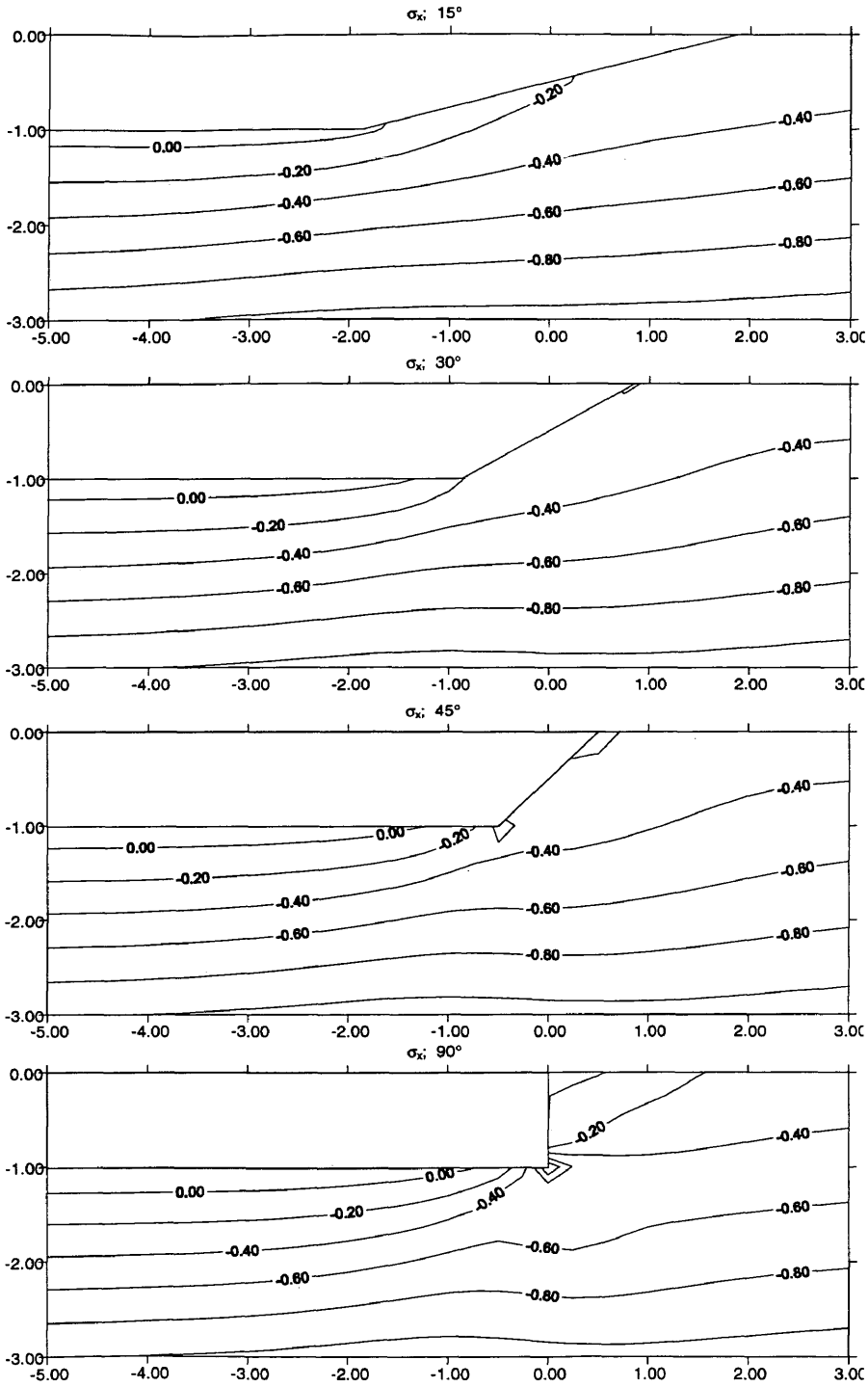

Figure 8-6: Horizontal Stresses in Various-Graded Slopes

Section 9

ELASTO-PLASTIC STRESS REDISTRIBUTION

This section departs from the focus upon linear-elastic responses in the soils of slopes. Elastic analyses often lead to generation of stresses that violate the Mohr-Coulomb failure criterion, and looks at what occurs mathematically during the stress-redistribution, or equilibration phase of the program FE-EMB1.f, written by D.V. Griffiths (1996), and based on Program 6.1 in his book (Smith and Griffiths, 1988). This finite element program is a more sophisticated model than the one used in earlier sections. It does not allow violation of the Mohr-Coulomb criterion and utilizes an iterative algorithm, based on visco-plasticity, which redistributes the stresses in a mesh until convergence or failure. Convergence indicates that the Mohr-Coulomb failure criterion has been met throughout the mesh and failure implies that convergence did not occur within a specified number of iterations for a given factor of safety. The factor of safety of a soil slope is the factor by which the original shear strength parameters are reduced such that the slope may be brought to the point of failure. Griffiths uses equations 9.1 and 9.2 for the factored shear strength parameters, c_f and ϕ_f in this program.

$$c_f = \frac{c}{FOS} \tag{9.1}$$

$$\phi_f = \arctan\left(\frac{\tan\phi}{FOS}\right) \tag{9.2}$$

Experiments were run using $\phi = 30°$, $c/\gamma h_1 = 0.30$, and $E = 1*10^5$ for a 45° embankment ($h_1 = s_1 = 2.0$). Figure 9-1 indicates that under these conditions, a factor of safety of 3.0 or greater cannot be achieved, but that factors of safety less than 3.0 can be. For this reason, four factors of safety (1.0, 1.5, 2.0, and 2.5) were run to convergence and a fifth (3.0) was run to failure. Table 9-1 lists the number of iterations for convergence to occur for each factor of safety. In all cases, the maximum number of iterations specified was 1000.

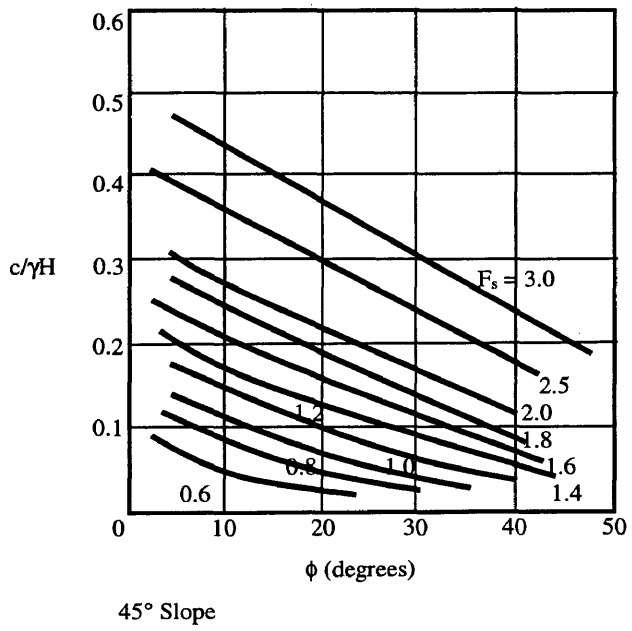

Figure 9-1: Contours of Equal Factors of Safety (after Singh, 1970)

Factor of Safety	Number of Iterations to Convergence
1.0	2
1.5	5
2.0	22
2.5	47
3.0	Failed

Table 9-1: Elasto-plastic Convergence for Specified Factors of Safety

The experiment using a factor of safety of 3.0 was run several times in order to obtain stress and displacement data throughout equilibration. The experiments using factors of safety less than 3.0 were run for comparison with qualities of the mid-run iterations for the FOS = 3.0 solution.

9.1 Mohr-Coulomb Failure Criterion

The graph below (Figure 9-2) illustrates the general pattern of convergence for all of the FOS experiments.

9.2 Influence of Stress Redistribution on Displacements

When gravity is "turned on" in the finite element program, the mesh deforms elastically and the stresses are then determined from this strain information. If Mohr-Coulomb failure criterion is violated, the stresses are redistributed around the region

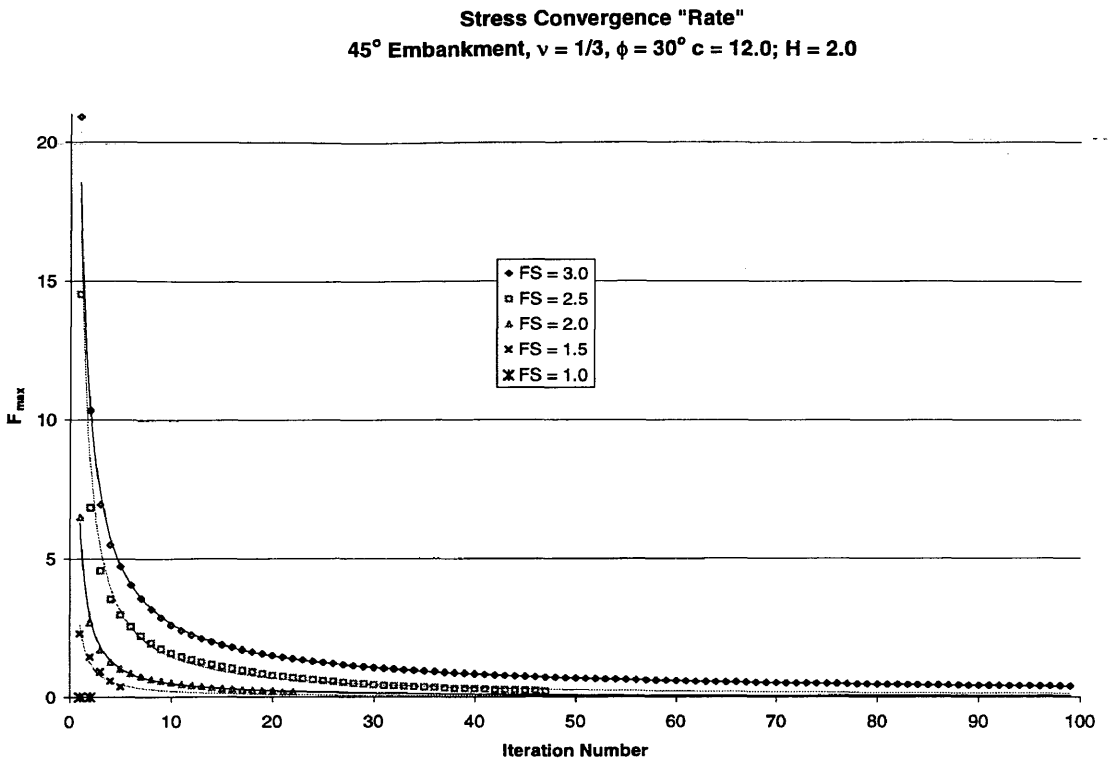

Figure 9-2: Elasto-plastic Stress Redistribution

containing the illegal stresses. This yields new deformation within the mesh. To illustrate these displacements, Figure 9-3 shows the original mesh, two of the interim meshes, and the final failed mesh for the FOS = 3.0 trial. Appendix J shows a more exhaustive series of the same experiment.

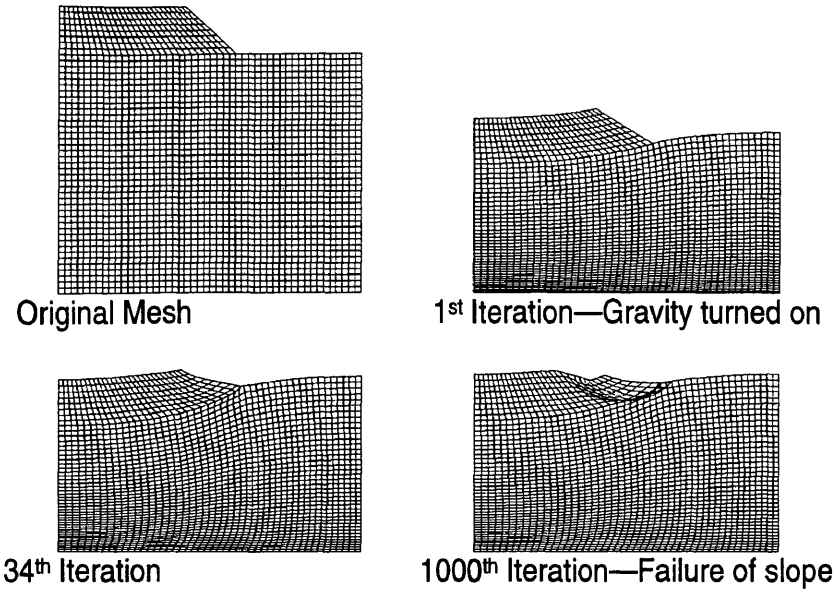

Figure 9-3: Displacements Due to Elasto-plastic Stress Redistribution

9.3 Limitations of the Linear Elastic Theory

The suitability of elastic theory for geotechnical problems was discussed in Section 2.3, above. Recall, that for 45° slopes with Poisson's Ratios less than 0.24, regions in the foundation appeared to violate the Mohr-Coulomb failure criterion (Figure 2-3). Indeed, when running the same slopes through the FE-EMB1 program, some stress redistributions do occur. Figure 9-4 and Figure 9-5 show the contrast between the elastic and elasto-plastic solutions for 45° slopes with Poisson's ratios of 0.20 and 0.23. These slopes required 11 and 7 iterations, respectively, to converge to a viable solution under the Mohr-Coulomb criterion.

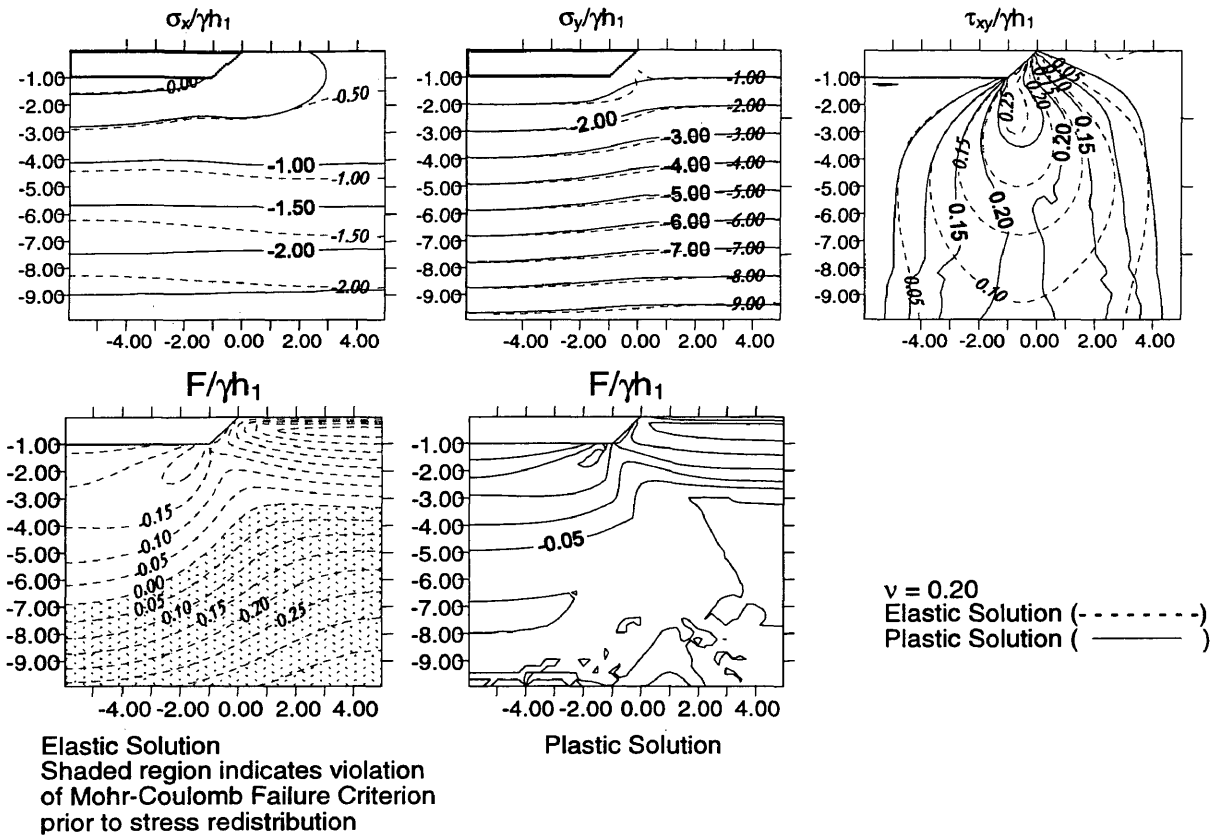

Figure 9-4: Elastic and Elasto-plastic Solutions for a 45° Slope with $\nu = 0.20$

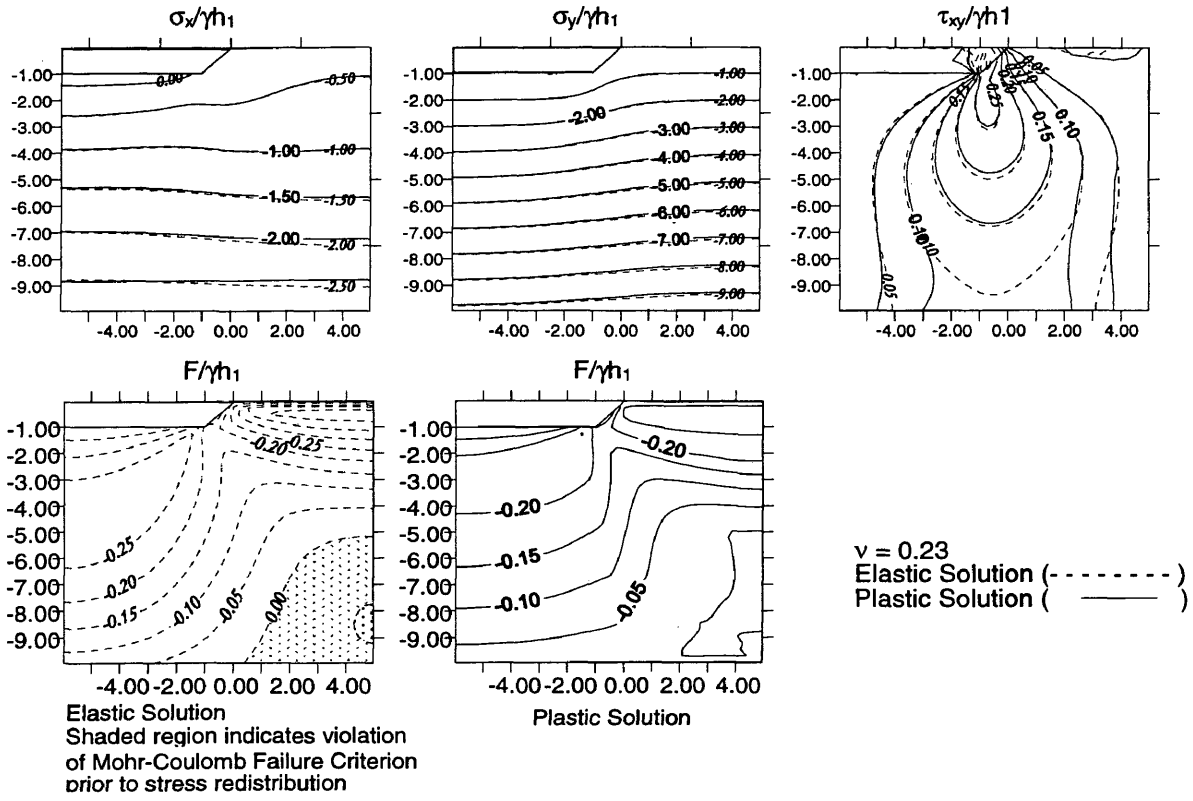

Figure 9-5: Elastic and Elasto-plastic Solutions for a 45° Slope with ν = 0.23

Figure 9-6 illustrates that for larger values of ν, the elastic solution is essentially equal to the solution that allows for plasticity because there is no violation of the Mohr-Coulomb criterion.

These final examples emphasize the stability of slopes in spite of a wide range of deformation. The deformed meshes of these embankments (and their foundations) make evident the effect of Poisson's ratio, or the compressibility, of geotechnical materials, see Figure 9-7. One aspect that is of interest here is the coincidence of a marginal failure of elastic theory with large deformations of the compressible material ($\nu = 0.20, 0.23$) versus the coupling of certain success of elastic theory associated with a fairly incompressible slope material ($\nu = 0.49$) (for $c/\gamma h = 0.30$ and $\phi = 30°$).

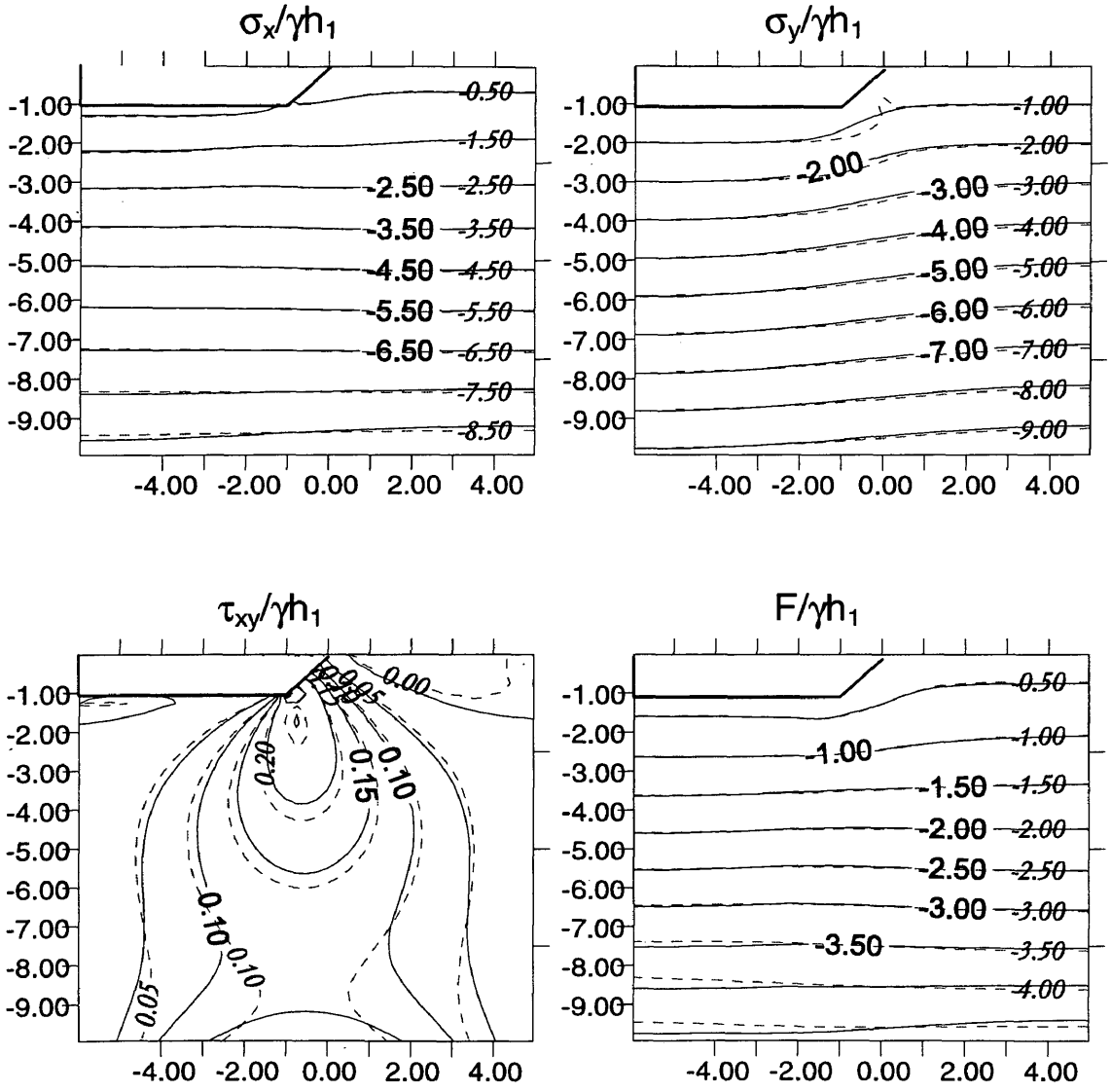

ν = 0.49
Elastic Solution (- - - - - -)
Plastic Solution (———)

Figure 9-6: Elastic and Elasto-plastic Solutions for a 45° Slope with ν = 0.49

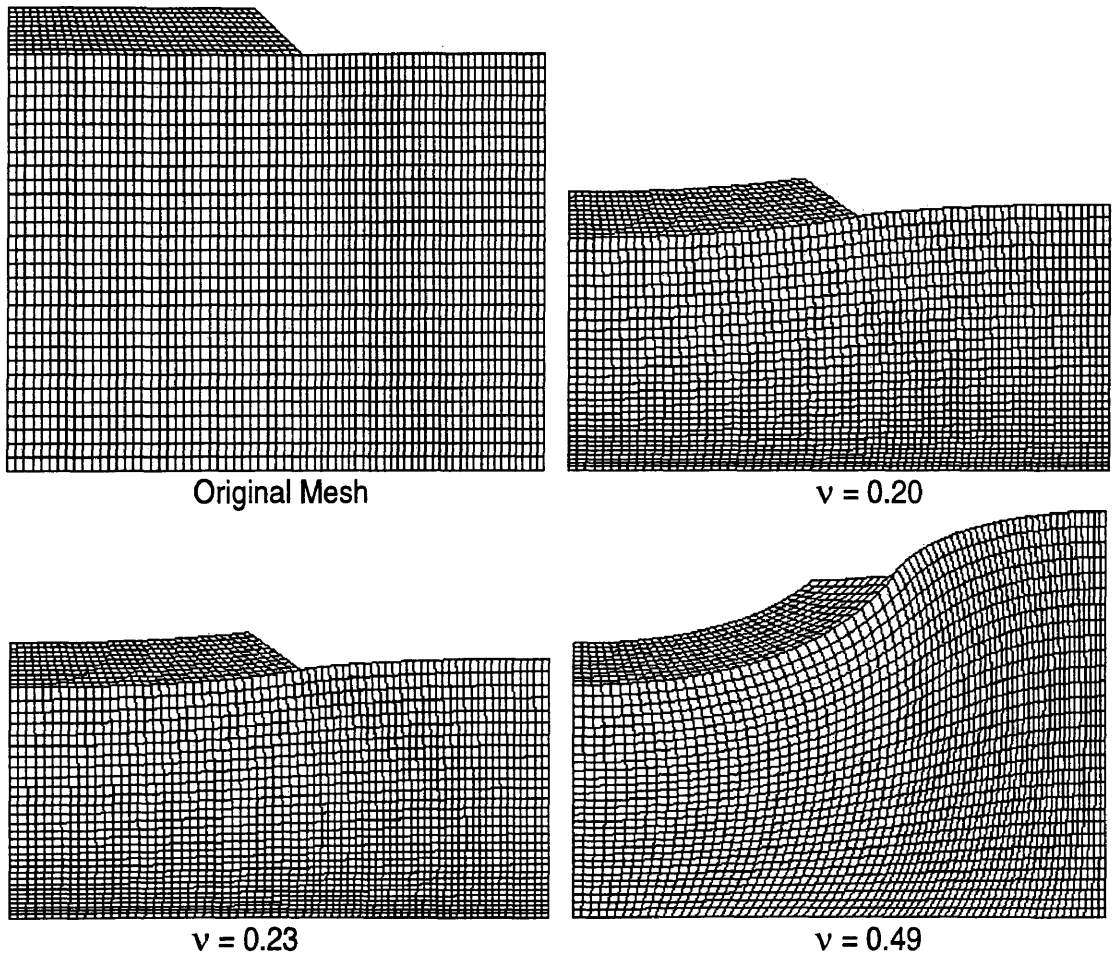

Figure 9-7: Compressibility Effects on Elastic Slope Deformation Under Gravitational Loads

Section 10

CONCLUDING REMARKS

Following a verification of the finite element program used for this research, the influences of several features related to the analysis of stresses in slopes under the assumption of elastic theory were examined. In particular, effects of slope and soil properties, as well as certain factors of the finite element method were scrutinized. Various means of representing and presenting the results of slope analyses were also considered.

In addition, a finite element program based on a visco-plastic algorithm was employed to explore the transitions of failure function contours as stresses were redistributed within a slope

10.1 Verification of the Finite Element Method

A comparison between an analytical and finite element model of the Boussinesq strip load problem was made; the results of which showed remarkable correspondence. Accordingly, the success of the elastic finite element solution was established.

10.2 Non-Dimensionalization of Stress Contours

Three methods for normalizing stress contours were presented. The scheme formulated by Clough and Woodward yielded a stress factor and two unique multipliers for each stress case—vertical horizontal and shear—such that their system could serve to estimate the stresses for several combinations of slope angle and Poisson's ratio in elastic embankments.

Poulos, Booker and Ring devised an analytical approach to determining slope stresses and utilized a constant divisor for non-dimensionalizing stresses. Their divisor requires the determination of the maximum possible height of the embankment, as if it were triangular. This height times the unit weight of the soil serves as their constant for normalization.

Finally, the method adopted for the current research work was also described by Savage and Denlinger. The unit weight of the soil times the actual height of the slope form a satisfactory and simply derived constant divisor for non-dimensionalizing stresses.

10.3 Influence of Poisson's Ratio

Under gravity loading, Poisson's ratio is one of only two factors that affect stresses in an elastic mass. It was demonstrated that there is a strong positive relationship between higher values of ν and increasing levels of horizontal stress in the embankment and foundation regions of the slopes studied. Similarly, shear stresses were shown to be

somewhat affected by the magnitude of ν, especially beneath the centers of the slopes.

10.4 Influence of Slope Angle

Slope angle is the second factor that affects stresses in elastic soils under gravitational loading. Two patterns of stress concentration were observed in horizontal and shear stress contours as slope angle was increased. For both stresses the change, characterized by bulbs of stress concentration, particularly below the slope toes, occurred between 35° and 45°.

10.5 Effects of Finite Element Mesh Size

The effects on stress contours induced by the placement of the finite element mesh boundaries were studied. It was shown that differences in the $\sigma_x/\gamma h_1$ and $\tau_{xy}/\gamma h_1$ contours are evident among the four sizes of meshes tested; however, the deviations are generally quite modest.

10.6 Effects of Element density

The results of a finite element model using three mesh densities were compared. It was found that there is virtually no effect on the normal stress values. However, the shear stress contours do exhibit a nominal amount of variation between the three meshes. In particular, the ovate contours directly under the center of the slope contract somewhat

as element density is increased.

10.7 Elasto-Plastic Stress Redistribution in Slopes

An investigation of the changes in the Mohr-Coulomb failure criterion and nodal displacements due to stress redistribution incurred by a finite element program based on elasto-plasticity was made. It was shown for a particular series of elastic slope analyses that exhibited violation of the failure criterion deep in the foundations, the contoured stresses for the elastic and plastic solutions did not vary appreciably. Nonetheless, the contours of Function F were considerably altered such that all regions of the embankment and foundation in these slope models no longer exhibited illegal values of F.

10.8 Animation as a Useful Visualization Technique

Animations using Microsoft® PowerPoint slide shows were utilized successfully as visualization techniques in the characterization of the trends manifested by each of the parametric studies and represented by contours of stresses and the failure function as well as displacements within a finite element mesh during stress redistribution.

Section 11

FURTHER STUDY

As with any research, the solutions to the initial problems inevitably lead to further questions about the conclusions reached. This study is no different. Following are a few directions which either could have been taken by this researcher or are likely candidates for extension to augment the work recorded in this thesis.

11.1 Re-assess Closed-Form Analytical Solution

A re-examination of the closed-form analytical solution for stresses in slopes and implementation of any necessary modifications could be beneficial for the reason that this solution takes both less computer time and memory than do the finite element solutions.

11.2 Comparison with Field Studies

Validation of the finite element solutions by comparison with field studies would improve the understanding of the variances with the numerical solutions and their inherent assumptions, e.g. material properties. Such an improved correlation between this calculative tool and actual slope stresses could engender increasingly better models.

11.3 More Conformal Mapping

With respect to enhancing automatic mesh generation, conformal mapping techniques may successfully augment the existing mesh generating subroutine. It is possible that such a mapping approach could simplify the arrangement of regions with greater or lesser element densities.

11.4 Varied Material Properties

Finite elements within a single mesh may be readily assigned numerous material properties. Experiments in which the slope and foundation materials are dissimilar reflect many situations. Additionally, often the core of an embankment is often of a different material than that which makes up the outer skin. Rigorous assessments of such configurations could lead to further simplification of analysis and design of embankments of this class.

11.5 Infinite Elements

Effects of the placement and type of boundaries of finite element meshes are not non-existent. Many documented solutions, e.g. Boussinesq, assume infinite depths. While this is not particularly realistic, it is a reasonable assumption in some cases. The use of infinite elements on the boundaries of a mesh could reduce the size of the problem, thus speeding calculation time. It would be interesting as well to determine if there is a

remarkable improvement in the correlation between the finite element and Boussinesq solutions.

REFERENCES CITED

Bardet,Jean-Pierre (1997), *Experimental Soil Mechanics*, Prentice Hall, USA.

Clough, Ray W., Woodward, Richard J. (July, 1967), *Analysis of Embankment Stresses and Deformations*, Journal of the Soil Mechanics and Foundations Division, ASCE, SM 4, pp. 529-549.

Das, Braja M. (1995), *Principles of Geotechnical Engineering 3rd ed.*, PWS Publishing Company, USA.

Davis, R. O., and Selvadurai, A. P. S. (1996), *Elasticity and Geomechanics*, Cambridge University Press, USA.

De Wet, M., and Hugo, F. (1988), *Evaluating the Design of an Earth Dam by Finite Element Analysis*, Int. J. for Numerical and Analytical Methods in Geomechanics, Vol. 12, pp. 573-578.

Griffiths, D. V. (May 1996), *FE-EMB2 and FE-EBM1: Slope stability software by finite elements*, Geomechanics Research Center, Colorado School of Mines,USA.

Lefebvre, Guy, Duncan, James M., and Wilson, Edward L. (July, 1973), *Three-Dimensional Finite Element Analyses of Dams*, Journal of the Soil Mechanics and Foundations Division, ASCE, SM 7, pp. 495-507.

Poulos, H.G., Booker, J. R., and Ring, G. J. (Dec., 1972), *Simplified Calculation of Embankment Deformations*, Soils and Foundations, Vol. 12, No. 4, pp. 1-17.

Savage, W. Z., and Denlinger, R. P. (1994), *Gravity-induced Stresses in Finite Slopes*, Computer Methods and Advances in Geomechanics, Siriwardane & Zaman (eds), Balkema, Rotterdam, pp. 2489-2492.

Savage, W. Z. (1994), *Gravity-induced Stresses in Finite Slopes*, Int. J. Rock Mech. Min. Sci. & Geomech. Abstr., Reprint, Vol. 31, No. 5, pp. 471-483.

Savage, William Z., and Swolfs, Henri S. (March 10, 1986), *Tectonic and Gravitational Stress in Long Symmetric Ridges and Valleys*, Jornal of Geophysical Research, Vol. 91, No. B3, pp. 3677-3685.

Savage, William Z., Powers, P. S., and Swolfs, Henri S. (1984), *In Situ Geomechanics of Crystalline and Sedimentary Rocks Part V: RVT--A FORTRAN Program for an Exact Elastic Solution for Tectonic and Gravity Stresses in Isolated Symmetric Ridges and Valleys*, USGS Open-File Report 84-827, Preliminary.

Singh, A. (1970), *Shear Strength and Stability of Man-Made Slopes*, Journal of the Soil Mechanics and Foundations Division, ASCE, Vol. 96, pp. 1879-1892.

Smith, I. M., and Griffiths, D. V. (1988), Programming the Finite Element Method 2nd ed., John Wiley & Sons Ltd.

SELECTED BIBLIOGRAPHY

Al-Khafaji, Amir Wadi, and Andersland, Orlando B. (1992), *Geotechnical Engineering and Soil Testing*, Saunders College Publishing, USA.

Amadei, B. (1996), *Importance of Anisotropy When Estimating and Measuring In Situ Stresses in Rock*, Int. J. Rock Mech. Min. Sci. & Geomech. Abstr., Vol. 33, No. 3, pp. 293-325.

Anireddy, H. R., and Ghose, A., K. (July, 1994), *Determination of in-situ horizontal stresses by hydraulic fracturing in underground coal mines*, Journal of Mines, Metals & Fuels, pp. 145-155.

Ashford, Scott A., and Sitar, Nicholas (1992), *Development of Analytical Methods for Evaluation of Seismic Stability of Coastal Bluffs in the San Francisco Bay Region*, USGS Geotechnical Engineering Report No. UCB/GT/92-12, University of California-Berkeley.

Bell, J. S. (June, 1996), *Petro Geoscience 1. In Situ Stresses in Sedimentary Rocks (Part 1): Measurement Techniques*, Geoscience Canada, Vol. 23, No. 2, pp. 85-100.

_____. (Sept., 1996), *Petro Geoscience 2. In Situ Stresses in Sedimentary Rocks (Part 1): Applications of Stress Measurements*, Geoscience Canada, Vol. 23, No. 3, pp. 135-153.

Boresi, Arthur, P., Schmidt, Richard J., and Sidebottom, Omar M. (1993), *Advanced Mechanics of Materials, 5th ed.*, John Wiley & Sons, Inc., USA.

Brackley, I. J. A., and Sanders, P. J. (1992), *In Situ measurement of total natural horizontal stresses in an expansive clay*, Géotechnique, Vol. 42, No. 2, pp. 443-451.

Bromhead, E. N. (1992), *The Stability of Slopes 2nd ed.*, Blackie Academic & Professional, Glasgow.

Brown, E. T., and Hoek, E. (1978), *Trends in Relationships between Measured In-Situ Stresses and Depth*, Int. J. Rock Mech. Min. Sci. & Geomech. Abstr., Vol. 15, pp. 211-215.

Chowdhury, R. N. (1978), *Slope Analysis*, Elsevier Scientific Publishing Company, Amsterdam.

Das, Braja M. (1995), *Principles of Foundation Engineering 3rd ed.*, PWS Publishing Company, USA.

Jaeger, Charles (1979), *Rock mechanics and engineering*, Cambridge University Press, Great Britain.

Jaeger, J. C., and Cook (1976), N. G. W., *Fundamentals of Rock Mechanics*, Halsted, New York.

Masood, Tahir, and Mitchell, James K. (Oct., 1993), *Estimation of In Situ Lateral Stresses in Soils by Cone-Penetration Test.*, Journal of Geotechnical Engineering, Vol. 119, No. 10, pp. 1624-1639.

Michalowski, Radoslaw L. (July, 1992), *Bearing Capacity of Nonhomogeneous Cohesive Soils Under Embankments*, Journal of Geotechnical Engineering, Vol. 118, No. 7, pp. 1098-1119.

Pande, G. N., Beer, G., and Williams, J. R. (1990), *Numerical Methods in Rock Mechanics*, John Wiley & Sons Ltd., Great Britain.

Popov, I. V., and Kotlov, F. V. (eds.) (1963), *The Stability of Slopes*, Transactions of the F. P. Savarenskii Hydrogeology Laboratory, Vol. 35, Consultants Bureau Enterprises, Inc., New York, NY, USA.

Poulos, H. G., and Davis, E. H. (1991), *Elastic Solutions for Soil and Rock Mechanics*, Centre for Geotechnical Research, University of Sydney, Australia.

Radbruch-Hall, D. H., Varnes, D. J. (1976), and Savage, W. Z., *Gravitational Spreading of Steep-sided Ridges ("Sackung") in Western United States*, Bulletin of the International Association of Engineering Geology, No. 14, pp. 23-35.

Savage, W. Z., and Swolfs, H. S. (1992), *Near-surface crustal stresses--theory and application*, Trends in Geophys. Res., Reprint, *1*, 217-250.

Savage, W. Z., Swolfs, H. S., and Amadei, B. (1992), *On the state of Stress in the Near-surface of the Earth's Crust*, Pageoph, Reprint, Vol. 138, No. 2, pp. 207-228.

Savage, W. Z., Swolfs, H. S., and Powers, P. S. (1985), *Gravitational Stresses in Long Symmetric Ridges and Valleys*, Int. J. Rock Mech. Min. Sci. & Geomech. Abstr., Vol. 22, No. 5, pp. 291-302.

Sheorey, P. R. (1996), *A Theory for In Situ Stresses in Isotropic and Transversely Isotropic Rock*, , Int. J. Rock Mech. Min. Sci. & Geomech. Abstr., Vol. 31, No. 1, pp. 23-34.

Terzaghi, Karl, and Peck, Ralph B. (1948), Soil Mechanics in Engineering Practice, John Wiley & Sons, Inc., USA.

Terzaghi, Karl (1943), *Theoretical Soil Mechanics*, John Wiley and Sons, Inc., New York.

Wiłun, Zenon, and Starzewski, Krzysztof (1975), *Soil Mechanics in Foundation Engineering 2nd ed., Vol 1, Properties of Soils and Site Investigations*, Surrey University Press, Great Britain.

_____. (1975), *Soil Mechanics in Foundation Engineering 2nd ed., Vol. 2 Theory and Practice*, Surrey University Press, Great Britain.

APPENDIX 1: Effects of Kriging Options

Included in this Appendix are graphical examples of the effects of options available in SURFER® for the Kriging method of point estimation. In addition, a table summarizing the values used is included. The purpose of the incorporation of this information is merely to provide a means for replication of the work done here; therefore, none of the options is specifically defined in this work. All examples use a grid with 50 lines in the x-direction and 19 lines in the y-direction.

Model #	Kriging Options										Search Options			
	Variogram Model			Nugget Effect		Anisotropy			Outside Data Treatment	Search Type	Search Rules			
	Type	Scale	Drift Type	Error Variance	Micro Variance	r1	r2	∠°			Data Per Sector	Min. Total Data	Max Empty Sectors
K-1a	Linear	0.0189	None	0	0	1.37	1.37	0	Do not Ignore	Quad	6	5	4
K-1b	Linear	0.0189	None	0	0	1.37	1.37	0	Ignore	Quad	6	5	4
K-1c	Linear	1.0	None	0	0	1.37	1.37	0	Do not Ignore	Quad	6	5	4
K-2a	Linear	0.0189	None	0	0	1.37	1.37	0	Do not Ignore	Oct	3	5	8
K-2b	Linear	0.0189	Linear	0	0	1.37	1.37	0	Do not Ignore	Quad	6	5	4
K-2c	Linear	0.0189	Linear	0	0	1.37	1.37	0	Ignore	Quad	6	5	4
K-3a	Linear	0.0189	None	0	0	1.37	1.37	30	Do not Ignore	Quad	6	5	4
K-3b	Linear	0.0189	None	0	0	1.37	1.37	0	Do not Ignore	Simple	24	5	1
K-3c	Linear	0.0189	None	0	0	1.37	1.37	0	Do not Ignore	Simple	6	5	1
K-4a	Linear	0.0189	None	0	0	1.37	1.37	0	Do not Ignore	Quad	24	5	4
K-4b	Linear	0.0189	None	0	0	1.37	1.37	0	Do not Ignore	Quad	10	5	4
K-4c	Linear	0.0189	None	0	0	1.37	1.37	0	Do not Ignore	Quad	6	1	4

Table A-1: Kriging Options

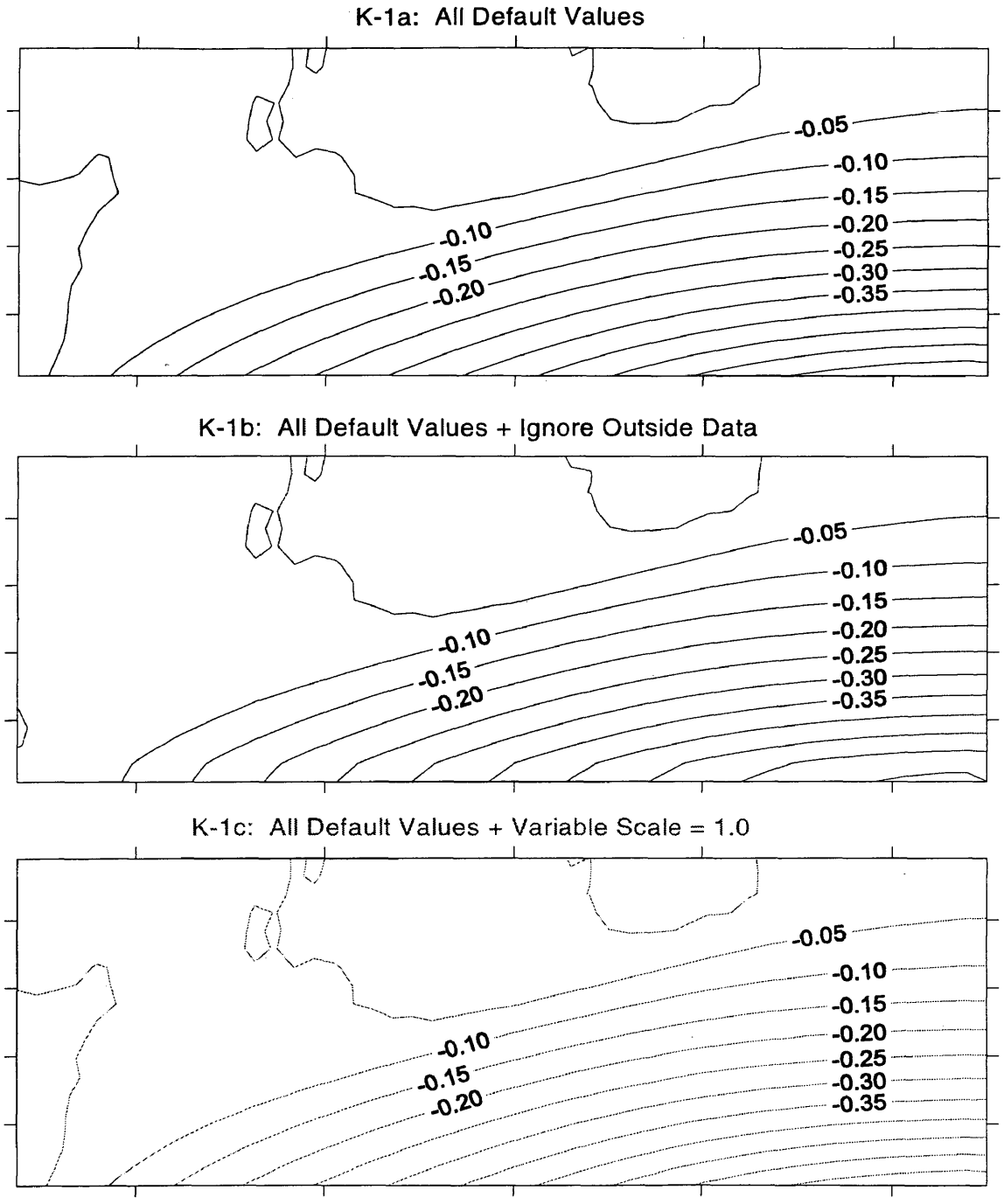

Figure A-1: Kriging Options K-1a, K-1b, and K-1c

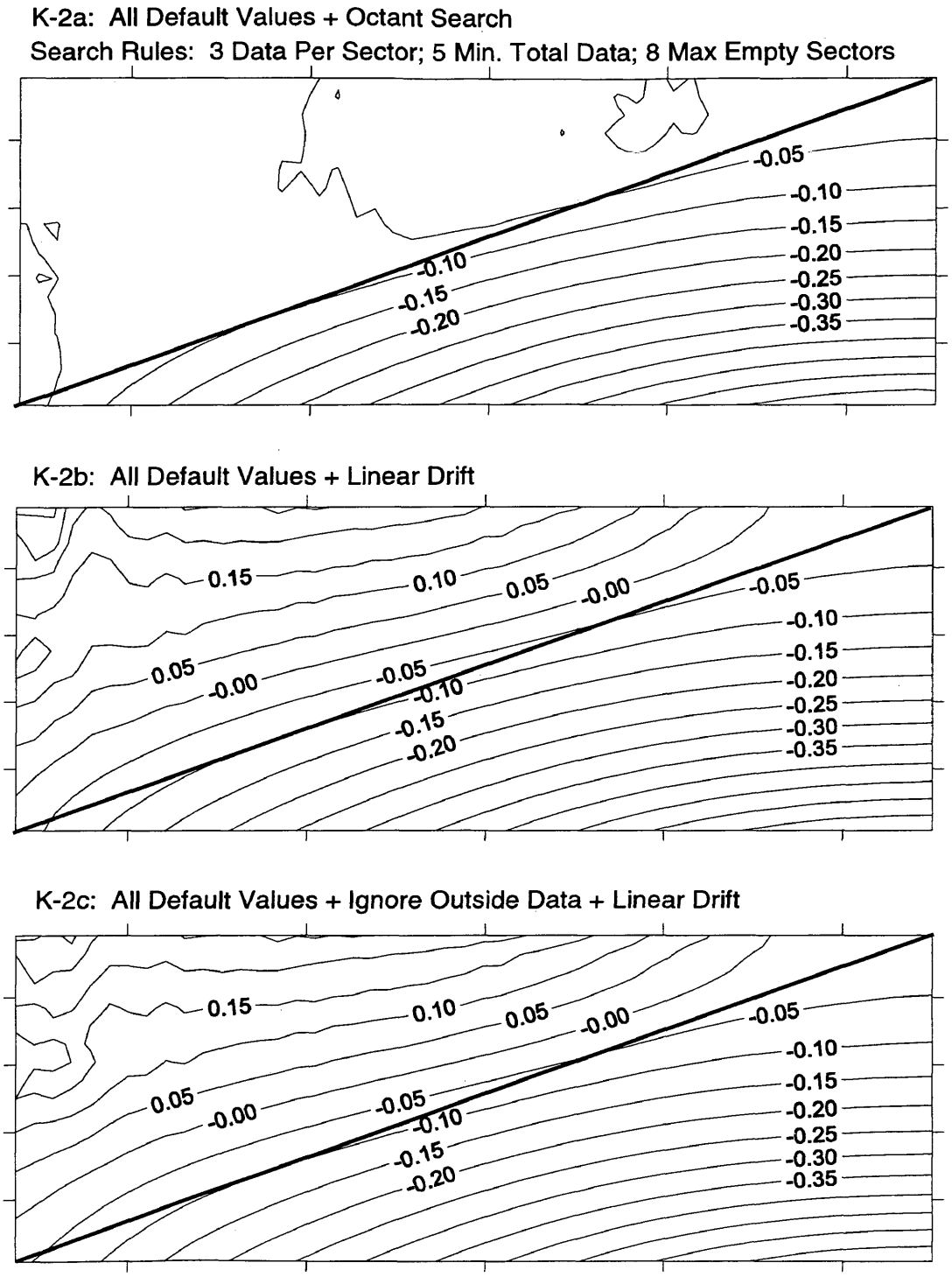

Figure A-2: Kriging Options: K-2a, K-2b, and K-2c

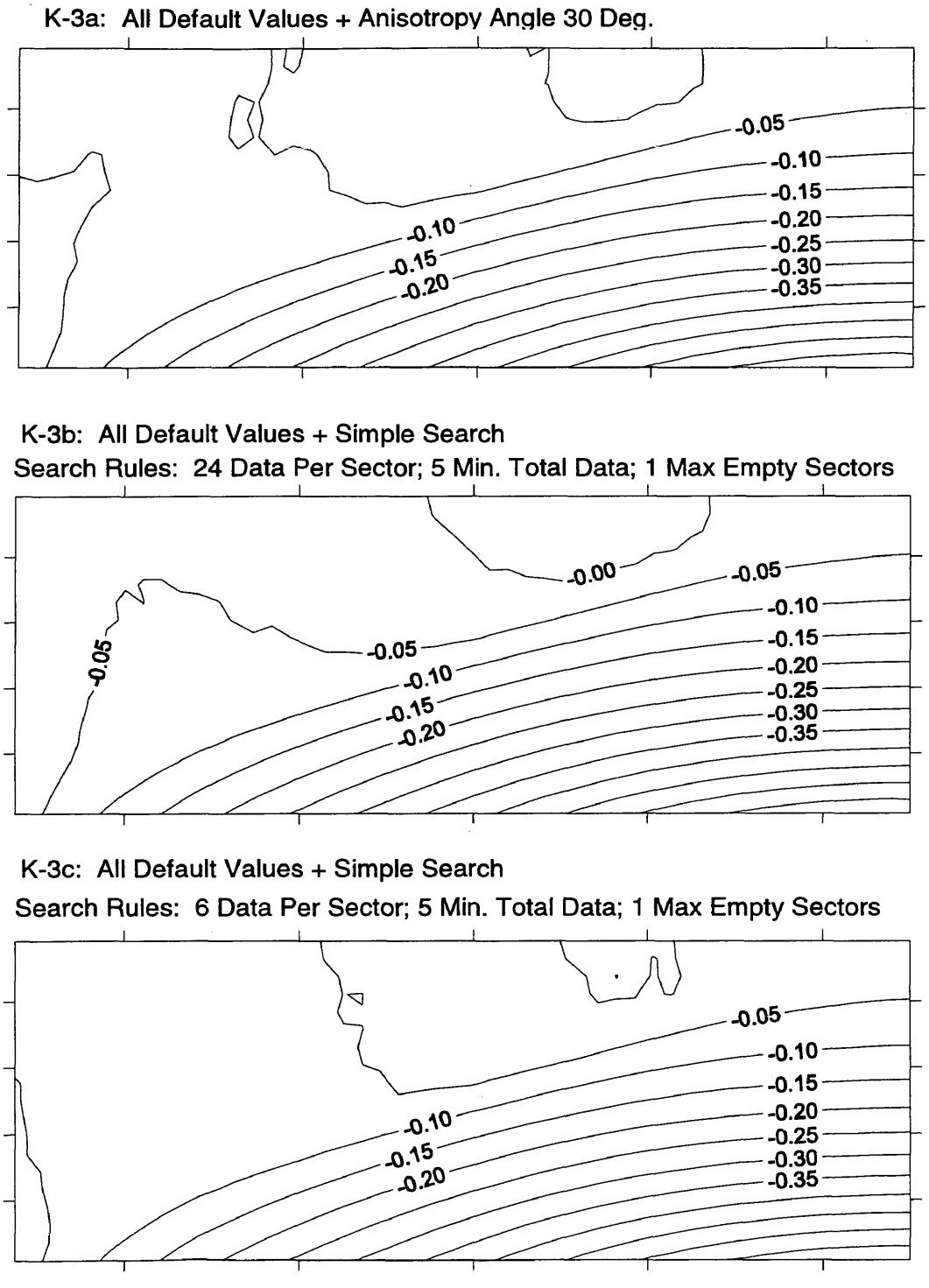

Figure A-3: Kriging Options: K-3a, K-3b, K-3c

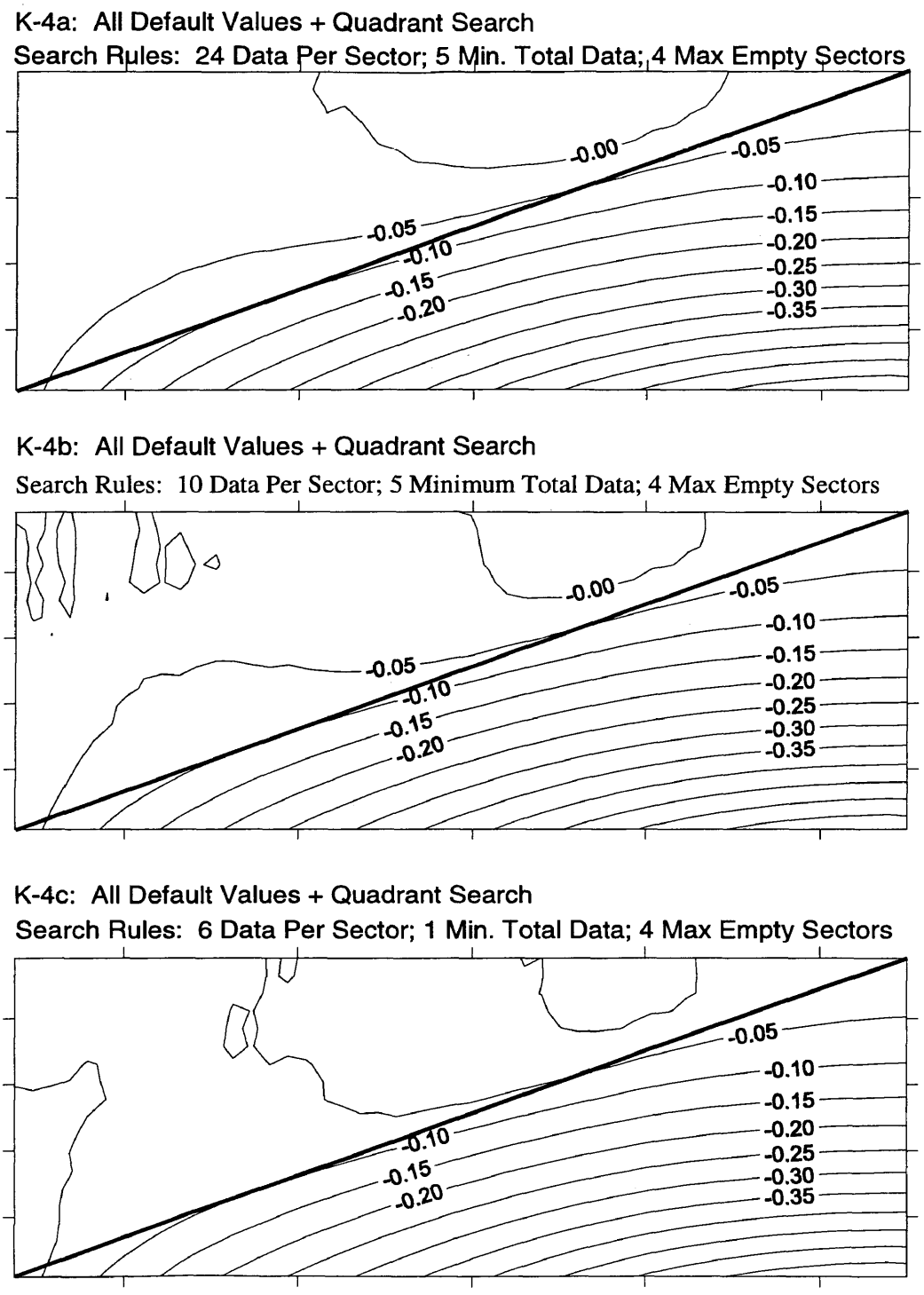

Figure A-4: Kriging Options: K-4a, K-4b, K-4c

APPENDIX 2: Finite Element Code (slope.f) and Sample Output

```
      program mp54r2
c
c      modified version of program 5.4 in text -
c
c      "PROGRAMMING THE FINITE ELEMENT METHOD"
c                    by
c           I.M. Smith and D.V. Griffiths
c
c      published by John Wiley and Sons (1988)
c
c      PLANE STRAIN ELASTIC ANALYSIS OF A RECTANGULAR SOLID
c      USING 8-NODE QUADRILATERAL ELEMENTS.
c      GENERAL PROGRAM
c
c      last update by D.V. Griffiths on dec 4, 1997
c
c     ALTERED, 1998 BY D. L. MICHELS TO PERFORM SEVERAL RUNS
C     AUTOMATICALLY VARYING DATA--NO INPUT DATA FILE REQUIRED
c
c     Alter next line to change problem size.
c
      parameter(ikv=20060000,iloads=55240,kpr=11,kel=9200,ino=75,
     +          ifix=20,inf=28001)
c
      real dee(4,4),samp(4,2),coord(8,2),jac(2,2),jac1(2,2),
     +der(2,8),deriv(2,8),bee(4,16),dbee(4,16),kvh(ikv),
     +btdb(16,16),km(16,16),eld(16),eps(4),sigma(4),disps(iloads),
     +bt(16,4),fun(8),kv(ikv),loads(iloads),comp(3),delta(3),
     +ym,pr,bdylds(iloads),eload(16),bload(16),
     +globc(inf,2),gc(2),val(ifix),gamma,clough,alpha
c
      integer g(16),no(ino),etype(kel),gnum(kel,8),
     +num(8),nf(inf,2),gg(kel,16),kdiag(iloads),node(ifix),
     +sense(ifix),cdex,pdex,adex,fdex,ibname
c
      character*3 name1
      character*2 name2,name3,name4
      character*9 basenm
      character*13 filenm
c
      data idee,ibee,idbee,ih/4*3/,idof,ibtdb,ibt,ikm/4*16/
      data ijac,ijac1,nodof,it,ider,ideriv,ngp/7*2/,icoord,nod/2*8/
```

```
      data isamp/4/, huge/1.e20/
c
c      input and initialisation
c
      ips=8
      iout=9
      igen=10
      ires=11
c
c     The following two lines are for file identification purposes
c     instituted by D.L.M., 1998.
c
            name1 = 'sca'
            name4 = 'lg'
c
c     BEGIN LOOP FOR POISSONS RATIO (pr)
c
       do 800 pdex=1,8
         if(pdex.eq.1)then
            pr = 0.0
            name2 = '00'
         else if(pdex.eq.2)then
            pr = 0.10
            name2 = '10'
         else if(pdex.eq.3)then
            pr = 0.20
            name2 = '20'
         else if(pdex.eq.4)then
            pr = 0.30
            name2 = '30'
         else if(pdex.eq.5)then
            pr = .33333
            name2 = '33'
         else if(pdex.eq.6)then
            pr = 0.40
            name2 = '40'
         else if(pdex.eq.7)then
            pr = 0.49
            name2 = '49'
         else if(pdex.eq.8)then
            pr = 0.4999
            name2 = '99'
         end if
c
c     BEGIN LOOP FOR ANGLE AND DIMENSION CHANGES
c
       do 900 adex=1,7
         if(adex.eq.1)then
            name3 = '15'
            nx1=29
```

```
  nx2=25
  ny1=5
  ny2=50
  w1=2.5
  s1=3.372
  w2=5.0
  h1=1.0
  h2=10.0
else if(adex.eq.2)then
  name3 = '45'
  nx1=17
  nx2=25
  ny1=5
  ny2=50
  w1=2.5
  s1=1.0
  w2=5.0
  h1=1.0
  h2=10.0
else if(adex.eq.3)then
  name3 = '85'
  nx1=12
  nx2=25
  ny1=5
  ny2=50
  w1=2.5
  s1=0.0875
  w2=5.0
  h1=1.0
  h2=10.0
else if(adex.eq.4)then
  name3 = '45'
  nx1=10
  nx2=15
  ny1=5
  ny2=20
  w1=5.0
  s1=1.0
  w2=5.0
  h1=1.0
  h2=10.0
else if(adex.eq.5)then
  name3 = '85'
  nx1=15
  nx2=15
  ny1=5
  ny2=20
  w1=5.0
  s1=0.087
  w2=5.0
```

```
            h1=1.0
            h2=10.0
          else if(adex.eq.6)then
            name3 = '90'
            nx1=35
            nx2=35
            ny1=10
            ny2=30
            w1=5.0
            s1=0.0
            w2=5.0
            h1=1.0
            h2=10.0
          else if(adex.eq.7)then
            name3 = '00'
            nx1=35
            nx2=35
            ny1=0
            ny2=30
            w1=5.0
            s1=0.0
            w2=5.0
            h1=0.0
            h2=10.0
          else if(adex.eq.8)then
c     This option is for mimicking Clough and Woodward's (1967) work
            name3 = 'cw'
            nx1=52
            nx2=0
            ny1=20
            ny2=0
            w1=1.25
            w2=0.0
            s1=26.25-1.25
            h1=10.0
            h2=0.0
            alpha = atan(h1/s1)
          end if
c
            c = 0.30
            phi = 30.0
c
c      CREATE BASE FILE NAME (name1+name2+name3)
c      AND OUTPUT FILES (.msh  .xls  .r)
c
       basenm(1:3) = name1(1:3)
       basenm(4:5) = name2(1:2)
       basenm(6:7) = name3(1:2)
       basenm(8:9) = name4(1:2)
       ibname = lnblnk(basenm)
```

```
        filenm = basenm(1:ibname)
        filenm(ibname+1:ibname+4) = '.msh'
        open(ips, file=filenm)
        filenm(ibname+1:ibname+4) = '.dat'
        open(iout, file=filenm)
        filenm(ibname+1:ibname+4) = '.r'
        open(ires, file=filenm)
c
c       CONTINUE ON WITH "original" SLOPE.F PROGRAM
c
c
      pi=acos(-1.)
      phi=phi*pi/180.
      siphi=sin(phi)
      cophi=cos(phi)
      call quad(nx1,nx2,ny1,ny2,w1,w2,s1,h1,h2,globc,nf,inf,
     +                gnum,kel,nels,nn,n,iw,igen)
c
      ntype=1
      ym=1.e5
      gamma=1.0
c
      do 5 ip=1,nels
    5 etype(ip)=1
      if(ntype.gt.1)read(10,*)(etype(ip),ip=1,nels)
c
      write(ires,*)
      write(ires,*)(' **************DATA SECTION**************')
      write(ires,*)
      write(ires,*)(' number of elements')
      write(ires,200)nels
      write(ires,*)(' number of nodes')
      write(ires,200)nn
      write(ires,*)(' number of property types')
      write(ires,200)ntype
      write(ires,*)(" Young's modulus and Poisson's
     +ratio for each type")
      write(ires,300)(ym,pr,i=1,ntype)
      write(ires,*)(' element types')
      write(ires,400)(etype(i),i=1,nels)
      call gauss(samp,isamp,ngp)
      n=1
      do 20 i=1,nn
      do 20 j=1,nodof
      if(nf(i,j).gt.n)n=nf(i,j)
   20 continue
c
      do 4 i=1,nn
 4       globc(i,1)=-globc(i,1)
      call mesh(globc,inf,nn,gnum,kel,nod,nels,ips)
```

```
      do 6 i=1,nn
 6       globc(i,1)=-globc(i,1)
c
c LOOP THE ELEMENTS TO SET UP GLOBAL GEOMETRY AND KDIAG
c
      do 25 i=1,n
   25 kdiag(i)=0
      do 30 ip=1,nels
      do 35 i=1,nod
      num(i)=gnum(ip,i)
      do 35 j=1,nodof
      k=(i-1)*nodof+j
      g(k)=nf(num(i),j)
   35 gg(ip,k)=g(k)
   30 call fkdiag(kdiag,g,idof)
      kdiag(1)=1
      do 40 i=2,n
   40 kdiag(i)=kdiag(i)+kdiag(i-1)
      ir=kdiag(n)
c
      write(ires,*)(' number of freedoms')
      write(ires,200)n
      write(ires,*)(' length of kv vector (skyline storage)')
      write(ires,200)ir
      call nulvec(kv,ir)
      call nulvec(loads,n)
c
c      ELEMENT STIFFNESS INTEGRATION AND ASSEMBLY
c
      do 45 ip=1,nels
      e=ym
      v=pr
      call fmdeps(dee,idee,e,v)
      do 50 i=1,nod
      num(i)=gnum(ip,i)
      do 50 j=1,nodof
      coord(i,j)=globc(num(i),j)
      k=(i-1)*nodof+j
   50 g(k)=gg(ip,k)
      call null(km,ikm,idof,idof)
      call nulvec(eld,idof)
      do 55 i=1,ngp
      do 55 j=1,ngp
      call fmquad(der,ider,fun,samp,isamp,i,j)
      call matmul(der,ider,coord,icoord,jac,ijac,it,nod,it)
      call twoby2(jac,ijac,jac1,ijac1,det)
      call matmul(jac1,ijac1,der,ider,deriv,ideriv,it,it,nod)
      call null(bee,ibee,ih,idof)
      call formb(bee,ibee,deriv,ideriv,nod)
      call matmul(dee,idee,bee,ibee,dbee,idbee,ih,ih,idof)
```

```
      call matran(bt,ibt,bee,ibee,ih,idof)
      call matmul(bt,ibt,dbee,idbee,btdb,ibtdb,idof,ih,idof)
      quot=det*samp(i,2)*samp(j,2)
      do 31 k=2,idof,2
 31      eld(k)=eld(k)+fun(k/2)*quot
      call msmult(btdb,ibtdb,quot,idof,idof)
  55  call matadd(km,ikm,btdb,ibtdb,idof,idof)
      do 41 k=1,idof
 41      if(g(k).ne.0)loads(g(k))=loads(g(k))-eld(k)*gamma
  45  call fsparv(kv,km,ikm,g,kdiag,idof)
      call veccop(kv,kvh,ir)
c
c
c      SOLVE EQUATIONS
c
      call veccop(loads,disps,n)
      call sparin(kv,n,kdiag)
      call spabac(kv,disps,n,kdiag)
      call linmls(kvh,disps,loads,n,kdiag)
c
c      PRINT NODAL DISPLACEMENTS
c
      write(ires,*)
      write(ires,*)('*************OUTPUT SECTION*************')
      write(ires,*)
      write(ires,*)(' Nodal Displacements')
      write(ires,*)(' node x-displacement   y-displacement')
      do 60 i=1,nn
      call nulvec(delta,nodof)
      do 58 j=1,nodof
  58  if(nf(i,j).ne.0)delta(j)=disps(nf(i,j))
  60  write(ires,'(i5,e12.4,5x,e12.4)')i,(delta(j),j=1,nodof)
c
c      INSPECT ALL GAUSS POINTS
c
c      ngp=3
c      call gauss(samp,isamp,ngp)
      write(ires,*)
      write(ires,*)(' Gauss point stresses')
      write(ires,*)
     >('Element    x         y          sig_x       sig_y       tau_xy ')
      call nulvec(bdylds,n)
      do 65 ip=1,nels
      call nulvec(bload,idof)
      e=ym
      v=pr
      call fmdeps(dee,idee,e,v)
      do 70 i=1,nod
      num(i)=gnum(ip,i)
      do 70 j=1,nodof
```

```
      coord(i,j)=globc(num(i),j)
      k=(i-1)*nodof+j
   70 g(k)=gg(ip,k)
      do 75 m=1,idof
      if(g(m).eq.0)eld(m)=0.
   75 if(g(m).ne.0)eld(m)=disps(g(m))
      do 80 i=1,ngp
      do 80 j=ngp,1,-1
      call fmquad(der,ider,fun,samp,isamp,i,j)
      call gcoord(fun,coord,icoord,nod,it,gc)
      call matmul(der,ider,coord,icoord,jac,ijac,it,nod,it)
      call twoby2(jac,ijac,jac1,ijac1,det)
      call matmul(jac1,ijac1,der,ider,deriv,ideriv,it,it,nod)
      call null(bee,ibee,ih,idof)
      call formb(bee,ibee,deriv,ideriv,nod)
      call matran(bt,ibt,bee,ibee,ih,idof)
      call mvmult(bee,ibee,eld,ih,idof,eps)
      call mvmult(dee,idee,eps,ih,ih,sigma)
      tmax = sqrt(((sigma(1) - sigma(2)) / 2.)**2 + sigma(3)**2)
      sigav = (sigma(1) + sigma(2))/2.
      sig1 = sigav - tmax
      sig3 = sigav + tmax
      f=(sig1+sig3)*siphi/2.-(sig1-sig3)/2.-c*cophi
      write(ires,'(1x,i5,2f9.2,3x,3e12.4)')
     >ip,-gc(1)+w1,gc(2),sig1/(gamma*1),
     >                   sig3/(gamma*1),
     >                      f/(gamma*1)
      write(iout,'(2f8.4,8e12.4)')
     >-gc(1)+w1,gc(2),sigma(1)/(gamma*h1),
     >                sigma(2)/(gamma*h1),
     >                sigma(3)/(gamma*h1),
     >                   f/(gamma*h1)
c     >                sig1/(gamma*1),
c     >                sig3/(gamma*1),
c     >                tmax/(gamma*1)
c
c THE FOLLOWING LINES CALCULATE AND PRINT CLOUGH
c AND WOODWARD'S STRESS FACTORS, K
c
c     if(gc(1) .le. w1)then
c      clough=abs(gc(2))
c     else if(gc(1) .gt. w1)then
c         clough=(((w1+s1)-gc(1))*tan(alpha))-gc(2)-h1
c     end if
c
c     write(iout,'(2f8.4,8e12.4)')
c    >gc(1),gc(2),
c    >                sigma(1)/(gamma*clough),
c    >                sigma(2)/(gamma*clough),
c    >                sigma(3)/(gamma*clough),
```

```
c     >                    f/(gamma*clough),
c     >                sigma(1)/(gamma*h1),
c     >                sigma(2)/(gamma*h1),
c     >                sigma(3)/(gamma*h1),
c     >                   f/(gamma*h1)
      call mvmult(bt,ibt,sigma,idof,ih,eload)
      quot=det*samp(i,2)*samp(j,2)
      do 85 k=1,idof
   85 bload(k)=bload(k)+eload(k)*quot
   80 continue
      do 90 m=1,idof
      if(g(m).eq.0)goto 90
      bdylds(g(m))=bdylds(g(m))+bload(m)
   90 continue
   65 continue
      write(ires,*)
      write(ires,*)(' Equilibrium check')
      write(ires,*)(' Stress convergence tolerance (%)')
      diff=0
      big=0.
      do 95 i=1,n
      if(abs(loads(i)).gt.big)big=abs(loads(i))
   95 if(abs(loads(i)-bdylds(i)).gt.diff)diff=abs(loads(i)-bdylds(i))
      write(11,'(f12.4)')diff/big*100.
  200 format(7i10)
  300 format(e13.4,f7.1)
  400 format(21i3)
c
      close(iout)
      close(ips)
      close(ires)
c
  950 continue
  900 continue
  800 continue
  700 continue
      stop
      end
c
c ***********************************************************************
c *                                                                     *
c *                          Subroutine mesh                            *
c *                                                                     *
c***********************************************************************
c  Version 1.1
c  Written by R. Daniel Lohnes, TUNS, May 9, 1994.
c  Updated: May 17, 1994 by Gordon A. Fenton.
c  Updated: Dec 4, 1997 by D.V. Griffiths
c  Updated: July, 1998 by D.L. Michels
c
```

```
c   PURPOSE     to create a post script file that will draw a
c               finite element mesh.
c
c  This routine draws a finite element mesh in PostScript
c       given the nodal coordinates and the node numbers
c       bounding each element.
c
c
c  Arguments to this routine are as follows;
c
c  coord    real array of size at least equal to the number of nodes in
c           the (or portion thereof) mesh to be drawn by 2 which
c           contains the (x,y) coordinates of each node. Thus
c           coord(i,1) is the x-coordinate and coord(i,2) is the
           y-coordinate of the i'th node. (input)
c
c  ic       leading dimension of the array coord as prescribed in the
c           calling routine. (input)
c
c  ien      integer array of size at least nod x nel containing the
c           node numbers bounding each element to be drawn, counting
c           clockwise. (input)
c
c  ie       leading dimension of the array ien as prescribed in the
c           calling routine. (input)
c
c  nod            number of nodes per element. (input)
c
c  nel            number of elements to be drawn on this call. (input)
c
c  ips              output channel for mesh plot
c-----------------------------------------------------------------------
--------
      subroutine mesh(coord,ic,nn,ien,ie,nod,nel,ips)
      real xmin,xmax,ymin,ymax,xln,yln,xorg,yorg
      dimension coord(ic,*)
      integer ien(ie,*)
      character*(*) psfile
      logical lshow
      data scale/72.0/
c                                        formats
   1  format(a,a,a)
   2  format(f5.2,a)
   3  format(2f9.2,a)
   4  format(2f9.2,a,f9.2,a)
c----------------------------- Start excutable statements -------------
--------
c                        open output file and compute scale factors
          write(ips,1)'%!PS-Adobe-1.0'
          write(ips,1)'%%DocumentFonts: none'
```

```
          write(ips,1)'%%Creator: mesh.f, ',title1
          write(ips,1)'%%Pages: 1'
          write(ips,1)'%%EndComments'
          write(ips,1)'/m {moveto} def'
          write(ips,1)'/l {lineto} def'
          write(ips,1)'/s {stroke} def'
          write(ips,1)'/c {closepath} def'
          write(ips,1)'%%EndProlog'
          write(ips,1)'%%Page: 0 1'
          write(ips,1)'gsave'
c
      xmin=coord(1,1)
      xmax=coord(1,1)
      ymin=coord(1,2)
      ymax=coord(1,2)
      do 21 i=2,nn
      if(coord(i,1).lt.xmin)xmin=coord(i,1)
      if(coord(i,1).gt.xmax)xmax=coord(i,1)
      if(coord(i,2).lt.ymin)ymin=coord(i,2)
      if(coord(i,2).gt.ymax)ymax=coord(i,2)
   21 continue
      width =xmax-xmin
      height=ymax-ymin
c
c    ALLOW 1.5" MARGIN MINIMUM ON EACH SIDE OF FIGURE
c
      if(height.ge.width)then
c
c       PORTRAIT MODE
c
      if(height.ge.11.0/8.5*width)then
c
c        HEIGHT GOVERNS THE SCALE
c
          sxy=scale*8.0/height
          xo = scale*0.5*(8.5-8.0*width/height)
          yo = scale*1.5
      else
c
c        WIDTH GOVERNS THE SCALE
c
          sxy=scale*5.5/width
          xo = scale*1.5
          yo = scale*0.5*(11.0-5.5*height/width)
      end if
c
      else
c
c       LANDSCAPE MODE
c
```

```
      write(ips,3) 612.0, 0.0, ' translate'
      write(ips,2) 90.0, ' rotate'
      if(width.ge.11.0/8.5*height)then
c
c       WIDTH GOVERNS THE SCALE
c
          sxy=scale*8.0/width
          xo = scale*1.5
          yo = scale*0.5*(8.5-8.0*height/width)
      else
c
c       HEIGHT GOVERNS THE SCALE
c
          sxy=scale*5.5/height
          xo = scale*0.5*(11.0-5.5*width/height)
          yo = scale*1.5
      end if
      end if
c
c                           DRAW THE MESH
c     The following three lines have been added by D. Michels, 1998
c     Their purpose is to unify the scaling of the mesh diagrams by
c     overriding the calculated scaling procedure (above).
      xo = 1.0
      yo = 1.0
      sxy = 30.0
c
      write(ips,3) xo, yo, ' translate'
      write(ips,2) 0.5, ' setlinewidth'
      do 20 i = 1, nel
         ii = ien(i,1)
         x  = sxy*(coord(ii,1) - xmin)
         y  = sxy*(coord(ii,2) - ymin)
         write(ips,3) x, y,' m'
         do 10 j = 2, nod
            jj = ien(i,j)
            x  = sxy*(coord(jj,1) - xmin)
            y  = sxy*(coord(jj,2) - ymin)
            write(ips,3) x, y,' l'
   10    continue
         write(ips,1)'c s'
   20 continue
c                                  close output file?
          write(ips,1)'grestore'
          write(ips,1)'showpage'
          write(ips,*)
          close(ips)

      return
      end
```

```
c
c*************************QUAD SUBROUTINE*****************************
c
      subroutine quad(nx1,nx2,ny1,ny2,w1,w2,s1,h1,h2,g_coord,nf,inf,
     +                g_num,maxel,nels,nn,n,iw,igen)
c
      real g_coord(inf,2),coord(8,2)
c
      integer nf(inf,2),g(16),num(8),g_num(maxel,8)
c
      nye=ny1+ny2
      nels=nx1*ny1+ny2*(nx1+nx2)
      nn=(3*nye+2)*nx1+2*nye+1+(3*ny2+2)*nx2
c
c  CALCULATIONS FOR NUMBER OF UNRESTRICTED FREEDOMS
c
c      ROLLERS ON THE SIDES, BOTTOM FIXED
      n=2*(nn-nye-2*(nx1+nx2)-1-ny2)
c
c      ROLLERS ON THE SIDES AND BOTTOM
c      n=2*(nn-nye-ny2-nx1-nx2)-3
c
      write(igen,*)n
      write(igen,*)nn
      write(igen,*)nels
c
c  CALCULATIONS FOR HALF BAND WIDTH
c
c      ROLLERS ON THE SIDES, BOTTOM FIXED
      iw=6*nye+5
c
c      ROLLERS ON THE SIDES AND BOTTOM
c      iw=6*nye+7
c
      nm=0
      ic=0
      do 81 i=1,2*nye
      nm=nm+1
      nf(nm,1)=0
      ic=ic+1
   81 nf(nm,2)=ic
      nm=nm+1
c                  BOTTOM CORNER NODE FULLY RESTRAINED
      nf(nm,1)=0
      nf(nm,2)=0
      do 82 j=1,nx1
      do 83 i=1,nye
      nm=nm+1
      ic=ic+1
      nf(nm,1)=ic
```

```
      ic=ic+1
   83 nf(nm,2)=ic
      nm=nm+1
c           BOTTOM NODES RESTRAINED IN X-DIR
      nf(nm,1)=0
c           BOTTOM NODES UNRESTRAINED IN X-DIR
c      ic=ic+1
c      nf(nm,1)=ic
c           BOTTOM NODES RESTRAINED IN Y-DIR
      nf(nm,2)=0
      do 84 i=1,2*nye
      nm=nm+1
      ic=ic+1
      nf(nm,1)=ic
      ic=ic+1
   84 nf(nm,2)=ic
      nm=nm+1
c           BOTTOM NODES RESTRAINED IN THE X-DIR
      nf(nm,1)=0
c           BOTTOM NODES UNRESTRAINED IN THE X-DIR
c      ic=ic+1
c      nf(nm,1)=ic
c           BOTTOM NODES RESTRAINED IN Y-DIR
      nf(nm,2)=0
   82 continue
      do 85 j=1,nx2
      do 86 i=1,ny2
      nm=nm+1
      ic=ic+1
      nf(nm,1)=ic
      ic=ic+1
   86 nf(nm,2)=ic
      nm=nm+1
c           BOTTOM CORNER NODE FULLY RESTRAINED
      nf(nm,1)=0
      nf(nm,2)=0
      do 87 i=1,2*ny2
      nm=nm+1
      if(j.eq.nx2)then
      nf(nm,1)=0
      else
      ic=ic+1
      nf(nm,1)=ic
      end if
      ic=ic+1
   87 nf(nm,2)=ic
      nm=nm+1
      nf(nm,1)=0
      nf(nm,2)=0
   85 continue
```

```
nm=0
do 8 ip=1,nx1+nx2
nys=1
if(ip.gt.nx1)nys=ny1+1
do 8 iq=nys,nye
nm=nm+1
nc=(3*nye+2)*nx1+2*ny1
facx=s1/ny1
facy=h1/ny1
facb=(w1+s1)/nx1
facs=0.
if(ny2.ne.0)facs=h2/ny2
frh=0.
if(nx2.ne.0)frh=w2/nx2
if(ip.le.nx1)then
  num(1)=(ip-1)*(3*nye+2)+2*iq+1
  num(2)=num(1)-1
  num(3)=num(1)-2
  num(4)=(ip-1)*(3*nye+2)+2*nye+iq+1
  num(5)=ip*(3*nye+2)+2*iq-1
  num(6)=num(5)+1
  num(7)=num(5)+2
  num(8)=num(4)+1
  if(iq.le.ny1)then
    coord(1,1)=(ip-1.)*(w1+iq*facx)/nx1
    coord(3,1)=(ip-1.)*(w1+(iq-1)*facx)/nx1
    coord(5,1)=ip*(w1+(iq-1)*facx)/nx1
    coord(7,1)=ip*(w1+iq*facx)/nx1
    coord(1,2)=-iq*facy
    coord(3,2)=-(iq-1)*facy
    coord(5,2)=-(iq-1)*facy
    coord(7,2)=-iq*facy
  else
    coord(1,1)=(ip-1.)*facb
    coord(3,1)=(ip-1.)*facb
    coord(5,1)=ip*facb
    coord(7,1)=ip*facb
    coord(1,2)=-h1-(iq-ny1)*facs
    coord(3,2)=-h1-(iq-ny1-1)*facs
    coord(5,2)=-h1-(iq-ny1-1)*facs
    coord(7,2)=-h1-(iq-ny1)*facs
  end if
else
  num(1)=nc+(ip-nx1-1)*(3*ny2+2)+2*(iq-ny1)+1
  num(2)=num(1)-1
  num(3)=num(1)-2
  num(4)=nc+(ip-nx1-1)*(3*ny2+2)+2*ny2+iq-ny1+1
  num(5)=nc+(ip-nx1)*(3*ny2+2)+2*(iq-ny1)-1
  num(6)=num(5)+1
  num(7)=num(5)+2
```

```
      num(8)=num(4)+1
      coord(1,1)=w1+s1+(ip-nx1-1)*frh
      coord(3,1)=coord(1,1)
      coord(5,1)=w1+s1+(ip-nx1)*frh
      coord(7,1)=coord(5,1)
      coord(1,2)=-h1-(iq-ny1)*facs
      coord(3,2)=-h1-(iq-ny1-1)*facs
      coord(5,2)=-h1-(iq-ny1-1)*facs
      coord(7,2)=-h1-(iq-ny1)*facs
    end if
    inc=0
    do 1 i=1,8
    do 1 j=1,2
    inc=inc+1
  1 g(inc)=nf(num(i),j)
    coord(2,1)=.5*(coord(1,1)+coord(3,1))
    coord(4,1)=.5*(coord(3,1)+coord(5,1))
    coord(6,1)=.5*(coord(5,1)+coord(7,1))
    coord(8,1)=.5*(coord(7,1)+coord(1,1))
    coord(2,2)=.5*(coord(1,2)+coord(3,2))
    coord(4,2)=.5*(coord(3,2)+coord(5,2))
    coord(6,2)=.5*(coord(5,2)+coord(7,2))
    coord(8,2)=.5*(coord(7,2)+coord(1,2))
    do 8 i=1,8
    g_num(nm,i)=num(i)
    k=2*i
    g_coord(num(i),1)=coord(i,1)
    g_coord(num(i),2)=coord(i,2)
8   continue
    return
    end
```

SAMPLE OUTPUT

X	Y	$\sigma_x/\gamma h_1$	$\sigma_y/\gamma h_1$	$\tau_{xy}/\gamma h_1$	$F/\gamma h_1$
5.4698	4.9698	-0.7211	-4.64E-01	-7.18E-01	2.56E-04
5.3872	4.8872	-0.7211	-4.64E-01	-7.17E-01	1.02E-03
5.4695	4.9695	-0.7789	-4.79E-01	-7.75E-01	3.90E-04
5.3861	4.8861	-0.7789	-4.79E-01	-7.74E-01	8.01E-04
5.4692	4.9692	-0.8211	-4.90E-01	-8.17E-01	3.51E-04
5.3852	4.8852	-0.8211	-4.90E-01	-8.17E-01	8.67E-04
5.4689	4.9689	-0.8789	-5.05E-01	-8.74E-01	5.87E-05
5.3841	4.8841	-0.8789	-5.05E-01	-8.74E-01	1.31E-03
5.4687	4.9687	-0.9211	-5.16E-01	-9.16E-01	1.08E-05
5.3833	4.8833	-0.9211	-5.16E-01	-9.15E-01	1.43E-03
5.4684	4.9684	-0.9789	-5.31E-01	-9.72E-01	1.88E-04
5.3821	4.8821	-0.9789	-5.32E-01	-9.72E-01	1.16E-03
5.4683	4.9683	-1.0704	-5.56E-01	-1.06E+00	2.66E-04
5.3817	4.8817	-1.0704	-5.56E-01	-1.06E+00	1.09E-03
5.4683	4.9683	-1.2629	-6.08E-01	-1.25E+00	2.80E-04
5.3817	4.8817	-1.2629	-6.08E-01	-1.25E+00	1.11E-03
5.4683	4.9683	-1.4038	-6.47E-01	-1.39E+00	3.71E-04
5.3817	4.8817	-1.4038	-6.47E-01	-1.39E+00	1.26E-03
5.4683	4.9683	-1.5962	-7.01E-01	-1.58E+00	4.35E-04
5.3817	4.8817	-1.5962	-7.01E-01	-1.58E+00	1.57E-03
5.4683	4.9683	-1.7371	-7.41E-01	-1.72E+00	5.17E-04
5.3817	4.8817	-1.7371	-7.41E-01	-1.72E+00	1.83E-03
5.4683	4.9683	-1.9296	-7.97E-01	-1.91E+00	6.35E-04
5.3817	4.8817	-1.9296	-7.97E-01	-1.91E+00	2.28E-03
5.4683	4.9683	-2.0704	-8.39E-01	-2.05E+00	6.28E-04
5.3817	4.8817	-2.0704	-8.39E-01	-2.05E+00	2.42E-03
5.4683	4.9683	-2.2629	-8.97E-01	-2.24E+00	6.99E-04
5.3817	4.8817	-2.2629	-8.97E-01	-2.24E+00	2.68E-03
5.4683	4.9683	-2.4038	-9.41E-01	-2.38E+00	7.96E-04
5.3817	4.8817	-2.4038	-9.41E-01	-2.38E+00	2.89E-03
5.4683	4.9683	-2.5962	-1.00E+00	-2.56E+00	9.22E-04
5.3817	4.8817	-2.5962	-1.00E+00	-2.56E+00	3.21E-03
5.4683	4.9683	-2.7371	-1.05E+00	-2.70E+00	9.60E-04
5.3817	4.8817	-2.7371	-1.05E+00	-2.70E+00	3.33E-03
5.4683	4.9683	-2.9296	-1.11E+00	-2.89E+00	9.50E-04
5.3817	4.8817	-2.9296	-1.11E+00	-2.89E+00	3.63E-03
5.4683	4.9683	-3.0704	-1.16E+00	-3.02E+00	1.01E-03
5.3817	4.8817	-3.0704	-1.16E+00	-3.02E+00	3.85E-03
5.4683	4.9683	-3.2629	-1.22E+00	-3.21E+00	1.11E-03
5.3817	4.8817	-3.2629	-1.22E+00	-3.21E+00	4.13E-03

APPENDIX C: Adaptations to FE Code for Conformal Mapping

1. Variables a and b added for symmetric slope problem (RVT)

```
      real a,b
c     for ridges, b should be positive;
c     for valleys, b should be negative
      b=-1.0
```

2. WITHIN LOOP FOR ANGLE AND DIMENSION CHANGES
Added 'option' solely for the symmetric slope problem

```
    else if(adex.eq.6)then
      name3 = '00'
      ny1=0
      s1=0.0
      h1=0.0
      w2=7.0
      nx2=20
      w1=7.0
      nx1=30
      h2=16.0
      ny2=60
    end if
```

3. Added a and b to the call for quad.f

```
      call quad(nx1,nx2,ny1,ny2,w1,w2,s1,h1,h2,globc,nf,inf,
     +                gnum,kel,nels,nn,n,iw,igen,a,b)
```

4. Adjusted write statements to normalize stresses using b

```
      write(iout,'(2f8.4,5e12.4)')
     >gc(1),gc(2),sigma(1)/(gamma*abs(b)),
     >               sigma(2)/(gamma*abs(b)),
     >               sigma(3)/(gamma*abs(b)),
     >                  f/(gamma*abs(b)),
     >                sig1/(gamma*abs(b)),
     >                sig3/(gamma*abs(b)),
     >                tmax/(gamma*abs(b))
```

5. Added a and b to the quad.f subroutine

```
      subroutine quad(nx1,nx2,ny1,ny2,w1,w2,s1,h1,h2,
      +                  g_coord,nf,inf,g_num,maxel,nels,nn,
      +                  n,iw,igen,a,b)

       real g_coord(inf,2),coord(8,2),u,v,a,b
```

6. Added 4 lines to map the rectangular mesh to a symmetric slope corresponding with Savage and Swolfs' RVT program.

```
       u=coord(i,1)
       v=coord(i,2)
       g_coord(num(i),1)=u+((a*b*u)/((u*u)+((v-a)*(v-a))))
       g_coord(num(i),2)=v-((a*b*(v-a))/((u*u)+((v-a)*(v-a))))
```

APPENDIX D: Finite Element Code: Boussinesq Solution

```
      PROGRAM PM54
C
C
C      MODIFIED PROGRAM 5.4   PLANE STRAIN OF AN ELASTIC
C      SOLID USING 8-NODE QUADRILATERAL ELEMENTS
C
C
C      ALTER NEXT LINE TO CHANGE PROBLEM SIZE
C
      PARAMETER(IKB1=2400,IKB2=126,ILOADS=2400,INF=1281,
     +          IVAL=100,INW=250,IND=500)
C
      REAL DEE(3,3),SAMP(4,2),COORD(8,2),JAC(2,2),JAC1(2,2),
     +DER(2,8),DERIV(2,8),BEE(3,16),DBEE(3,16),VAL(IVAL),
     +BTDB(16,16),KM(16,16),ELD(16),EPS(3),SIGMA(3),GC(2),
     +BT(16,3),FUN(8),KB(IKB1,IKB2),LOADS(ILOADS),WID(INW),DEP(IND)
      INTEGER NF(INF,2),G(16),NO(IVAL)
      DATA IDEE,IBEE,IDBEE,IH/4*3/,IDOF,IBTDB,IBT,IKM/4*16/
      DATA IJAC,IJAC1,NODOF,IT,IDER,IDERIV/6*2/,ICOORD,NOD/2*8/
      DATA ISAMP/4/
C
C      INPUT AND INITIALISATION
C
      open(5,file='bsq5Cin.d')
      READ(5,*)NXE,NYE,N,IW,NN,NR,NGP,E,V
      READ(5,*)(WID(I),I=1,NXE+1)
      READ(5,*)(DEP(I),I=1,NYE+1)
      CALL READNF(NF,INF,NN,NODOF,NR)
      IWP1=IW+1
      CALL NULL(KB,IKB1,N,IWP1)
      CALL FMDEPS(DEE,IDEE,E,V)
      CALL GAUSS(SAMP,ISAMP,NGP)
C
C      ELEMENT STIFFNESS INTEGRATION AND ASSEMBLY
C
      DO 10 IP=1,NXE
      DO 10 IQ=1,NYE
      CALL GEOV8Y(IP,IQ,NYE,WID,DEP,COORD,ICOORD,G,NF,INF)
      CALL NULL(KM,IKM,IDOF,IDOF)
      DO 20 I=1,NGP
      DO 20 J=1,NGP
      CALL FMQUAD(DER,IDER,FUN,SAMP,ISAMP,I,J)
      CALL MATMUL(DER,IDER,COORD,ICOORD,JAC,IJAC,IT,NOD,IT)
```

```
      CALL TWOBY2(JAC,IJAC,JAC1,IJAC1,DET)
      CALL MATMUL(JAC1,IJAC1,DER,IDER,DERIV,IDERIV,IT,IT,NOD)
      CALL NULL(BEE,IBEE,IH,IDOF)
      CALL FORMB(BEE,IBEE,DERIV,IDERIV,NOD)
      CALL MATMUL(DEE,IDEE,BEE,IBEE,DBEE,IDBEE,IH,IH,IDOF)
      CALL MATRAN(BT,IBT,BEE,IBEE,IH,IDOF)
      CALL MATMUL(BT,IBT,DBEE,IDBEE,BTDB,IBTDB,IDOF,IH,IDOF)
      QUOT=DET*SAMP(I,2)*SAMP(J,2)
      CALL MSMULT(BTDB,IBTDB,QUOT,IDOF,IDOF)
   20 CALL MATADD(KM,IKM,BTDB,IBTDB,IDOF,IDOF)
   10 CALL FORMKB(KB,IKB1,KM,IKM,G,IW,IDOF)
C
C      EQUATION SOLUTION
C
      CALL NULVEC(LOADS,N)
C
C      FIXED DISPLACEMENT DATA
C
      READ(5,*)IFIX,(NO(I),VAL(I),I=1,IFIX)
      DO 25 I=1,IFIX
      KB(NO(I),IWP1)=KB(NO(I),IWP1)+1.E20
   25 LOADS(NO(I))=KB(NO(I),IWP1)*VAL(I)
C
      READ(5,*)NL,(K,LOADS(K),I=1,NL)
      CALL CHOLIN(KB,IKB1,N,IW)
      CALL CHOBAC(KB,IKB1,LOADS,N,IW)
c      CALL PRINTV(LOADS,N)
C
C      RECOVER STRAINS AND STRESSES AT ELEMENT CENTRES
c
      open(8,file='bsqcout.dat')
C
c      NGP=1
c      CALL GAUSS(SAMP,ISAMP,NGP)
      DO 30 IP=1,NXE
      DO 30 IQ=1,NYE
      CALL GEOV8Y(IP,IQ,NYE,WID,DEP,COORD,ICOORD,G,NF,INF)
      DO 40 M=1,IDOF
      IF(G(M).EQ.0)ELD(M)=0.
   40 IF(G(M).NE.0)ELD(M)=LOADS(G(M))
      DO 30 I=1,NGP
      DO 30 J=1,NGP
      CALL FMQUAD(DER,IDER,FUN,SAMP,ISAMP,I,J)
      CALL MATMUL(DER,IDER,COORD,ICOORD,JAC,IJAC,IT,NOD,IT)
      CALL TWOBY2(JAC,IJAC,JAC1,IJAC1,DET)
      CALL MATMUL(JAC1,IJAC1,DER,IDER,DERIV,IDERIV,IT,IT,NOD)
      CALL NULL(BEE,IBEE,IH,IDOF)
      CALL FORMB(BEE,IBEE,DERIV,IDERIV,NOD)
      CALL MVMULT(BEE,IBEE,ELD,IH,IDOF,EPS)
      CALL MVMULT(DEE,IDEE,EPS,IH,IH,SIGMA)
```

```
c       CALL PRINTV(SIGMA,IH)
        call GCOORD(FUN,COORD,ICOORD,NOD,IT,GC)
        write(8,'(2f8.4,5e12.4)')
       +       GC(1), GC(2), SIGMA(1), SIGMA(2), SIGMA(3)
    30 CONTINUE
        STOP
        END
```

APPENDIX E: FORTRAN Code for Analytic Boussinesq Solution

```
program boussinesq
!
! assume q=1.0
! assume half width of footing is   1.0 (b=2.0)
! assume half  width of problem is  3.0
! assume total depth of problem is 10.0
!
implicit none
!
real::b=1.0,width=2.5,depth=5.0,q=1.0
!
!integer::i,j,nx=15,ny=50 ! a coarser discretisation
 integer::i,j,nx=75,ny=100,iout
!
real::xinc,yinc,l1,l2,alp,bet,x,shftx,y,negy,sigx,sigz,txz,pi
!
iout = 11
open(iout,file='anbsq5.dat')
pi=4.*atan(1.)
xinc=real(width/nx); yinc=real(depth/ny)
do i=-nx/3, 2*nx/3
do j=1,ny
  x=real(i*xinc); y=real(j*yinc)
  l1=sqrt((b+x)**2+y**2)
  l2=sqrt(x**2+y**2)
  alp=acos((l1**2+l2**2-b**2)/(2.*l1*l2))
  bet=atan(x/y)
  sigx=q/pi*(alp-sin(alp)*cos(alp+2.*bet))
  sigz=q/pi*(alp+sin(alp)*cos(alp+2.*bet))
  txz =q/pi*(sin(alp)*sin(alp+2.*bet))
  negy=-y
  shftx=x+0.5
  write(11,'(5f12.4)')shftx,negy,sigx,sigz,txz
end do
end do
end program boussinesq
```

APPENDIX F: Mesh Size Variations

Finite element variables used for mesh size comparisons with constant centerline

(after Poulos et al)

	Small mesh			Wide/shallow mesh			Deep/narrow mesh			Large mesh		
	15°	45°	85°	15°	45°	85°	15°	45°	85°	15°	45°	85°
nx1	29	17	12	29	17	12	29	17	12	29	17	12
nx2	12	12	12	25	25	25	12	12	12	25	25	25
ny1	5	5	5	5	5	5	5	5	5	5	5	5
ny2	25	25	25	25	25	25	50	50	50	50	50	50
w1	2.5	2.5	2.5	2.5	2.5	2.5	2.5	2.5	2.5	2.5	2.5	2.5
w2	2.5	2.5	2.5	5.0	5.0	5.0	2.5	2.5	2.5	5.0	5.0	5.0
s1	3.372	1.000	0.0875	3.372	1.000	0.0875	3.372	1.000	0.0875	3.372	1.000	0.0875
h1	1.0	1.0	1.0	1.0	1.0	1.0	1.0	1.0	1.0	1.0	1.0	1.0
h2	5.0	5.0	5.0	5.0	5.0	5.0	10.0	10.0	10.0	10.0	10.0	10.0

Table F-1 : FE Variables for Mesh Size Variants

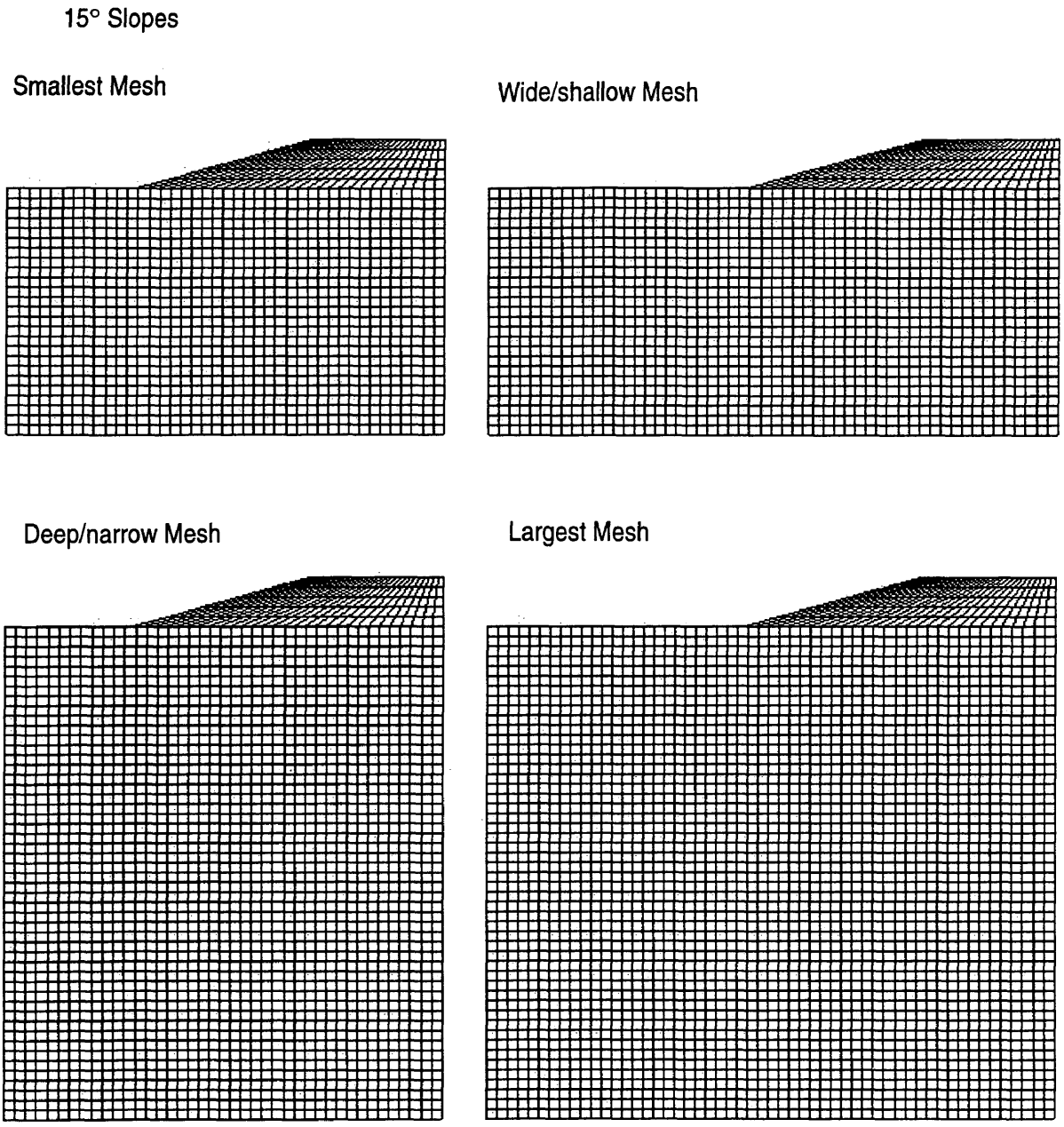

Figure F-1: Mesh Size Variants, 15° Slope Angle

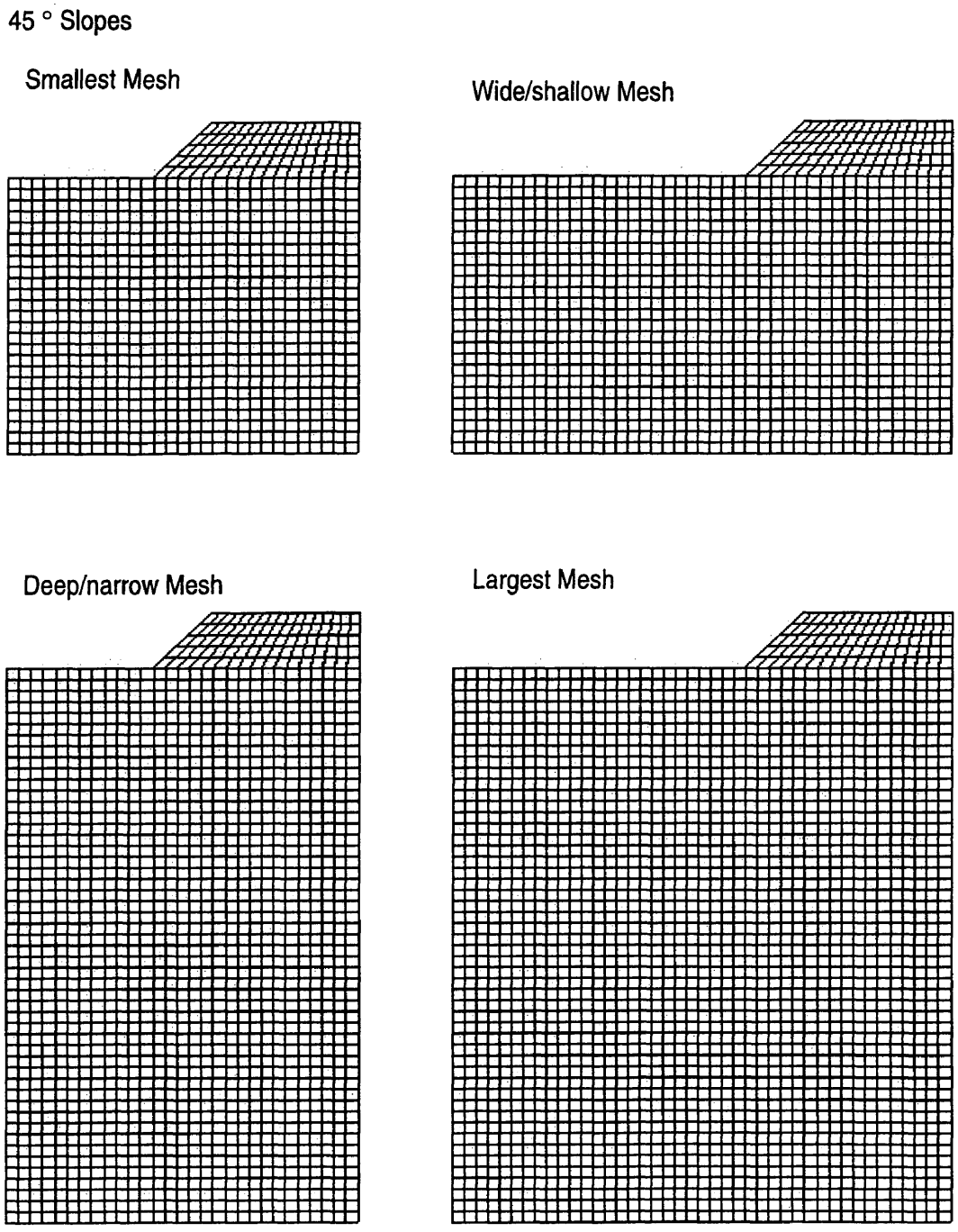

Figure F-2: Mesh Size Variants, 45° Slope Angle

85° Slopes

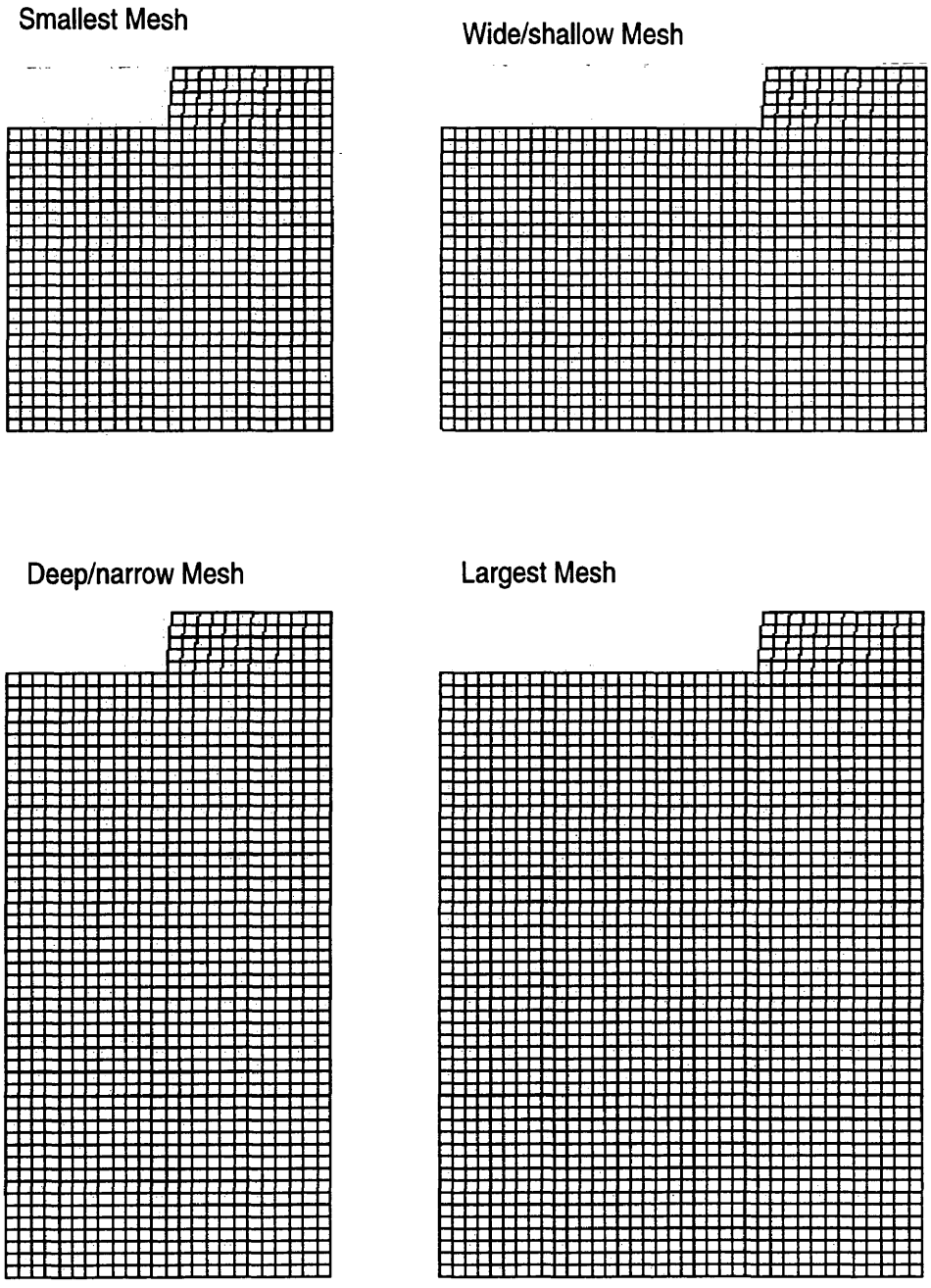

Figure F-3: Mesh Size Variants, 85° Slope Angle

APPENDIX G: Element Density Variations

Variables Used for Element Density Comparisons

	Sparsest		Mid-dense		Densest	
	15°	45°	15°	45°	15°	45°
nx1	20	15	41	30	60	43
nx2	12	12	25	25	40	40
ny1	2	2	5	5	7	7
ny2	25	25	50	50	70	70
w1	5.0	5.0	5.0	5.0	5.0	5.0
w2	5.0	5.0	5.0	5.0	5.0	5.0
s1	3.372	1.000	3.372	1.000	3.372	1.000
h1	1.0	1.0	1.0	1.0	1.0	1.0
h2	10.0	10.0	10.0	10.0	10.0	10.0

Table G-1: FE Variables for Element Density Variants

	Sparsest		Mid-dense		Densest	
	15°	45°	15°	45°	15°	45°
nx1/(w1+s1)	2.4	2.5	4.9	5.0	7.2	7.2
nx2/w2	2.4	2.4	5	5	8	8
ny1/h1	2.0	2.0	5.0	5.0	7.0	7.0
ny2/h2	2.5	2.5	5.0	5.0	7.0	7.0

Table G-2: Element Densities

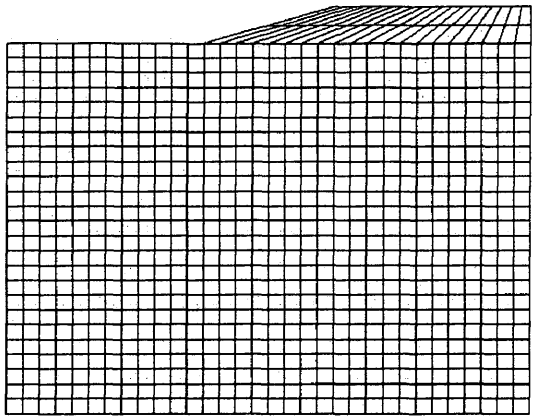

Lowest Element Density
15° Slope

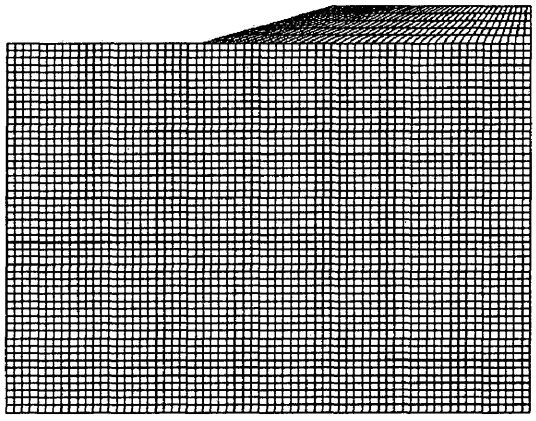

Medium Element Density
15° Slope

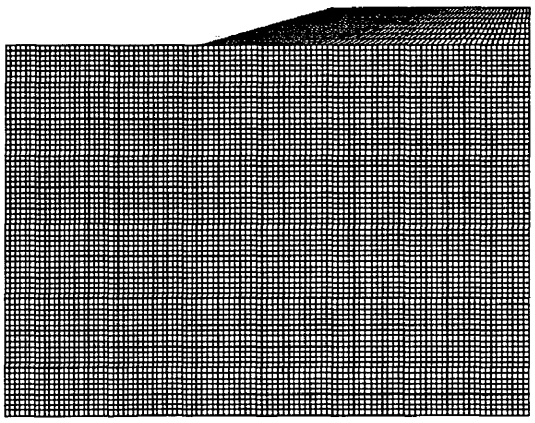

Greatest Element Density
15° Slope

Figure G-1: Mesh Density Variants, 15° Slope Angle

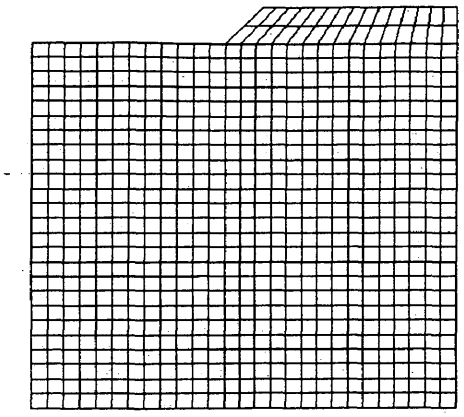

Lowest Element Density
45° Slope

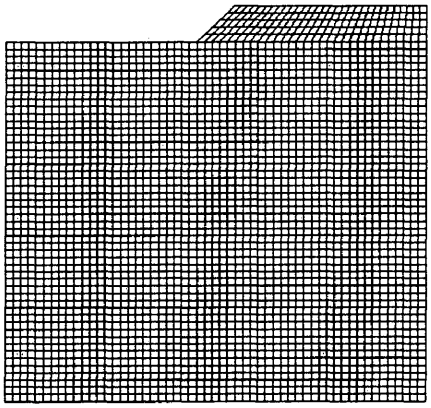

Medium Element Density
45° Slope

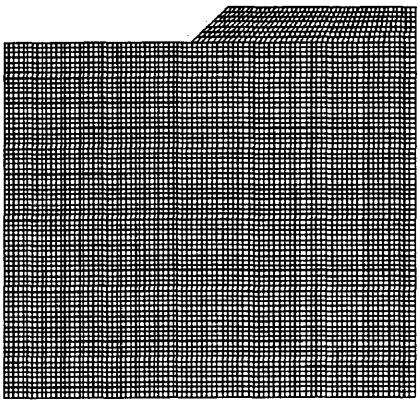

Greatest Element Density
45° Slope

Figure G-2: Mesh Density Variants, 45° Slope Angle

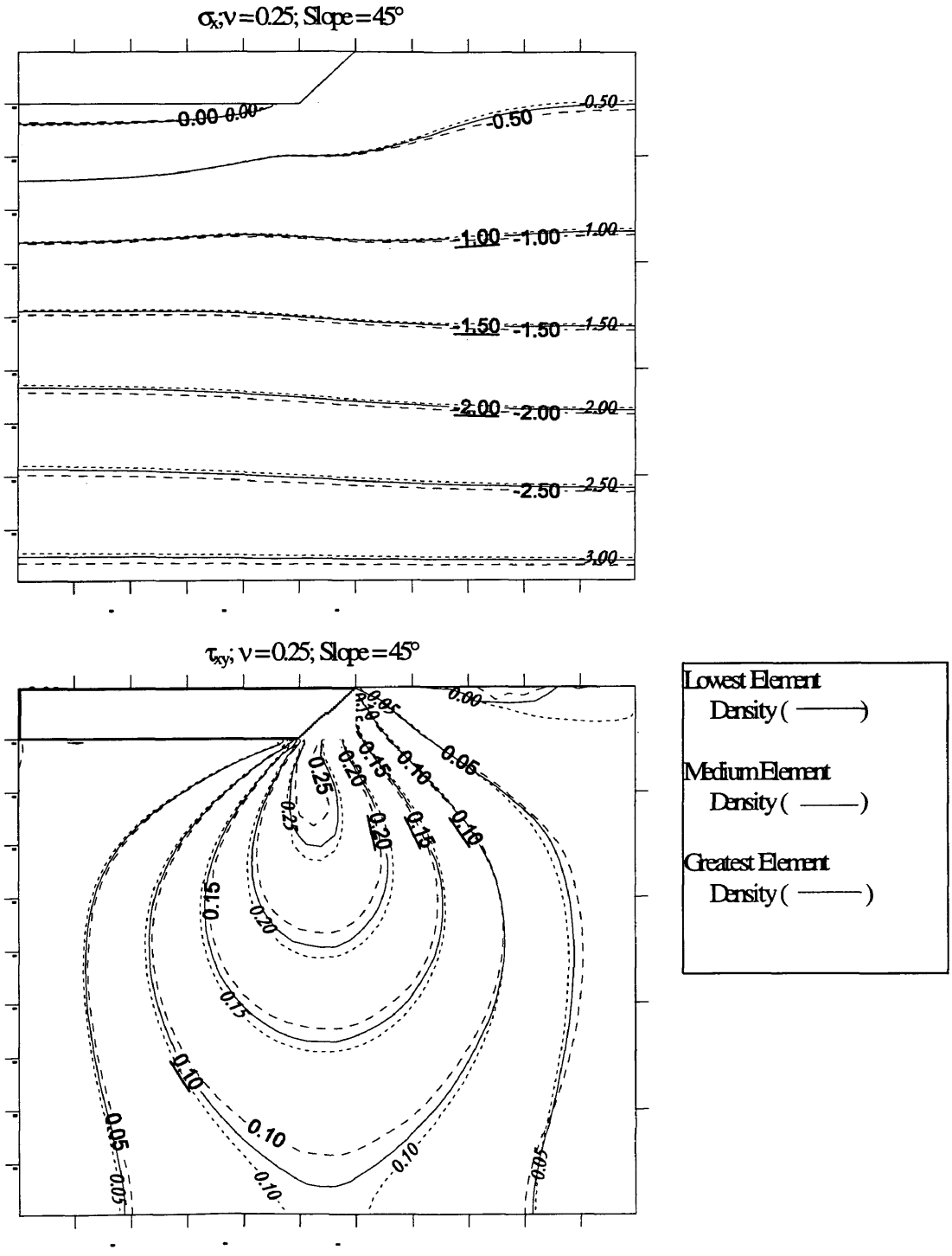

Figure G-3: Element Density Effects, 45° Slope Angle

APPENDIX H: Effects of Poisson's Ratio

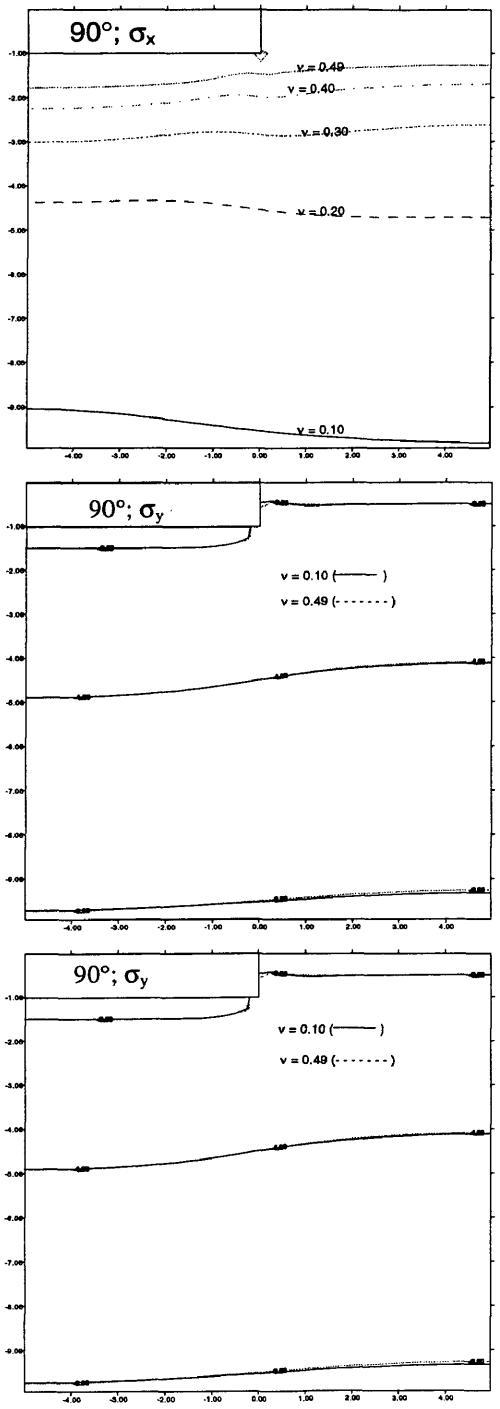

Figure H-1: ν Effects, 90° Slope Angle

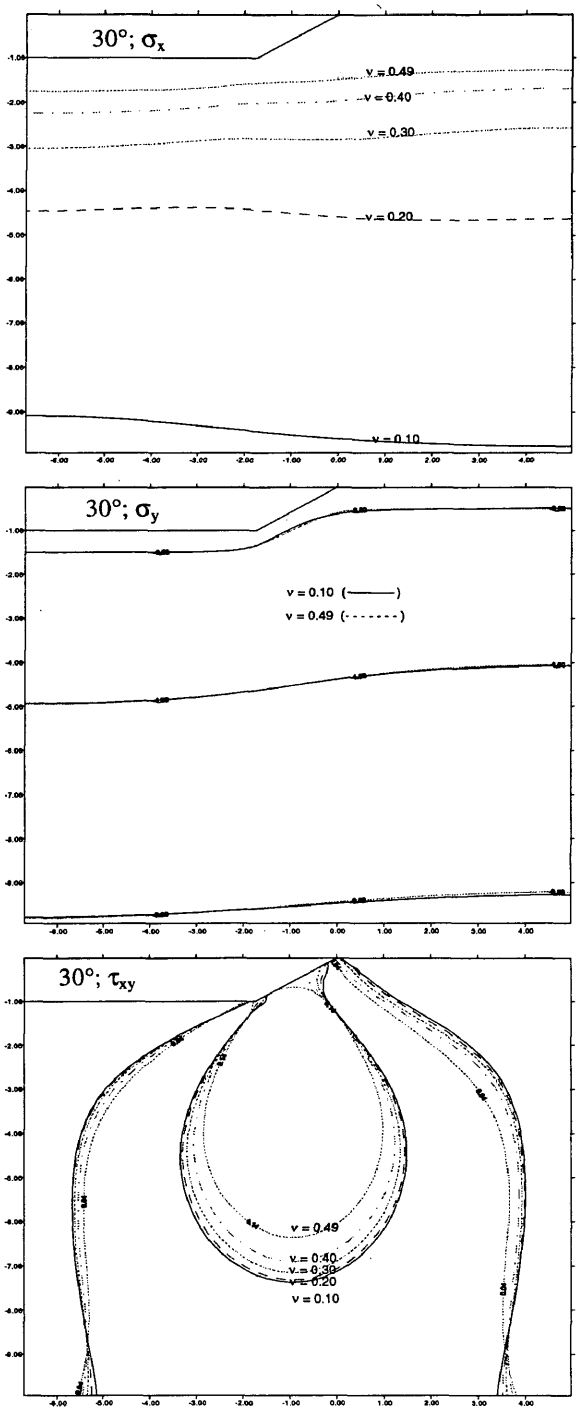

Figure H-2: ν Effects, 30° Slope Angle

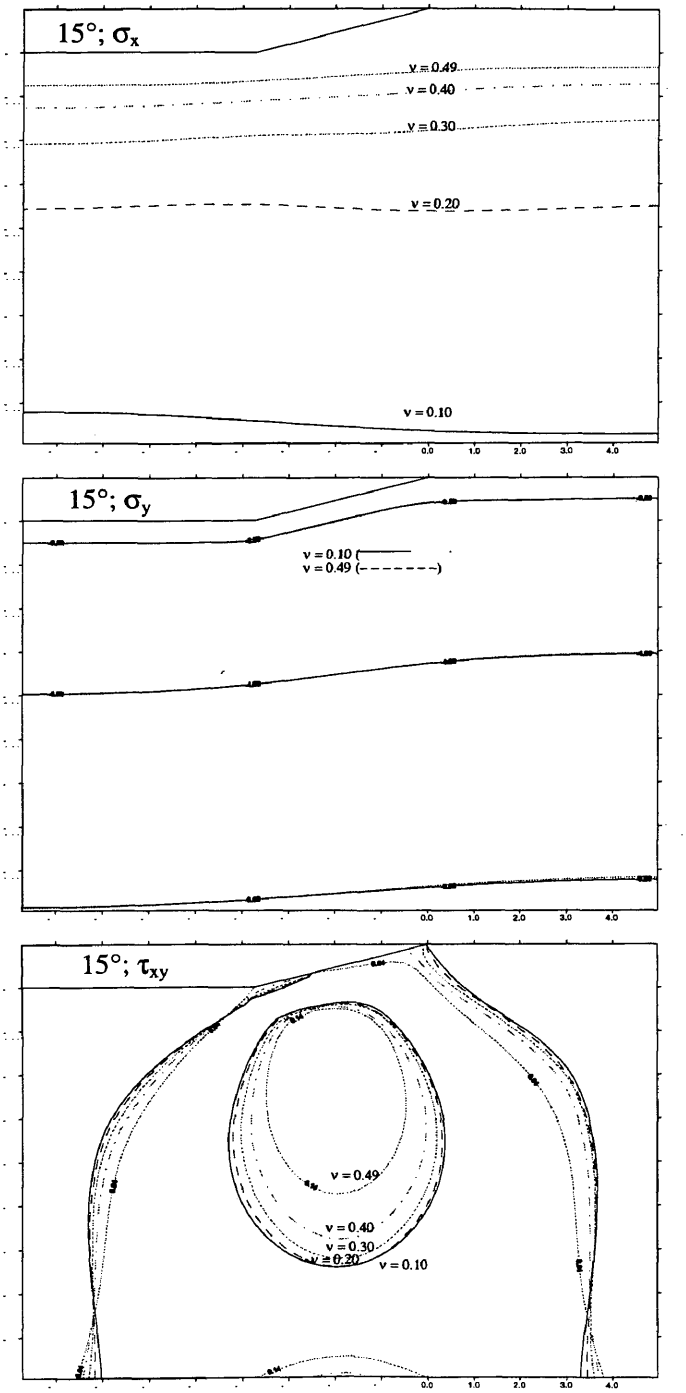

Figure H-3: ν Effects, 15° Slope Angle

APPENDIX I: Slope Angle Effects

Contained in this appendix are renditions of shear and horizontal stresses in slopes with angles of 15°, 20°, 25°, 30°, 35°, 45°, 55°, 65°, 75°, 85°, and 90°. Their inclusion is intended to show the stress variations due to grade more gradually than is done in the main text of this document.

It should be noted that the original meshes used to generate these graphs contained two different centerlines. For the 15°, 30°, 45°, 85° and 90° slopes, w_1 was equal to 5.0; whereas, w_1 was half that length (2.5) in the remaining meshes. Element densities and all other factors were consistent between the two groups. The boundary effect is evident in both the shear and horizontal stress contours; this is most apparent in the latter group. Nevertheless, the overall trends follow the discussion in the main text.

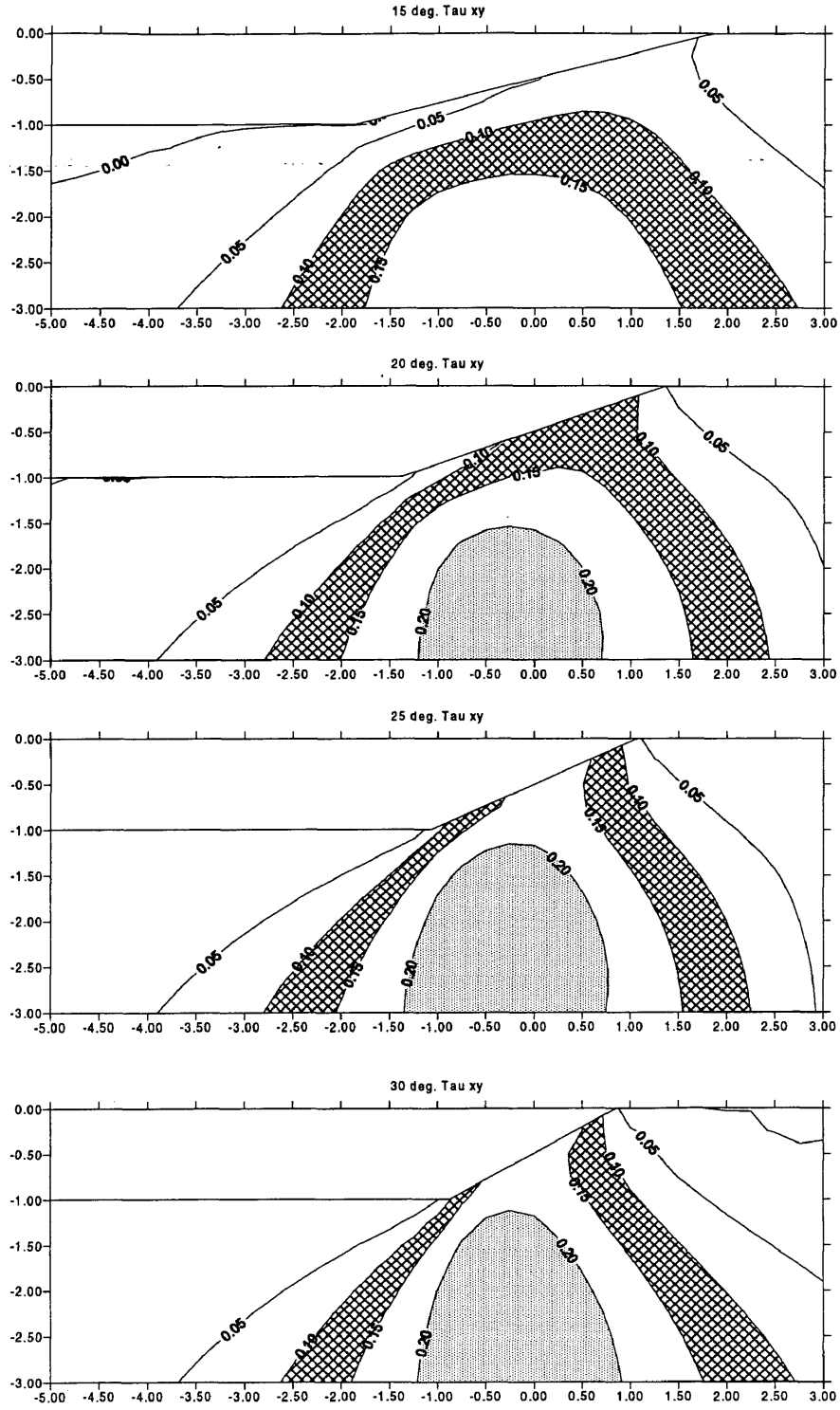

Figure I-1: τ_{xy}; 15°, 20°, 25°,30°

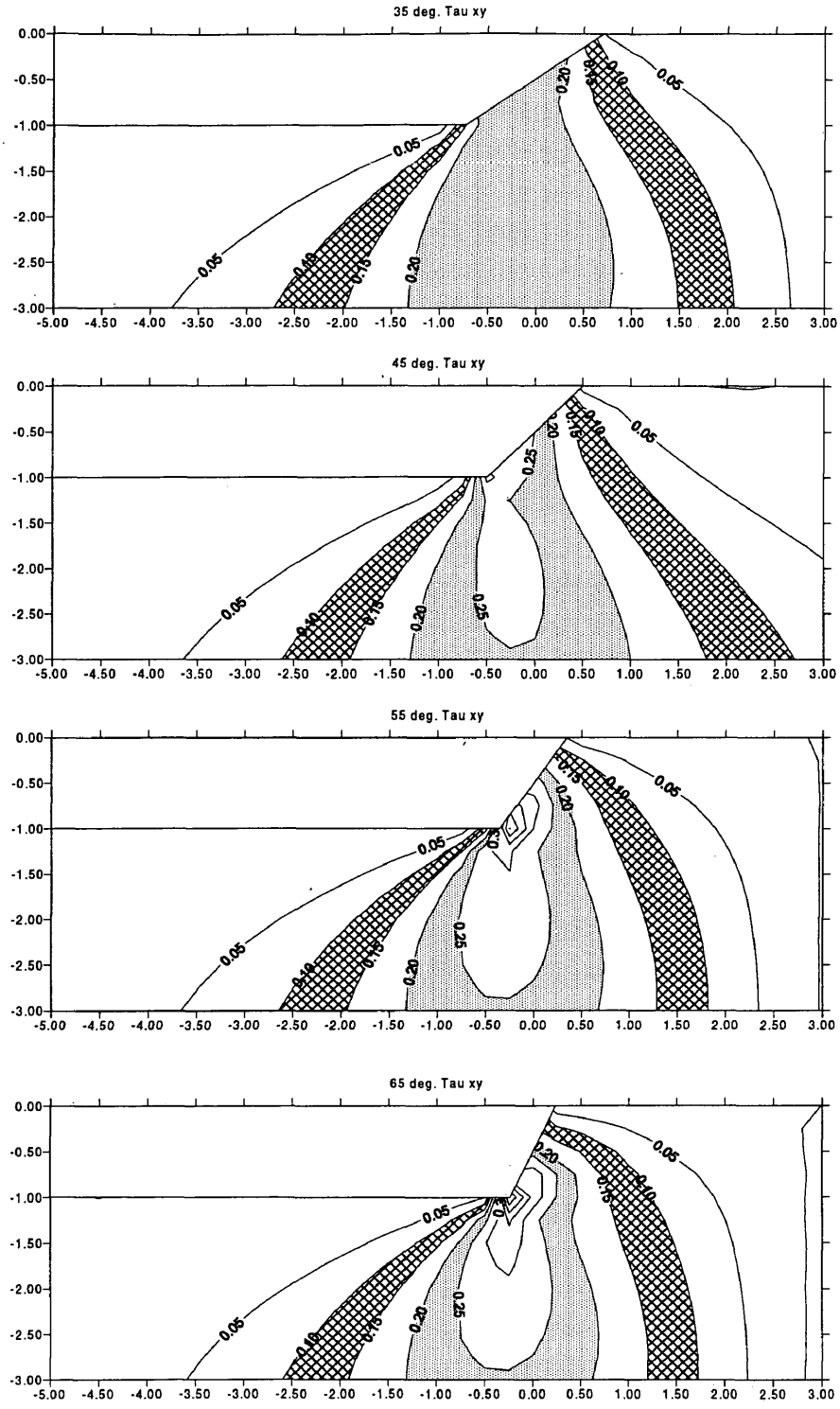

Figure I-2: τ_{xy}; 35°, 45°, 55°, 65°

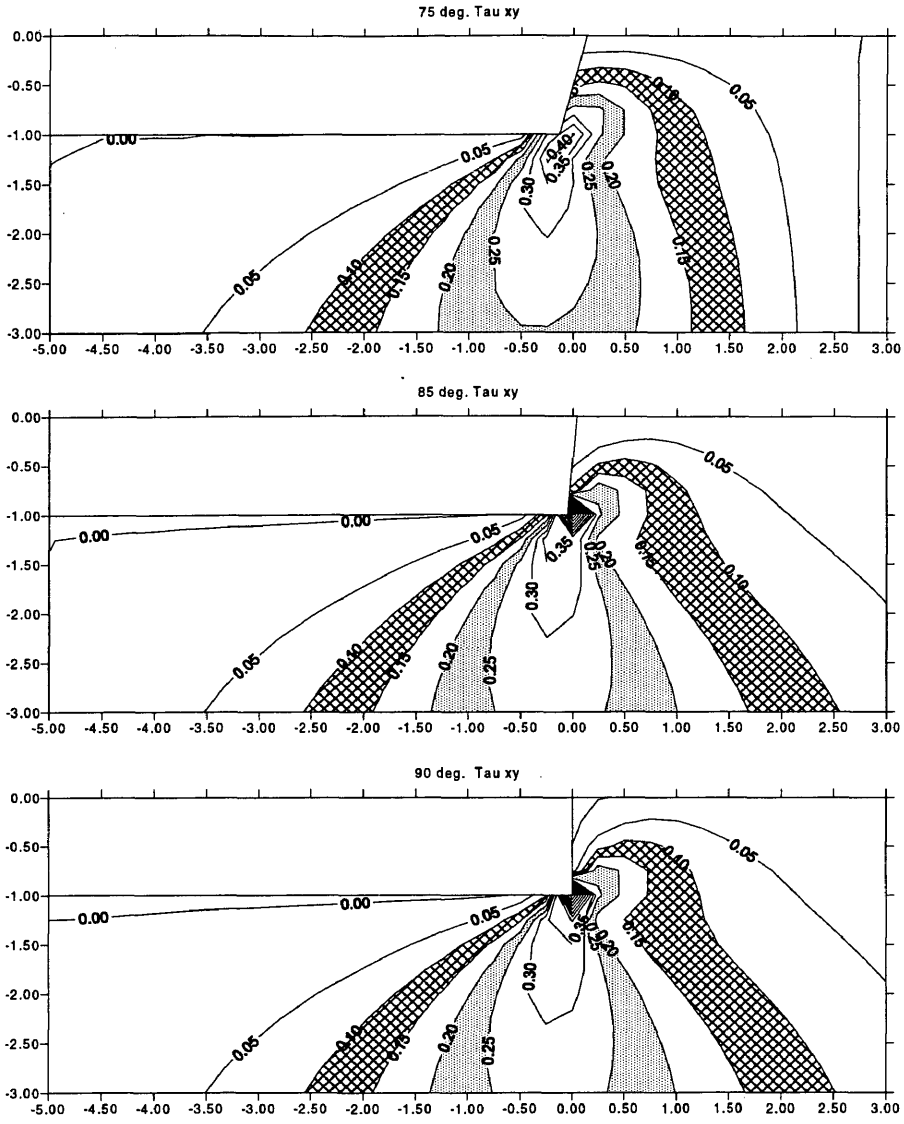

Figure I-3: τ_{xy}; 75°, 85°, 90°

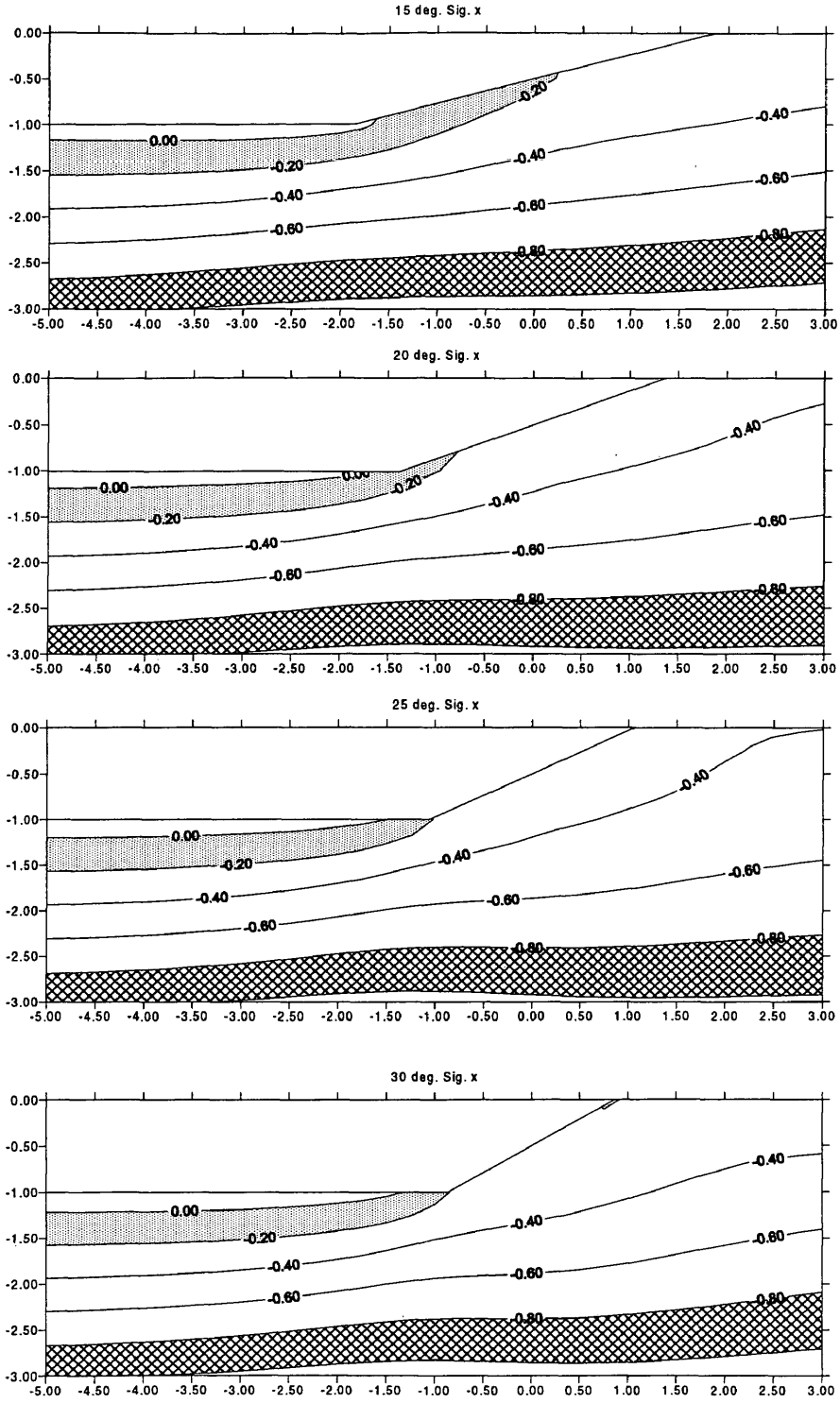

Figure I-4: σ_x; 15°, 20°, 25°,30°

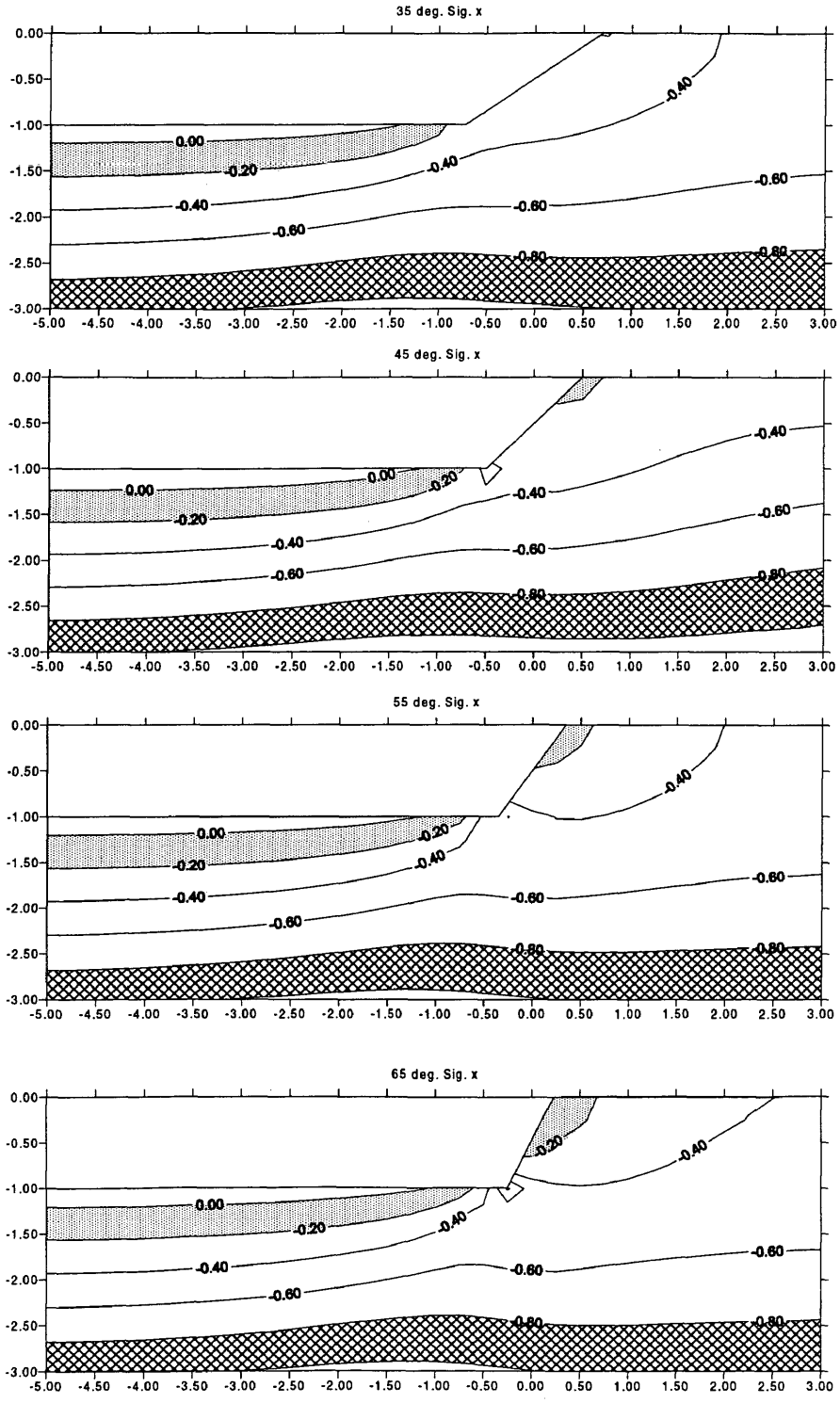

Figure I-5: σ_x; 35°, 45°, 55°, 65°

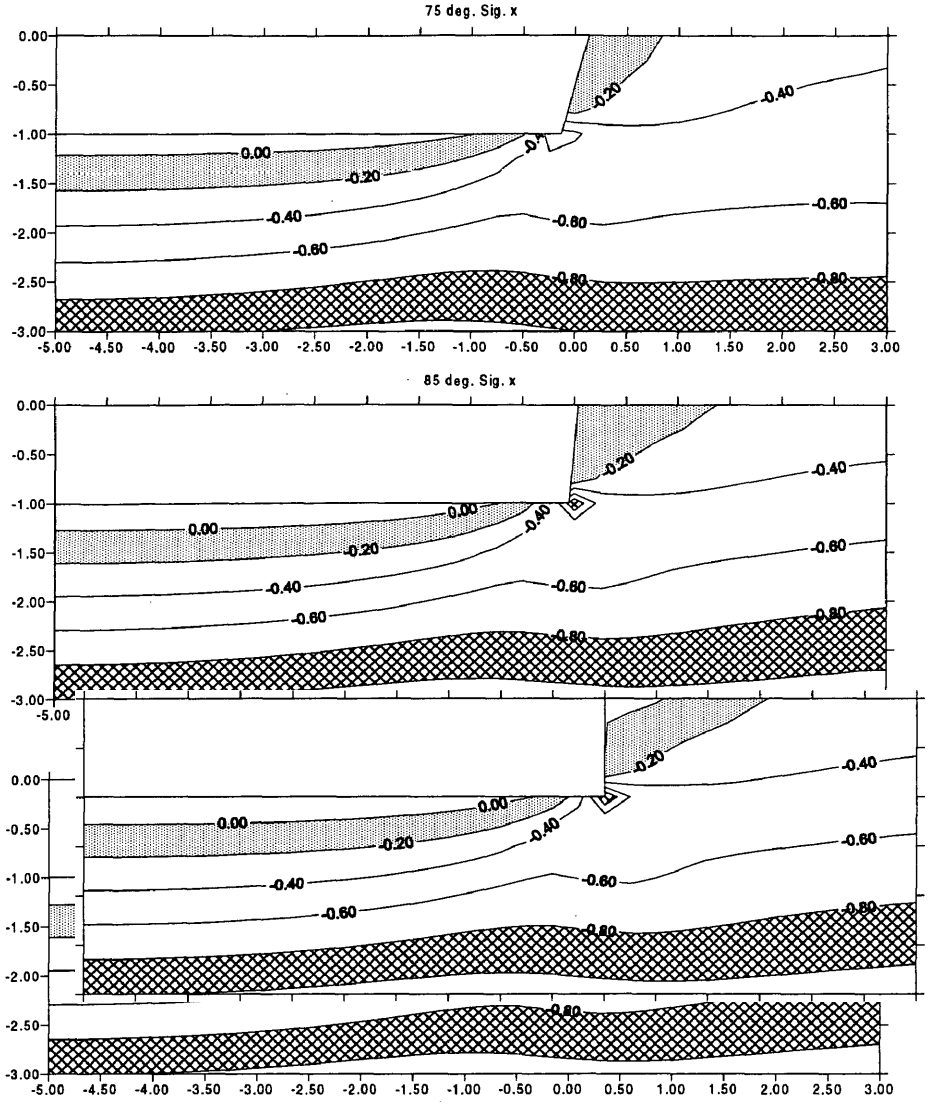

Figure I-6: σ_x; 75°, 85°, 90°

APPENDIX J: Mesh Displacements Due to Visco-plastic Stress Redistribution

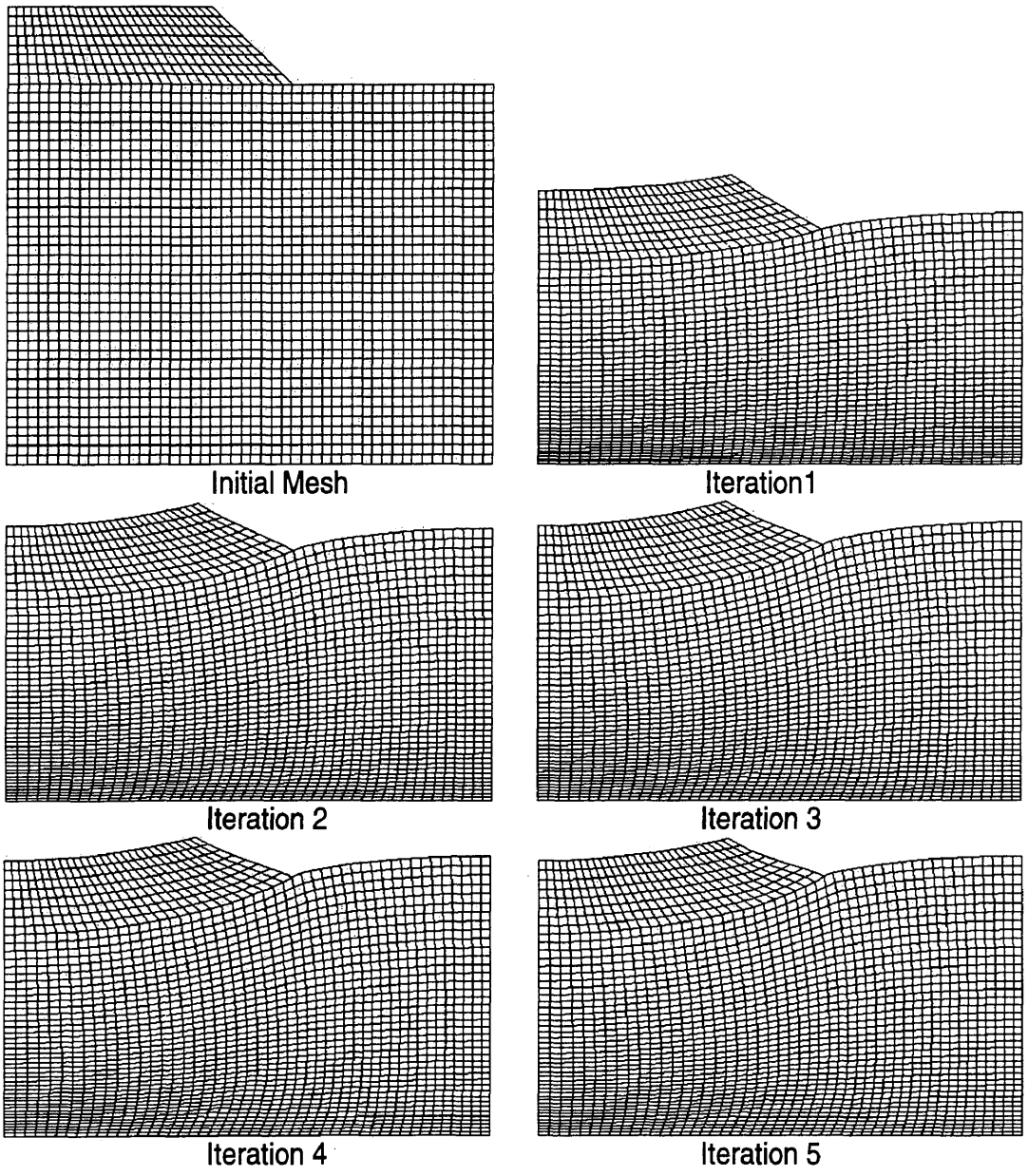

Figure J-1: Mesh Displacements 1

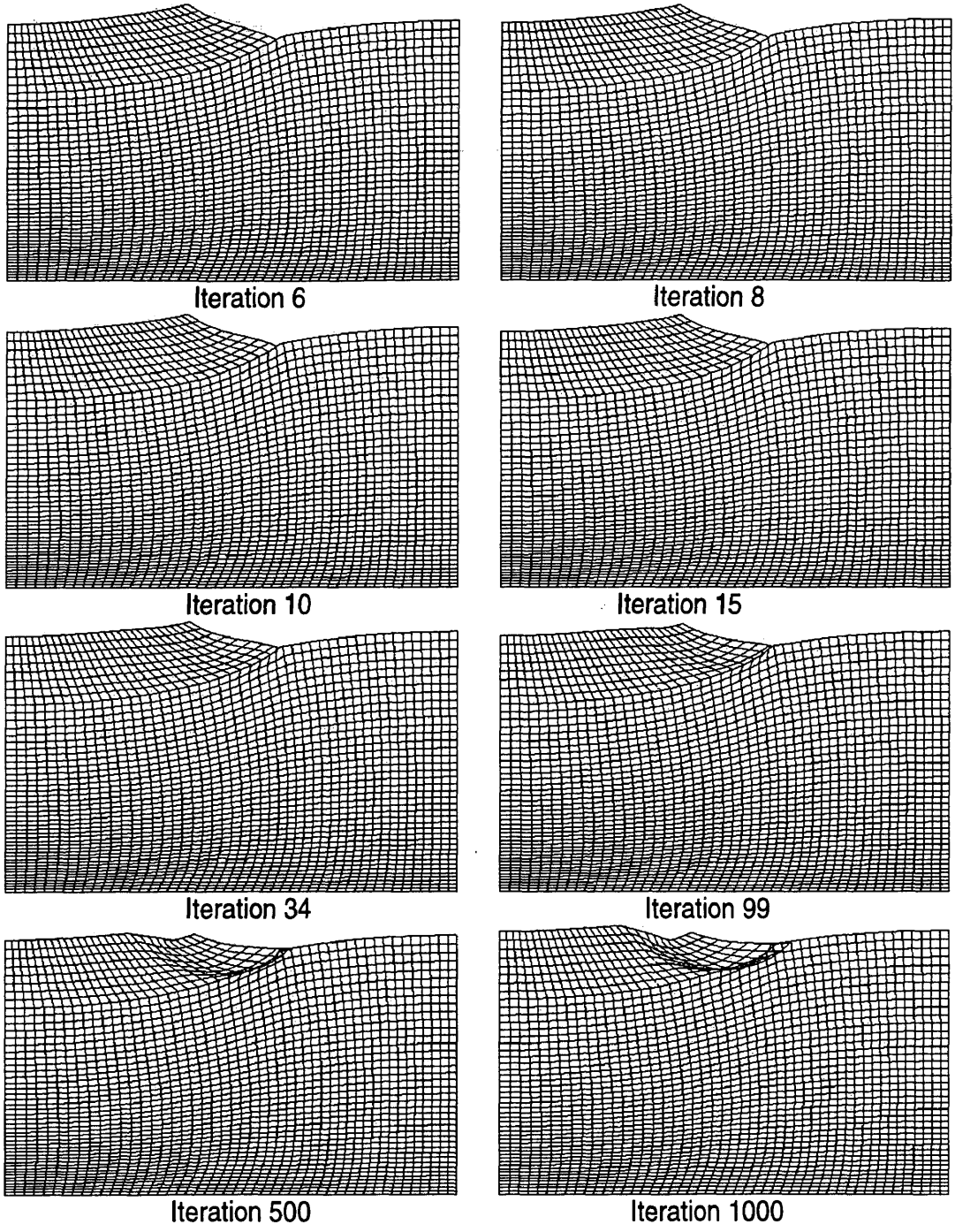

Figure J-1: Mesh Displacements 2